Dysprosium Mid-Infrared Fibre Lasers

By

Matthew Majewski

A thesis submitted to Macquarie University
for the degree of Doctor of Philosophy
Department of Engineering
January 2018

© Matthew Majewski, 2018.

Typeset in LaTeX 2_ε.

Except where acknowledged in the customary manner, the material presented in this thesis is, to the best of my knowledge, original and has not been submitted in whole or part for a degree in any university.

Matthew Majewski

Acknowledgements

Over the course of my PhD work I have occasionally thought about (and semi-frequently been asked about by my partner) who I would be thanking in the acknowledgements. I have read some very lengthy acknowledgements, and though I could certainly make a long list of people who have had an influence on me both personally and in my professional career, this will likely be brief. I find myself even now writing this certainly over-thinking the process. So rather than the carefully measured, revised, and revised again, words that I hope make up the actual content of this thesis, I will aim for a more stream of consciousness approach here. I will almost certainly be forgetting certain people in this process, and for that I apologize, though honestly you probably weren't reading this anyway.

I would start with the people with most recent impact, specifically with this foray into the academic world. First among them has to be my supervisor Prof. Stuart Jackson. I first met Stuart while attempting to arrange a part-time PhD project as part of my last industry employment, and though I immediately liked him, I suspected his level of optimism in regards to the probable success of various experiments may not always mesh with my own outlook. Over the last several years actually working together this has been proven true on occasion, though rather than a negative I think this has actually been a net positive. RFK is quoted to have said "There are those that look at things the way they are, and ask why? I dream of things that never were, and ask why not?", and while these words are certainly over-dramatic in reference to working on lasers in a lab, it is relevant. A good technical team needs a balance of viewpoints, and I think we have achieved that rather well. I would also like to thank Dr. Robert Woodward, who is a recent addition to our research group but has at least for me had a profound impact. I spent much of the beginning of my PhD project working with only Stuart, and often alone. Rob's presence, along with his clear skill re-invigorated my approach to research in a crucial way, and his patience in taking the time to answer my many, and often repeated, questions is more than appreciated. Finally in regards to people at the university, I would like to thank Dr. (hopefully by now at least) Sergei Antipov. Though we did not really get a chance to work directly together, we shared laboratory space for a time and our projects shared some cross-over. As two students, it was both enriching and often fun to try to solve various problems ourselves.

Prior to starting this research project, I spent several years working in industry, and I am extremely grateful for having lived in both worlds, as I think many people only truly see one of them, and there are clear positives (and negatives) to each. Though the people mentioned above had direct impact on this specific research project, I would never have been here if not for several of the great people I have worked with in industry, and I would like to thank them here. First Dr. Dan Hogenboom, who was my first 'boss' in a laser research position.

Beyond just being responsible for my entry into the world of lasers, he was instrumental in encouraging me to continue with education beyond my undergraduate degree. I have often recalled his advice that pursuing a PhD was a waste of time, and one of his biggest mistakes. Though I am fairly certain we would not have crossed paths if he had not pursued one himself, and completing my own now, I hope that this remains the only piece of bad advice he has ever given. Further, I would sincerely thank Paul Lewis, who fought hard to get me a position working on a project at GE. Though that ultimately failed (through no fault of his own) he was instrumental in arranging the position that brought me to Australia seven years ago, and where I currently sit writing this. He was the first (in my professional life) to congratulate me on receiving a scholarship for a PhD project and was the most vocal in advising me it was the right thing to do. Finally, for those in my previous life in industry, the most sincere thanks goes to Dr. Stephanus Van Heerden, Fani. His influence truly allowed me to mature as a scientist, even in an industrial setting. His willingness to discuss various ideas at length, and the freedom he afforded me to conduct experiments in the lab, I find to have been truly unique in an industrial setting, and had a profound impact on my development. To do this on top of also having to meet strict deadlines was indeed impressive. I also doubt that I will encounter many others in a management position who are such strong advocates for all of their employees.

Finally, this would not be complete without some personal thanks, much of which is owed to my partner Amelia. You have been incredibly patient with me during this time, especially towards the end when the work got hectic and I could not contribute as much to our life together (thank you for the lunches). I know you did not always follow my various rants about the issue of the day in the lab, but you tried, and most importantly listened, which is mostly all I ever needed. You are quite literally the only other person in the world who understands what the last 7 years has been like, on a giant island on the other side of the world from our home and family, thank you for just being.

And lastly I would like to thank my mother, Joanne Majewski, who was patient through my teenage years, and encouraged me to actually pursue higher education, instead of just being a smart pizza maker.

Abstract

Optical sources in the mid-infrared have enabled an increasing number of applications in fields such as sensing, materials processing, and defence. While traditional mid-IR sources have often been based on nonlinear conversion in parametric oscillator devices, these systems are bulky, costly, and inefficient. In contrast, the past few decades have seen fluoride glass based mid-IR fibre lasers advance from small scale laboratory demonstration, to advanced developmental systems, and even recently commercial products. The majority of this class of lasers have been based on erbium, or to a lesser extent, holmium-doped gain media. Both systems have achieved multi-watt output power, and have been demonstrated as ultra-fast pulsed systems down to pico- and even femto-second pulse duration. However, these systems share two fundamental limitations. One, the conversion efficiency is limited to less than 50%, which has led to a distinct slowdown in output power scalability. Two, both systems are limited in bandwidth, translating to holes in the optical spectrum which can be covered by fibre lasers.

There is a third dopant element which exhibits emission in the same spectral region, but has been largely ignored: dysprosium. While the few demonstrations of dysprosium-doped mid-IR fibre lasers did not exceed performance of competing systems, there is much untapped potential remaining which is what this thesis aims to address. Specifically, two novel optical pumping schemes based on near- and mid-infrared are investigated which address the limitations of the previous dysprosium efforts, and the competing erbium and holmium-based systems. Further, the viability of progressing these systems to operation in the pulsed regime is considered. As a whole, these investigations aim to both solidify dysprosium as a viable candidate for mid-IR fibre laser emission, and deepen the collective understanding of dysprosium as an active rare earth dopant.

Contents

List of Figures

1 Introduction

A common goal in many modern industries is the pursuit of so-called *disruptive technology*; ground-breaking innovation which is claimed by many tech-sector startups. But when a technology becomes truly ubiquitous in modern society, it can be easy to overlook how disruptive it was, and how profound an impact it continues to make. The laser - *light amplification by stimulated emission of radiation* - is perhaps one of the best examples of this. Theodore Maiman demonstrated operation of the first laser in 1960 using a ruby crystal [1], and several other variants of laser quickly followed. While the significance of these achievements were certainly not overlooked by the scientific community, it is said that even proponents of continued development deemed lasers a 'solution in search of a problem'.

It would be hard to understate how successful this 'search' has been, as the global laser market is currently valued well into the billions of dollars. The variety of laser applications now is staggering, ranging from medical and scientific, to military, industrial, and even consumer arenas. Highlighting this wide diversity, conceptually identical technology is responsible not only for terawatt power used in fusion research, but scanning your groceries or even a toy on a key-chain. Despite this great success, laser research continues to be a vibrant field, continually advancing technology and providing deeper understanding of existing devices and laser physics as a whole. This is where the work presented in this thesis lies: an effort to advance fibre laser technology and contribute to the collective knowledge.

1.1 Fibre lasers

While the technological development in the field of lasers at large is impressive, the fibre laser specifically deserves special attention. Simply put, a fibre laser employs an optical fibre as the active element, in place of the crystals and gases common in other varieties of laser. This is unique in the sense that the form of the active medium - the optical fibre - is itself a major technological breakthrough. Optical fibres comprise a substantial portion of the global data communication networks that have become a critical component of modern infrastructure. In addition to maturing into a giant commercial industry, the field of fibre optics, with a key contribution from Charles Kao [2] has even generated a Nobel Prize.

The concept of a laser based on optical fibre offers several distinct advantages. A serious design concern in most lasers is the dissipation of waste heat generated by the process of converting pump power into useful laser light output. This generally dictates the total efficiency of a laser system, and can be the major limitation in continued power scaling. A fibre geometry ensures not only that the generated heat is distributed over a comparatively long active length, but that the surface area to volume ratio of the active element is in many cases orders of magnitude larger than other solid state systems. Both of these aspects contribute to efficient cooling of a fibre laser system. Additionally, fibre lasers offer literal flexibility, capable of replacing articulated mirror systems in lasers used for surgery or materials processing. Further, fibre lasers have benefited greatly from the accompanying advancement of fibre optic components such as wavelength division multiplexers (WDM's), beam combiners, and fibre Bragg gratings (FBG's), allowing for *all fibre* systems with no bulk or free space components. This reduces cost, weight, system complexity, and perhaps most importantly for the experimentalist, eliminates the need for careful optical system alignment.

While the demonstration of a laser based on active optical fibre dates back to shortly after the first demonstration of the laser itself [3], it was not until relatively recently that the fibre laser has seen wide-scale success. However, the magnitude of that success is undeniable, with the market for fibre lasers growing over the last decade by as much as 50% per year, now accounting for a sizeable portion of the total laser market [4]. Along the way have been major advancements across several key performance parameters. Perhaps most significant to the industrial and military segments is the scale up of output power from fibre laser systems. From output power of 100 W [5], to 10's [6], and even 100's [7] of kilowatts of output power, rivalling if not surpassing that of other solid state systems. Pulsed operation of fibre lasers has also seen substantial advancement, with ultrafast systems emitting pulses as short as 10's of femtoseconds [8]. The high peak power of these systems has enabled a host of new systems and applications based on nonlinear effects [9]. Finally, the range of wavelengths covered by fibre lasers is increasing, with systems emerging to directly penetrate the mid-infrared spectrum, which will be our focus here.

1.2 The mid-infrared region of the spectrum

The precise definition of the mid-infrared (mid-IR) region of the electromagnetic spectrum is unfortunately subject to some ambiguity, with author definitions ranging from 3–8 [10], 3–50 [11], and 2–20 µm [12]. From a fibre optics point of view, it is perhaps most convenient to describe the mid-IR as the spectral region beyond the common transparency window of silica glass (2.2 µm), and limited on the long wavelength side by the transmission of chalcogenide optical fibres (20 µm) [13]. However one defines the exact spectral limits, there is no debate that laser sources in the mid-IR have wide ranging applications.

1.2.1 Significance

Though specific applications are widely varied, the vast majority of applications of mid-IR light revolve around one central theme: molecular absorption. From this fundamental principle, the bulk of applications can be divided into distinct categories: to either avoid, or specifically target this absorption. For example see the atmospheric transmission data presented in figure 1.1 where we see regions of high transmission between 3–4 and 8–12 µm. Sources in these regions could be used for free space communication, or military infrared countermeasures for example. One could take the inverse approach as well by noting that

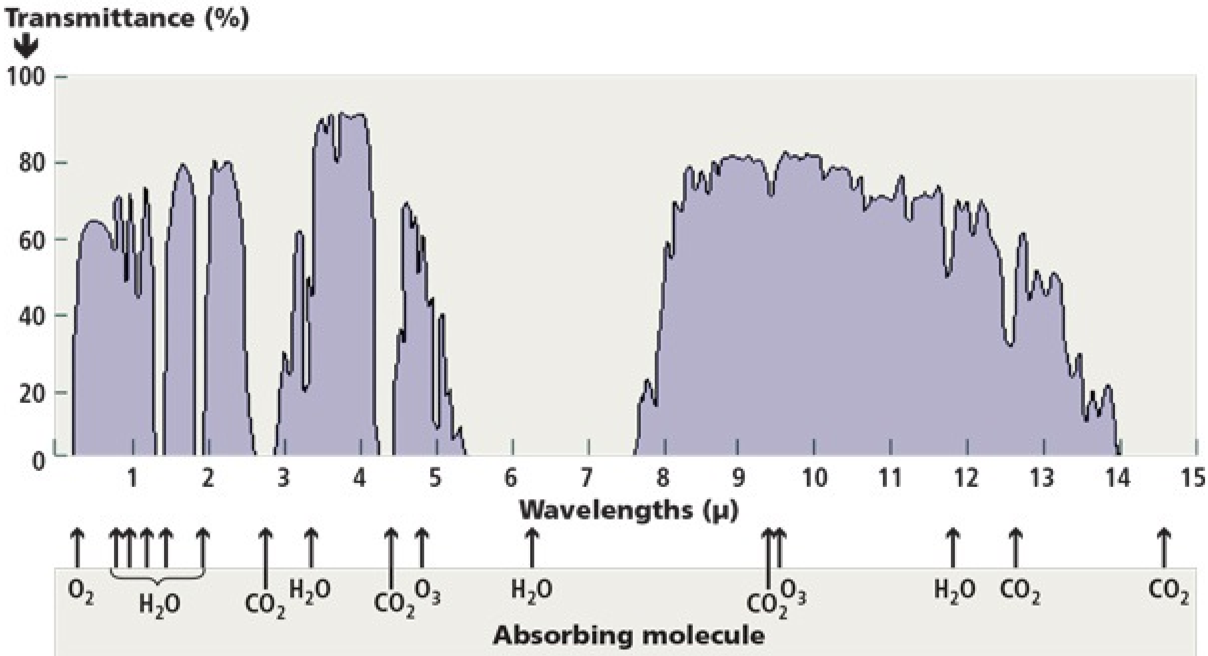

FIGURE 1.1: Atmospheric absorption with contributions from the relevant molecules indicated. Adapted from [14].

molecular absorption in this region is due to characteristic vibrational transitions which provide a so-called *molecular fingerprint*. Thus broadband or tunable optical sources over this region could provide very sensitive detection of a variety of important chemicals [15]. This has implications over a variety of fields; for example environmental monitoring of greenhouse gases such as nitrogen oxide compounds, or detection of nerve agents such as VX or Sarin for military/defence. Absorption can also be targeted with high power for more active applications, such as targeting water absorption in tissue for surgery [16], or even controlling chemical reaction processes [17].

1.2.2 Available sources of mid-IR laser emission

Perhaps the most successful mid-infrared laser source to date, at least in terms of unit volume, is the carbon dioxide, CO_2, laser emitting around 9.6 or more commonly 10.6 µm. Carbon dioxide lasers are widely employed in industrial applications such as cutting and welding, but also see use as surgical tools, as well as the basis of some laser radar systems.

It should not be surprising that there are several other variant of molecular gas based lasers emitting in the mid-IR, as some of these same vibrational transitions can be made to lase under the right pumping conditions. A closely related cousin to the carbon dioxide laser is the CO laser, emitting around 5 µm. Other examples include the HBr laser around 4 µm, the HF laser emitting around 2.9 µm, or its deuterium variant DF, emitting around 3.8 µm. Though capable of very high output power, all of these systems are generally quite bulky and rely on high energy electrical discharge pumping, often in conjunction with carefully designed gas circulation.

Another common means of generating mid-IR light is the optical parametric oscillator (OPO). This method relies on a resonant cavity around a crystal with high optical nonlinearity. When pumped with a laser of sufficient intensity, this arrangement will generate two new lower frequencies (longer wavelengths). As this process requires the phases of the relevant fields to be reasonably well matched in the nonlinear crystal, tuning of the cavity or crystal orientation leads to a continuous tuning of the output frequency. The result is a continuously tunable device which can be rather compact with proper design. However, OPO's rely on a high spatial brightness pump beam, which can present an issue in output power scaling, and given that the pump wavelength is fixed, the system efficiency naturally decreases as longer wavelength output is achieved.

A more recent addition to the family of mid-IR optical sources is the quantum cascade laser (QCL) [18]. While still in the category of semiconductor lasers, QCL's are unique in that they do not rely on electron-hole recombination to generate photons, but rather a series of quantum tunnelling events. While the physics alone of this invention is undeniably clever, it is the actual performance of these devices which is perhaps even more impressive. QCL's can be designed to cover the entire mid-IR spectrum, and have even been demonstrated out to the terahertz region [19]. Though generally limited in output power, these devices can achieve efficiency superior to that of most OPO's, reaching 50% [20].

1.3 Fibre lasers around 3µm

Though each of the systems mentioned above has benefits, due to the inherent advantages of fibre lasers previously discussed, fibres lasers emitting in the mid-IR are highly desirable. Recently, thulium fibre systems emitting around 2 µm have become more commonplace, with several vendors offering commercial systems. As discussed, by some definitions this would not be considered mid-IR, and by others, just barely. Pushing further slightly in output wavelength was a holmium-doped fibre emitting at 2.2 µm [21]. As all common fibre lasers are based on silica glass hosts, this represents a fundamental limit in the achievable emission wavelength, as multiphonon (see chapter 2) absorption dominates beyond 2 µm and silica is no longer optically transparent. To achieve a truly mid-IR laser then, will require alternative glasses.

1.3.1 Fluoride glasses for mid-IR fibres

As we have stated, silica is not a viable host for mid-IR fibres due to the limited transparency window. There are however several alternative glass compositions which exhibit transparency well into the mid-IR as shown in figure 1.2. In terms purely of transmission

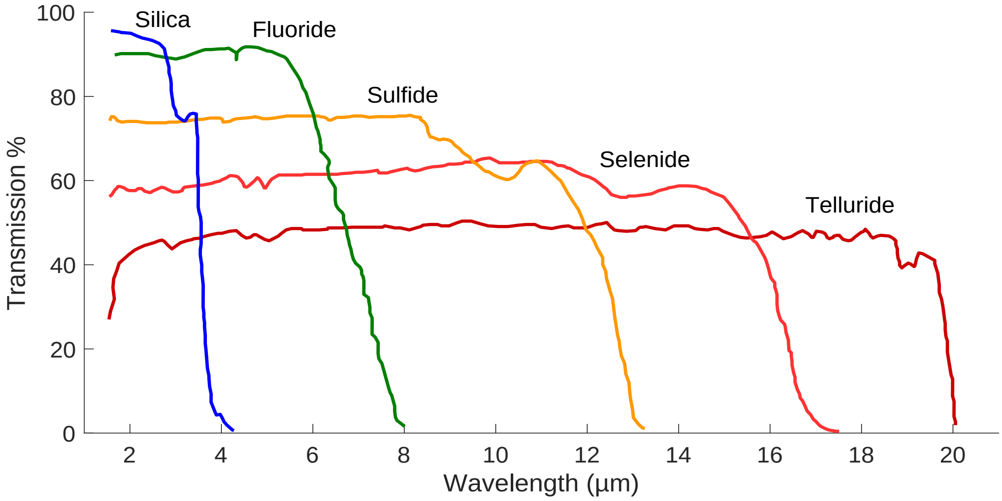

Figure 1.2: Transmission of several glasses drawn for optical fibres. Adapted from [13].

window broadness, it would appear that the *chalcogenide* (sulfide, selenide, and telluride) glasses are ideal candidates for mid-IR fibre lasers. In practice however, this has to date been proven to not be the case. While emission from several rare earth doped chalcogenide glasses has been demonstrated [22, 23], currently there has only been one successful demonstration of a rare earth doped chalcogenide fibre laser, based on Nd^{3+} and emitting around 1 µm [24]. There have been a variety of reasons proposed to explain this, many of which revolving around glass processing techniques [25]. There is much continued work aimed at addressing these issues, and the progress made indicates there may still be potential for successful realization of rare earth doped chalcogenide mid-IR fibre lasers [26]. Despite the challenges of achieving direct laser oscillation in doped chalcogenide fibre, there have been several successful examples of mid-IR sources which exploit the relatively large optical non-linearity of chalcogenide fibre. For example, Raman fibre lasers have been demonstrated beyond 3 µm [27], and supercontinuum generation in tapered chalcogenide fibre is capable of covering wide ranges of the mid-IR spectrum [28].

For effective realization of mid-IR fibre lasers, we are then left to focus our attention on the family of fluoride based glasses, specifically those based on AlF_3, InF_3, and ZrF_4. All three glasses are capable of being drawn into optical fibres, and though suppliers are small in number, fluoride fibre is commercially available. The optical attenuation of the various fluoride fibres is shown in figure 1.3. We see that beyond 3.5 µm InF_3 (or *fluoroindate*) glass possesses the lowest attenuation, which has generated some recent investigation into its viability as a laser host [30, 31]. While AlF_3 glass exhibits larger attenuation across most of the spectrum, its possesses a higher glass transition temperature T_g, translating to a increased damage threshold, and allowing AlF_3 glass to see some utility as a high power delivery fibre [32]. It is however the zirconium based glasses, ZrF_4, which exhibit the lowest attenuation over most of the spectrum, and have allowed for many successful demonstrations of rare earth doped fibre laser, making ZrF_4-based glass the focus of our present work.

Glass based on zirconium fluoride was first discovered in 1975 by Poulain and Lucas

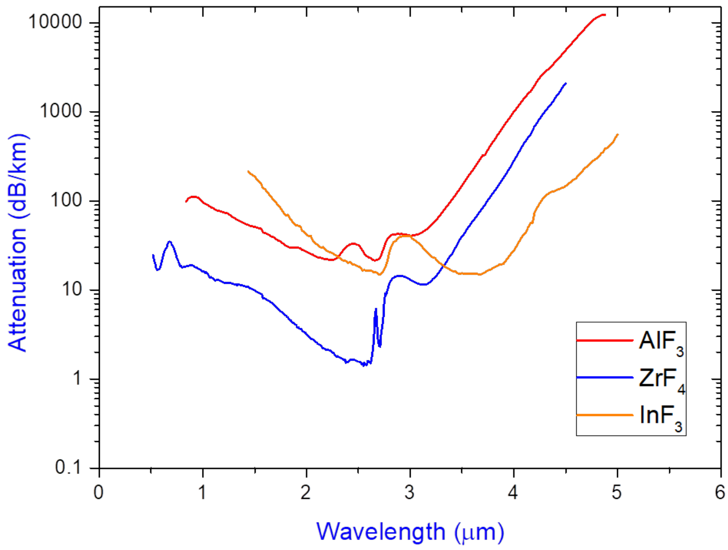

FIGURE 1.3: Attenuation of fluoride optical fibres. Adapted from [29].

accidentally as they were attempting to fabricate doped crystals of the ZrF_4-BaF_2-NaF system [33, 34]. Though these initial glasses were not highly stable, within a relatively short time frame it was discovered that the addition of LaF_3 [35], and subsequently, AlF_3 [36] resulted in significant stability increase. Finally, the addition of NaF reduced crystallization tendency [37], producing the most successful fluoride glass for laser applications: ZrF_4-BaF_2-LaF_3-AlF_3-NaF, or as it is most commonly known - ZBLAN. Of particular note for laser development utilizing ZBLAN is that it already contains a lanthanide compound, meaning that substitution in part with other rare earth compounds will not substantially alter the glass composition, thus doping with active rare earth ions can be readily achieved.

All loss mechanisms in a glass can be grouped as either intrinsic, or extrinsic in nature. Intrinsic losses in ZBLAN over the mid-IR spectral region are defined only by scattering losses, and multiphonon absorption (see chapter 2) which is responsible for the steady increase in attenuation across all fluoride compounds beyond 4 µm seen in figure 1.3. While intrinsic scattering loss for ZBLAN is actually less than silica [38], the drawing process allows for non-negligible formation of scattering crystal sites, which interestingly have been shown to be dramatically reduced by drawing in a zero gravity environment [39].

For many lasers based on ZBLAN glass, it has been rather the extrinsic loss that is the dominant mechanism, specifically the loss due to absorption by impurities in the glass. As the bulk of mid-IR fibre lasers emit in the 3 micron region, arguably the most significant impurity is the hydroxyl ion (OH^{-1}) as it has an absorption peak around 2.9 µm and can be introduced into the glass even under strict environmental control. Referring back to the attenuation data in figure 1.3 we can indeed see a local maxima around 2.9 µm for all fluoride compounds that can be attributed to hydroxyl impurity.

1.3.2 State of the field: successes and challenges

Identifying a suitable glass host is obviously a necessary step in mid-IR fibre laser development, but we must also identify appropriate rare earth dopants. There are three ions for which mid-IR laser emission from a ZBLAN fibre have been demonstrated, holmium, erbium, and as we will focus on in this work, dysprosium. Partial energy level diagrams indicating possible pump absorptions and relevant radiative transitions are shown for each ion in figures 1.4, 1.5, and 1.6. The longest wavelength yet generated from a ZBLAN fibre laser

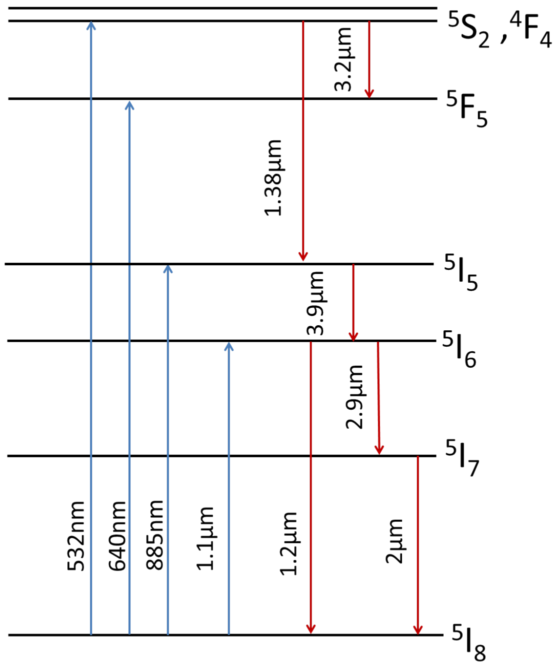

Figure 1.4: Energy level diagram of Ho^{3+} in ZBLAN; blue arrows indicate pump absorption, red arrows indicate radiative transitions.

was based on the Ho^{3+} transition $^5I_5 \rightarrow {}^5I_6$ emitting at 3.9 µm [40], though this required both cascade lasing and cryogenic cooling of the fibre. Somewhat shorter in wavelength, the $^4F_{9/2} \rightarrow {}^4I_{9/2}$ transition of Er^{3+} has been demonstrated at room temperature with emission at 3.45 µm [41] and has been shown to be broadly tunable over a range of 450 nm to a maximum of 3.78 µm [42].

Aside from these examples, the remainder of the work concerning mid-IR ZBLAN fibre lasers has focused on emission around three microns, with the vast majority of efforts directed at either Er^{3+} or Ho^{3+}. The three micron transition of both ions is interesting in that they are *self-terminating* i.e. the lower laser level has a longer lifetime than the upper level (see chapter 3) and therefore should not exhibit continuous wave (CW) laser action. Excited state absorption of pump radiation was offered as an explanation in the initial demonstration of laser emission from both ions [43, 44], though the output power was minimal in each instance. Since then however, the CW output power of 3 µm ZBLAN fibre lasers has improved markedly as seen in figure 1.7. Holmium based sources have benefited from co-doping with Pr^{3+}, which depopulates the lower laser level and has led to multi-watt output

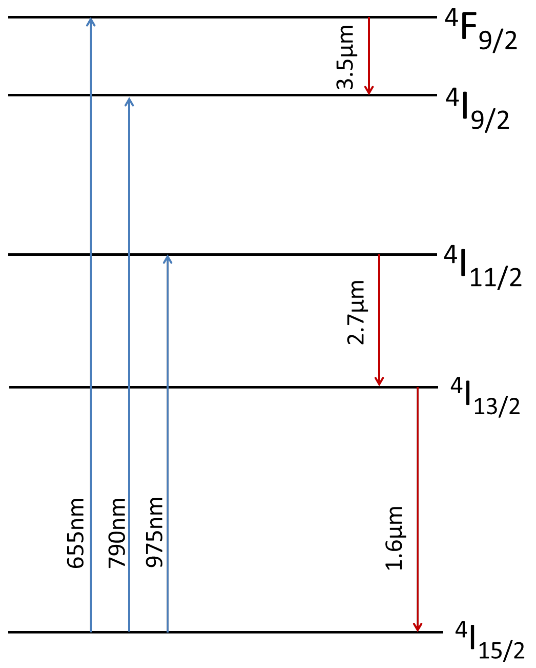

FIGURE 1.5: Energy level diagram of Er^{3+} in ZBLAN; blue arrows indicate pump absorption, red arrows indicate radiative transitions.

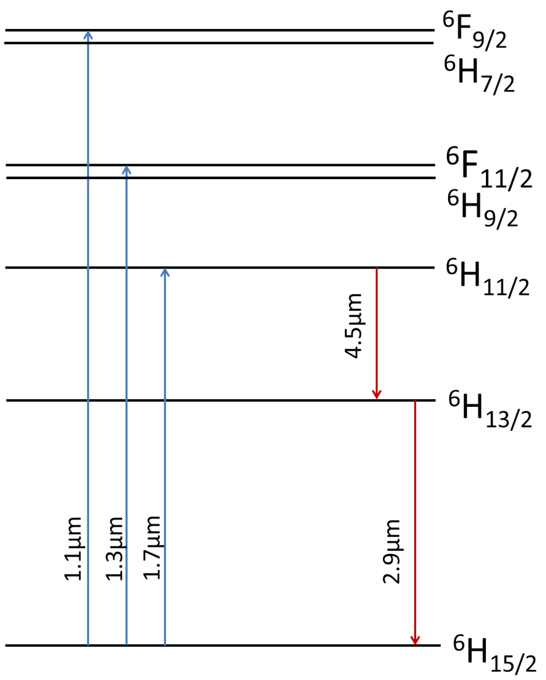

FIGURE 1.6: Energy level diagram of Dy^{3+} in ZBLAN; blue arrows indicate pump absorption, red arrows indicate radiative transitions.

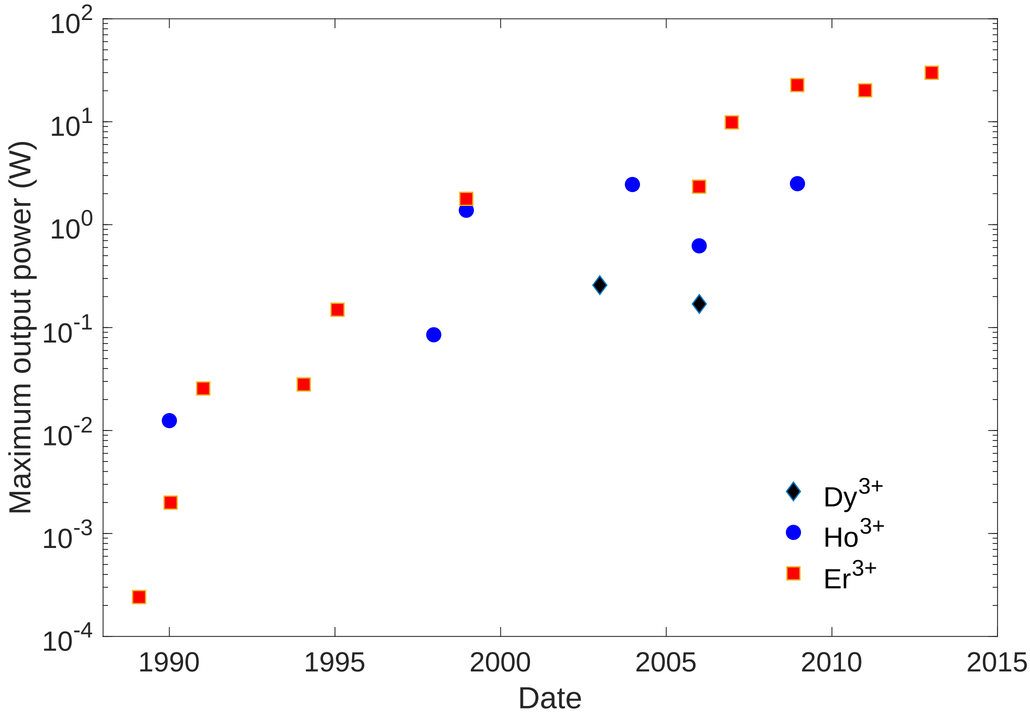

Figure 1.7: Historical progress of CW output power around 3 µm from a ZBLAN fibre laser.

[45]. Erbium sources have seen even more impressive increase in output power, utilizing very high doping levels, allowing for up-conversion energy transfer between erbium ions to depopulate the lower laser level, reaching a recent record of 30 W CW output [46]. However, one may notice on inspection of figure 1.7, that the output power appears to be approaching a scalability limit. A contributing factor is that both types of system rely on near-infrared optical pumping, which sets the *Stokes limit* (energy difference between pump and laser photons) to well below 50%. The excess energy is majority converted to waste heat, and with a comparatively (to silica) low T_g, ZBLAN can be particularly vulnerable to thermal damage. While this has been mitigated somewhat recently by a cascade lasing scheme in erbium, efficiency still does not exceed 50% [47] and fibre thermal load remains an issue in continued output power scaling.

Pulsed operation of 3 micron class fibre lasers has also seen substantial improvement in recent years, particularly in the ultrafast regime [48]. Erbium has been demonstrated as a mode-locked system emitting pulses as short as 207 fs [49]. However, the emission spectrum of Er^{3+} overlaps with the absorption lines of water vapour, which was suggested to have a negative impact on the lower limit of achievable pulse duration. Supporting this belief was the recent demonstration of a Ho^{3+} mode-locked system with emission somewhat removed from the water vapour absorption, and further reduced pulse duration of 180 fs [50].

1.4 Dysprosium and thesis progression

In the general progress of three micron class fibre lasers, dysprosium has largely been neglected, with experimental demonstrations representing only two data points in figure 1.7, both of which falling well short of the other systems in terms of output [51, 52]. While there are some legitimate scientific and technological reasons for this apparent lack of interest which we will discuss in later chapters, dysprosium also offers distinct potential which has not been fully explored. For example, there are two pumping schemes for three micron emission from dysprosium which have yet to be investigated, at 1.7 and 2.8 µm, both of which represent a Stokes limit efficiency substantially higher than either erbium or holmium based systems. Second, the three micron transition of dysprosium exhibits larger bandwidth than the other two systems, offering the potential for emission at wavelengths previously inaccessible directly by fibre lasers. While a main aim of this thesis is the successful experimental demonstration of various dysprosium fibre laser systems, an increase in the collective knowledge of mid-IR emitting rare earths should be achieved regardless of the particular experimental outcomes.

From these introductory considerations of mid-IR ZBLAN fibre lasers, we will move on in chapter 2 to a theoretical treatment of rare earths in general, with particular discussion of the optical properties of the dysprosium ion following. Theoretical content is continued in chapter 3, where several important concepts general to fibre optics will be introduced. Further, basic laser theory will be covered, both in generality and specifically in context of optical fibres. The theoretical aspects introduced in these two chapters should provide the foundation from which to understand the goals of the experimental work presented in subsequent chapters, and is required for the analysis of the results generated. Chapter 4 investigates a resonant, or *inband* pumping scheme aimed at achieving high optical conversion efficiency. Chapter 5 is devoted to the development of a 1700 nm pump source which is then implemented experimentally in a dysprosium fibre system in chapter 6.

2

Dysprosium and the rare earth dopants

While chapter 1 provides an overview of fibre lasers in general, and specifically the field of mid-IR fibre lasers, this chapter will present a more detailed discussion of the properties of mid-IR active ions. The concepts in section 2.1 form a theoretical framework applicable to the optical properties of all rare-earths, where in section 2.2 this will be applied more specifically to dysprosium. Further, the 3 micron transition of dysprosium is considered in detail, with a view towards the new experimental work to be presented in the following chapters.

2.1 Optical properties of rare earth ions

Of the many variants of laser device that have been studied or found commercially viable application, those based on solid state gain media (in which fibre lasers are included) have been perhaps the most successful. Solid state lasers are most often crystals or glasses which have been doped with rare earth ions, almost exclusively of the trivalent form $[\mathrm{RE}]^{3+}$ of a lanthanide element (figure 2.1). As an aside, despite the term *rare earth*, dysprosium is not particularly rare and in fact the current market price is 350 USD/kg [54]; mass-wise, this is orders of magnitude more dysprosium than in all of the fibre used in this thesis.

What follows is intended to be somewhat general in nature, as the study of rare earths and their optical properties is a rich field with literature too numerous to cite in totality here. However, should the reader be inclined, more detailed discussion of rare earth and solid state lasers can be found for example in [55] and [56]. More specifically, we will loosely follow the treatment of [57].

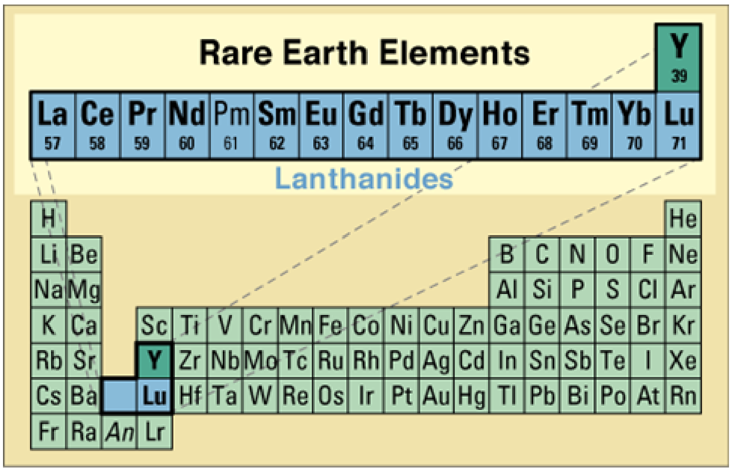

FIGURE 2.1: Periodic table of the elements showing the lanthanide series of rare earths. Image adapted from [53].

2.1.1 Electronic structure and transitions

The electronic configuration of elements in the lanthanide series are characterized by the increasing occupation of the $4f$ electron shell. It is transitions between these $4f$ states which are responsible for the observed optical spectra of trivalent rare earth ions [58]. An important effect in the optical properties of these lanthanides is the so-called *lanthanide contraction* [59], which describes a reduction in the spatial extent of the $4f$ wave functions with increasing atomic number. This in turn means that transitions of the $4f$ states are effectively shielded from external environmental effects. This results in some very beneficial effects: a relative insensitivity to host, and a weak effect of phonon-assisted transitions, resulting in sharp emission lines of high radiative efficiency, in contrast to emission from transition metals.

The electronic structure of these transitions can be described by considering the total Hamiltonian of an ion in a host

$$H = H_{free\,ion} + V_{ion\,host} \tag{2.1}$$

where $H_{free\,ion}$ is the Hamiltonian of the ion in isolation and $V_{ion\,host}$ accounts for interactions of the ion with the host. Though we have just stated that the latter term is relatively weak due to the lanthanide contraction, it is not negligible. The interaction of the ion with the electric field of the host, results in Stark splitting of individual energy levels, giving rise to energy levels comprised of closely spaced sub-levels. Due to the small energy separation, in practice these are generally treated as manifolds in thermal equilibrium.

2.1.2 Radiative transitions

Beyond understanding the electronic structure of a rare earth ion, we are also interested in further defining the interaction of light with the ion. While we would need to rely on Einstein himself for a full description [60], we can simplify the picture by employing the concepts of the aforenamed A and B coefficients.

Consider first the process of absorption of light by a rare earth ion. If electromagnetic radiation (photons) of density Φ, is incident on a system of rare earth ions in the ground state, represented by population density N_1, it will be absorbed provided the frequency of the radiation ν matches a specific transition energy gap $h\nu$, where h is Planck's constant, thus exciting the ion to a higher energy state with population density N_2. The rate at which this process occurs can be described as

$$\frac{dN_1}{dt} = -B_{1,2}\Phi N_1 \tag{2.2}$$

where B is the Einstein coefficient for stimulated transition. Once excited to the higher energy state, the ion will spontaneously decay back to the ground state via the emission of a photon with energy equal to the gap of the two states. The rate of this process is similarly described but with the Einstein $A_{2,1}$ coefficient.

$$\frac{dN_2}{dt} = -A_{2,1}N_2 \tag{2.3}$$

For a large number of ions, as is always the case in real laser systems, this spontaneous process can be described statistically by an exponential decay of the excited state population with a characteristic lifetime of

$$\tau_{2,1} = A_{2,1}^{-1} \tag{2.4}$$

While this lifetime can in principle be measured empirically, via a fluorescence measurement for example, as we will see in section 2.1.3 other factors bear consideration. Further, in a real system, there may be and often are many intermediate energy states between the ground state and excited state. Spontaneous emission to these intermediate states may also occur, so that the total decay rate of the upper state is the summation of rates to all other possible states.

$$\frac{1}{\tau_{2,1,total}} = \sum_i A_{2,i} \tag{2.5}$$

With the more realistic lifetime from (2.5) we can then define an important quantity: branching ratio β

$$\beta_{2,i} = \frac{A_{2,1}}{\sum_i A_{2,i}} = A_{2,1}\tau_{2,1,total} \tag{2.6}$$

The branching ratio defines the fraction of total decays that occur through a particular intermediate energy level and can have a significant impact on laser performance.

So far, we have the stimulated transition from ground to excited state, and the spontaneous transition from the excited state back down. We also require to know the rate of stimulated transitions from the excited state, which is described simply as the reverse of (2.2), as this is the basis of coherent laser emission. A more complete derivation can be found in [56], but we can summarize the result that considering thermal equilibrium and the blackbody radiation law, we can relate the rate of spontaneous to stimulated emission as

$$\frac{A_{2,1}}{B_{2,1}} = \frac{8\pi\nu^3 h}{c^3} \tag{2.7}$$

At this point it is also convenient to introduce the concept of cross section. Measurements of light interaction with rare earths in practice are more often conveniently described by an absorption coefficient

$$I_{out} = I_{in} e^{-\alpha L} \tag{2.8}$$

or gain (amplification) coefficient

$$I_{out} = I_{in} e^{gL} \tag{2.9}$$

where optical intensities I and interaction length L are easily measurable. We then desire a quantity directly relating g or α to the density of rare earth ions in a ground or excited state $N_{1,2}$, which we can define as the absorption and emission cross sections.

$$\sigma_a = \frac{\alpha}{N_1} \tag{2.10}$$

$$\sigma_e = \frac{g}{N_2} \tag{2.11}$$

The cross sections can in turn be related to the Einstein coefficients.

$$\sigma_e(\nu) = \frac{A_{2,1}\lambda^2}{8\pi n^2}\psi(\nu) \tag{2.12}$$

$$\sigma_a(\nu) = \frac{B_{1,2}h\nu}{c}\psi(\nu) \tag{2.13}$$

where n is the index of refraction of the medium (host) and $\psi(\nu)$ is a lineshape function which will depend on the particular transition.

Though the above gives us the requisite theory, we are now left with the need to actually quantify these transition rates. From quantum mechanical principles, in theory one could calculate the strength and lineshape of all the relevant transitions if the exact nature of the level splitting is known. However, not only is this well out of the scope of this thesis, but would prove to be a nearly intractable problem in most circumstances. Fortunately, a semi-empirical technique was developed independently by both Judd [61] and Ofelt [62]. Judd-Ofelt analysis has since become fundamental in the study of rare earth optical properties. For a complete derivation the interested reader can refer to the original work or more recent treatments that focus on application [63, 64]. In brief summary, three empirical intensity parameters are used to fit the integrated absorption from a measured spectrum. These parameters are then used to calculate the radiative transition strength for any transition.

While Judd-Ofelt analysis is a very useful tool, for laser development purposes we are concerned with numerical quantities for the relevant transition cross sections. As Judd-Ofelt deals with integrated strengths, we must use additional means to extract both cross sections. Generally absorption cross section can be obtained from measurement as ion concentration is known with reasonable accuracy. Extraction of the intensity parameters from measured spectrum then allows calculation of the emission cross section at the fluorescence peak with the Füchtbauer-Ladenburg equation [65].

$$\sigma_e(\bar{\lambda}) = \frac{\bar{\lambda}^4}{8\pi c n^2 \tau_{rad}} \frac{I(\lambda)}{\int I(\lambda) d\Lambda} \tag{2.14}$$

In practice if one can measure a fluorescence spectrum, it can then be scaled by calculation of (2.14) to produce quantitative emission cross sections across the band.

A simpler way to relate the two cross sections is the McCumber relation [66]

$$\sigma_e(\nu) = \sigma_a(\nu) \exp\left(\frac{E_0 - h\nu}{k_B T}\right) \tag{2.15}$$

where k_B is Boltzmann's constant, T is temperature, and E_0 is the energy difference between the two levels. To calculate absolute values with this relation, the parameter E_0 must be accurately known (noting also it has temperature dependence), which can be done if the energies of individual Stark levels are known. Alternatively, this parameter can be reasonably well estimated with an equidistant energy assumption [67]. While there has been some disagreement on the limitations of this relation as it applies to rare earths in amorphous (glass) hosts [68], as is the case in most fibre lasers, it can be shown to still have useful validity in glass hosts with careful accounting of experimental errors [69].

2.1.3 Non-radiative transitions and other processes

In addition to the radiative transitions for absorption and emission described above, transitions that result from interaction of the ion with vibrations of the host (phonons) also often play an important role. While the energy separation between the ground and first excited state is often many times the highest energy phonon of the host, an excited ion can undergo multiphonon relaxation to the ground state [70].

The rate of decay between any two levels through multiphonon relaxation is a function exponentially dependant on the separation energy by

$$W_{nr} = C\left[n(T) + 1\right]^p \exp(-\alpha \Delta E) \tag{2.16}$$

where p is the number of phonons required to bridge the energy gap of ΔE, and C and α are host-dependant parameters. The term $n(T)$ defines the number of phonons as a function of temperature, following Bose-Einstein statistics.

$$n(T) = \frac{1}{\exp(h\nu/k_B T) - 1} \tag{2.17}$$

In both (2.16) and (2.17), the host dependent terms (including $h\nu$ or *phonon energy*) are empirically independent of rare earth, with the notable exception of dysprosium as we will see in section 2.2. The phonon energy of silicate glass is 1100 cm^{-1}, as compared to 500 cm^{-1} in ZBLAN [71], indicating that lower lying levels will be more effectively quenched by multiphonon relaxation in silicate glass. The inverse process of multiphonon absorption is significant at higher energies (shorter wavelengths) in silica as well, defining a transparency window that does not extend into the mid-IR. Though determining all of the relevant parameters to determine the non-radiative decay rate may see a daunting task, when we consider that this effect reduces the observed lifetime τ of the level as compared to that calculated by Judd-Ofelt analysis τ_r, the definition of nonradiative rate W_{nr} reduces to the simple form

$$W_{nr} = \frac{1}{\tau} - \frac{1}{\tau_r} \tag{2.18}$$

Though we expect that the transitional effects outlined above are sufficient for the description of the Dy^{3+} systems presented in this thesis, for completeness we briefly mention a few other process of significance in various rare earth laser systems.

Cross-relaxation occurs when an excited ion transfers a portion of its energy to a neighbouring ion, leaving both in an intermediate excitation level. This can be detrimental if for example the intermediate level is non-radiatively coupled to the ground state, as this presents a mechanism of quenching the excitation. In 2 µm Tm^{3+} doped fibre lasers for example cross relaxation can be a significant effect [72].

Cooperative up-conversion is the process by which an excited ion donates its energy to another excited ion, de-exciting the donor, and exciting the acceptor to a higher level. In some cases this is an inefficiency mechanism, while in others it is exploited to design lasers which emit at wavelengths shorter than the pump, which would impossible without this effect [73].

Energy transfer is a more general term for the exchange of energy between ions, but it is perhaps mostly identified with the exchange of energy between two dissimilar ions in a co-doping situation. This can be used to effect efficient pump absorption by an ion species which does not strongly absorb. In this instance a co-dopant is chosen which does exhibit pump absorption while also having an excited state energy closely matched to an excited state of the acceptor dopant ion. The result is effective pump absorption by the acceptor, and is a common strategy in the design of diode pumped Er^{3+}/Yb^{3+} fibre lasers. Energy transfer between co-dopants is also used to de-populate the lower level of a transition, eliminating what would otherwise be a population bottleneck prohibiting sustained population inversion (inversion is covered in chapter 3), as is the case in Ho^{3+}/Pr^{3+} fibre lasers [74].

Finally, while it is not an energy transfer process, we must also mention the effect of excited state absorption (ESA). This is the situation when an excited ion absorbs an additional photon(s), and is excited to a higher lying energy level. Often this results in radiative emission from the higher energy level back to the ground state, which is effectively a loss mechanism in terms of laser performance. In the Er^{3+} doped ZBLAN systems which currently lead the field of 3 µm fibre lasers, ESA is a well known effect [75], and as we will see, may play an important role some Dy^{3+} based systems.

2.2 Dysprosium as laser active ion

Having covered the theory required to understand electronic transitions in rare earth doped material, we now look at how these concepts apply to dysprosium specifically. While the study of the spectra of trivalent rare earths and their respective transition dynamics in glass hosts have been well studied [58, 76, 77], Dy^{3+} in particular, while not strictly excluded from these works, has received comparatively much less attention. Erbium and neodymium on the other hand, have been extensively studied, including specifically in a fibre geometry [78] owing in part to their applications in telecommunication. As a result, current work on the development of Dy^{3+}-doped sources, and specifically fluoride glass (ZBLAN) based sources, relies heavily on relatively few spectroscopic studies of electronic structure and transition dynamics [79, 80].

2.2.1 Sources based on dysprosium doping

Inspection of the energy level diagram in figure 2.2 provides some insight on the historical lack of interest. We see that all of the lower lying levels, up to the $^4F_{9/2}$ level, are separated

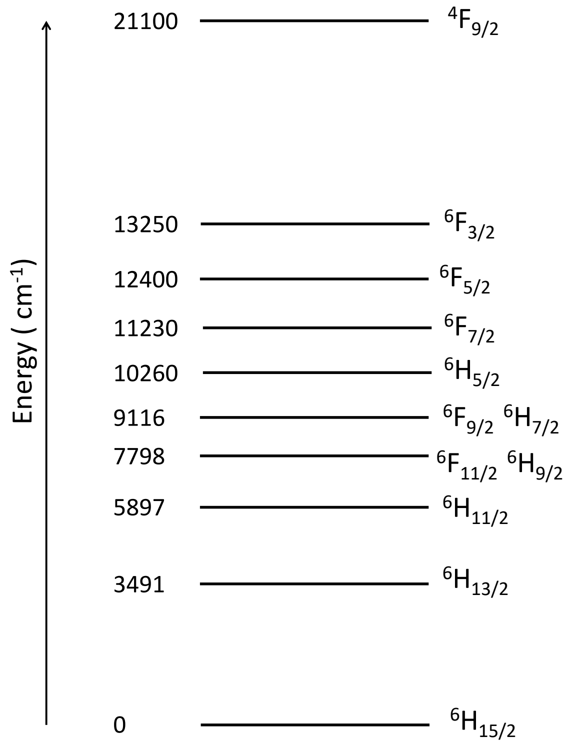

Figure 2.2: Energy level diagram of Dy^{3+} in ZLBA glass.

by less than 3500 cm^{-1}, and in most cases much less. Recalling the discussion of multiphonon relaxation in section 2.1.3 emission from all of these levels will be strongly quenched in silica glass. Further, though from Judd-Ofelt analysis we know that strong emission from the $^4F_{9/2}$ level is possible, to effectively pump those levels would require high brightness sources in the blue end of the visible spectrum or even shorter in the UV, which even today remains a technical challenge. However, there is some traction in this area, motivating further study of the emission properties of Dy^{3+}-doped ZBLAN [81]. In particular, the recent emergence of gallium nitride laser diodes (GaN) allowed for demonstration of an efficient yellow dysprosium laser [82].

The remaining work focused on emission from Dy^{3+}-doped sources has focused rather on the lower lying energy levels, requiring by definition low phonon energy host crystals or glasses. In particular, emission from the $^6H_{11/2} \rightarrow {^6H_{13/2}}$ transition around 4.3 µm has been demonstrated in YLF [83]. Further increase in efficiency of this transition has also been demonstrated in a $PbGa_2S_4$ host pumped by both an Er:YLF source [84], and perhaps more impressively by a commercial diode laser at at 1.7 µm [85].

Emission from this transition falls beyond the effective transmission window of ZBLAN, preventing the development of 4 µm ZBLAN fibre lasers. However, both InF_3 and chalcogenide glass based fibres are potentially viable alternatives. Demonstration of lasing action of Dy^{3+} in either glass host has to date proven elusive, with work largely limited to spectroscopic study and numerical model [30, 86, 87].

2.2.2 The $^6H_{13/2} \rightarrow {}^6H_{15/2}$ transition at 3µm

Aside from the transitions mentioned above, historically the $^6H_{13/2} \rightarrow {}^6H_{15/2}$ transition emitting around 3 µm has received the most attention. Laser emission from this transition was first demonstrated in a BaY_2F_8 crystal in 1973 [88]. While certainly ground-breaking, this demonstration relied on inefficient flash-lamp pumping, and required liquid nitrogen cooling of the active crystal. Room temperature operation of a LaF_3 based system was made possible by pumping directly with a neodymium laser source [89]. More recently, laser emission at an impressive wavelength of 3.4 µm was demonstrated from a highly doped $BaYb_2F_8$ crystal [90].

Our true aim here however, is fibre-based dysprosium laser sources, and for this we need to turn to Dy^{3+}:ZBLAN. The emission spectrum of Dy^{3+}:ZBLAN is presented in figure 2.3, showing the transition as quite broad, and centred near 2.9 µm.

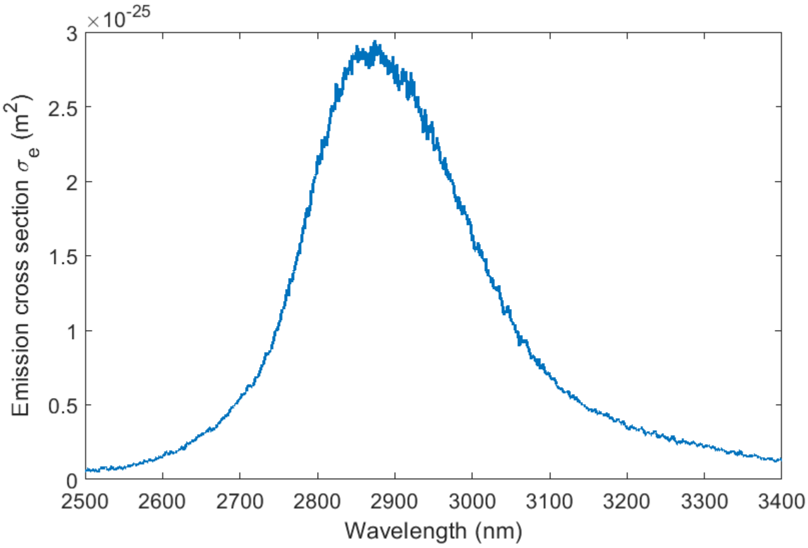

FIGURE 2.3: Emission cross section of Dy^{3+} in ZLBAN glass.

For efficient pumping, we desire an absorption level which is strongly non-radiatively coupled to the $^6H_{13/2}$ upper laser level. As noted in section 1.3.1, the multiphonon absorption edge for ZBLAN is nominally 4 µm, translating to an energy separation of 2500 cm^{-1}. From the energy level diagram (figure 2.2) all the levels above $^6H_{13/2}$ are separated by less than this amount, indicating strong multiphonon relaxation. Thus every low-lying level up to $^6F_{3/2}$ absorbing around 754 nm could make for a suitable pump transition. While there are high-power diode lasers which would overlap quite well with some of these lower lying levels, it is important to note that the laser transition terminates on the ground state, meaning that re-absorption of laser emission is largely unavoidable. Effective diode pumping of a ground state terminated transition often requires an additional energy transfer process to increase effective absorption, for example co-doping such as in Er/Yb lasers at 1550 nm, or cross relaxation in Tm doped lasers emitting at 2 µm.

In addition to these considerations, we also note that targeting short pump wavelengths represents a large quantum defect. For all of these reasons, efforts at development of dysprosium ZBLAN fibre lasers have been restricted to targeting pump absorption at 1 µm and beyond. Figure 2.4 shows the absorption spectrum of Dy^{3+}:ZBLAN from 1 µm to the

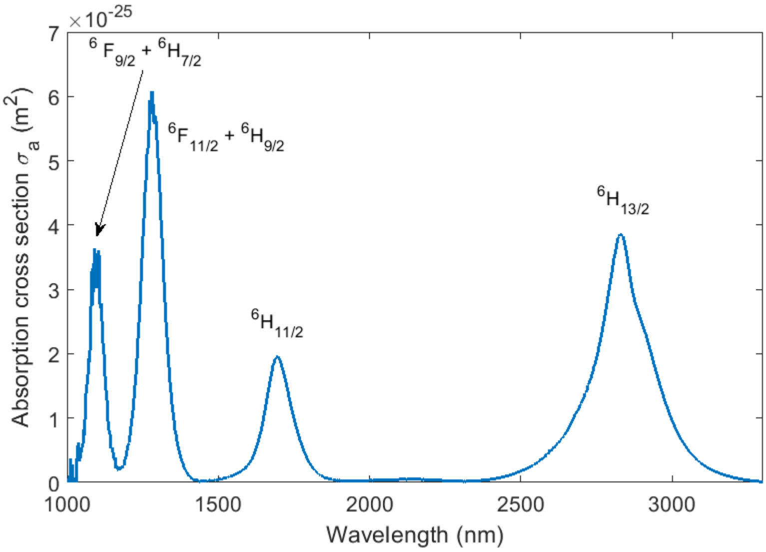

Figure 2.4: Absorption spectrum of Dy^{3+} in ZLBAN glass; transitions responsible for each peak are indicated.

intrinsic absorption of the $^6H_{13/2} \rightarrow {}^6H_{15/2}$ transition itself. In terms of pump wavelength there are four possibilities in this range: 1.1, 1.3, 1.7 and 2.8 µm.

The first demonstration of a Dy^{3+}:ZBLAN fibre laser employed a Yb^{3+} fibre laser as a pump source targeting the thermally coupled $^6F_{9/2}$ and $^6H_{7/2}$ levels [51]. This laser exhibited a fairly low slope efficiency with respect to absorbed pump power of 4.5%. A yellow fluorescence was observed in this work under strong pumping conditions, indicating pump excited state absorption (ESA), which can at least in part explain the low overall efficiency. The ESA process for this particular case is shown graphically by the energy levels in figure 2.5. Here population in the upper laser level allows absorption of a pump photon, exciting the ion to $^6F_{5/2}$. An additional absorption event from this level leads to excitation to the $^4F_{9/2}$ level, which is strongly coupled radiatively to the upper laser level $^6H_{13/2}$ by an emission of *yellow* photons around 570 nm. Subsequent work with the same pumping scheme sought to reduce the potential influence of ESA by altering the output coupler reflectivity (see chapter 3 for laser basics) [91]. The aim was to reduce population in the upper laser level by increasing intra-cavity flux, which resulted in a reported efficiency increase to 23%.

A reduction in fundamental quantum defect was achieved by targeting absorption further in the infrared at 1.3 µm by employing a Nd:YAG laser [52] as the pump source. Pumping at this wavelength is also thought to reduce the impact of ESA as excitation to the radiatively coupled upper levels is not possible. However, inspection of the energy levels in figure 2.2 indicates excitation from the upper laser level to $^6F_{7/2}$ is possible. While this level is strongly

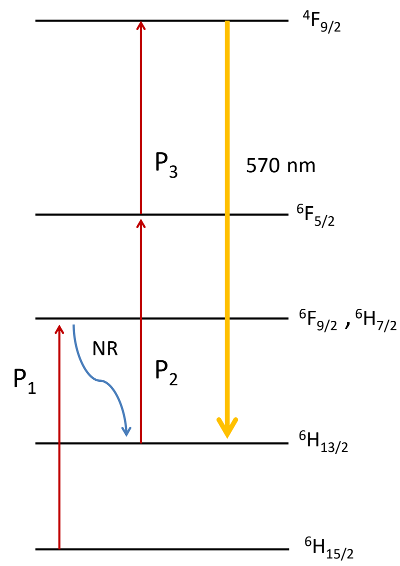

FIGURE 2.5: Excited state absorption process under strong pumping by 1.1 µm. Pump absorption non-radiatively decays to the upper laser level, where two subsequent absorption events excite the ion to the long lived $^4F_{9/2}$ level which then radiatively emits around 570 nm back to $^6H_{13/2}$.

coupled back to the upper laser level via multiphonon relaxation, this still represents a reduction in overall efficiency as pump power is in fraction lost to phonons. This may help explain why the reported efficiency for this work was still less than half of the inherent Stokes limit.

Before moving on, there is an important point of discussion in regards to the multiphonon relaxation rates of dysprosium energy levels. Following the concepts introduced in section 2.1, we know that the radiative lifetime τ_r of the $^6H_{13/2}$ upper laser level (or indeed any level) can be calculated via Judd-Ofelt analysis. This has been done for both ZBLA, and ZBLAN glass and the calculations produce a value for τ of 51.2 ms and 46.8 ms respectively [79, 80]. With the measured lifetime of 640 µs we can calculate via (2.18) a non-radiative rate W_{nr} of 1563 s^{-1}. The same procedure is applied to the $^6H_{11/2}$ level, yielding 1.25 µs and 8×10^5 for τ and W_{nr} respectively. The lifetimes and non-radiative decay rates W_{nr} for all the low-lying levels are summarized in table 2.1; as expected all but the upper laser level are strongly quenched by multiphonon relaxation.

These values for W_{nr} are well represented by the "energy gap law" (2.16), and allow calculation of the non-radiative rate of any energy level. The parameters in the energy gap relation are considered as only host-dependent, defining that non-radiative rates of any rare earth are a function only of the separation in energy of the levels involved. Measurements across various other rare earths have shown this assumption to hold quite well [92–94]. Non-radiative rates for dysprosium however, are an order of magnitude larger, which has yet to be comprehensively explained.

Energy transfer to OH^{-1} may have been a possibility, as this has been attributed to an observed reduction in $^6H_{13/2}$ lifetime with ion concentration [80]. However the calculated energy transfer rate indicated by the reduction in lifetime was deemed negligible as compared to multiphonon relaxation. Quimby has shown this phenomenon to not be specific to host,

Level (position)	Total lifetime τ (%)	Non-radiative decay rate (s^{-1})
$^6F_{3/2}$ (13250 cm^{-1})	0.3 ns	6.6×10^6
$^6F_{5/2}$ (12400 cm^{-1})	9 ns	6.6×10^6
$^6F_{7/2}$ (11300 cm^{-1})	152 ns	6.6×10^6
$^6H_{7/2}$, $^6F_{9/2}$ (9116 cm^{-1})	6 ns	1.7×10^8
$^6H_{9/2}$, $^6F_{11/2}$ (7798 cm^{-1})	100 ns	1×10^7
$^6H_{11/2}$ (5897 cm^{-1})	1.25 µs	8×10^5
$^6H_{13/2}$ (3491 cm^{-1})	641 µs	1539

Table 2.1: Lifetimes and non-radiative decay rates (W_{nr}) for the low-lying levels of Dy^{3+} in ZBLAN. Data from Ref [80].

and alternatively proposes an increased electron-phonon coupling strength due to ad-mixing of electronic levels as a possible explanation [92].

2.3 Summary and further research

The foundational rare earth concepts presented in this chapter perhaps provide further insight into why dysprosium has remained comparatively under-studied as a laser ion. Additionally, while we note that this work is preceded by demonstrations of Dy^{3+}:ZBLAN fibre lasers, the totality of previous work represents only a fraction of possible investigation.

In considering the development of Dy^{3+}:ZBLAN fibre lasers to this point, we can refer back to the absorption spectrum in figure 2.4 and clearly see that only half of the defined pumping possibilities have been investigated. Targeting pump absorption at 1.7 µm and 2.8 µm will be the focus for the remainder of this thesis, with each offering unique possibilities in laser system performance.

Pumping at 2.8 µm (*in-band pumping* chapter 4) aims to address the most significant shortcoming not only of previous Dy^{3+}:ZBLAN fibre lasers but that of any mid-IR fibre laser: efficiency. From a quantum defect point of view, in-band pumping is the most efficient scheme, and dysprosium offers the unique advantage in the field of mid-IR ions in that its mid-IR transitions are close to ground state. In fact the 3 µm transition terminates on the $^6H_{15/2}$ ground state, implying a factor of 3 increase in Stokes limit over any other ion emitting in that region. Further, by employing an Er^{3+}:ZBLAN fibre laser as the pump source, we aim to leverage recent advances in that technology to demonstrate rare earths working in tandem to increase capabilities of the overall mid-IR fibre field.

Targeting the absorption at 1.7 µm on the other hand, while perhaps not as efficient, offers many of its own advantages. It represents a substantial reduction in quantum defect over previous work. Additionally, it further reduces potential impact of ESA, as pump absorption from neither the $^6H_{11/2}$ pump, nor $^6H_{13/2}$ upper laser level is directly resonant with higher energy levels. And perhaps most importantly from an engineering and technology development point of view, this pumping scheme allows for the use of silica fibre based components. This will have an impact on both ease of use and cost, points which arguably remain a roadblock for all mid-IR fibre sources.

Finally, there are two key points which have yet to be addressed in any previous work on Dy^{3+} based fibre sources: tunability (continuous or otherwise) and pulsation. The emission spectrum in figure 2.3, combined with the knowledge that room temperature operation in a crystalline host has been demonstrated at 3.4 µm [90] passively implies not only that a large continuous tuning range may be possible, but that Dy^{3+} may cover spectral regions inaccessible directly by other ions. This same broad potential gain bandwidth also has implications for the possibility of pulsed operation, and specifically mode-locked operation (chapter 6). While even long pulses from a fibre in this wavelength range would represent technological novelty, such broad gain bandwidth, if realizable, would suggest mode-locked pulses of less than 100 fs. Tangible progress on either of these fronts would further support the central thesis that dysprosium fibre lasers warrant further research and development effort from the mid-IR field at large.

3

Theory: optical fibre and lasers

The discussion up to this point has made frequent mention of concepts surrounding optical fibres and lasers in general, not directly addressing theoretical considerations of either. While the overarching aim of this thesis centres on experimental demonstration of dysprosium fibre lasers and their untapped potential, the work would be incomplete without treatment of the basic principles of optical fibres and laser physics. We will endeavour in this chapter to cover key aspects of fibre and laser theory. By no means is the material presented meant to be exhaustive, as even separately, fibre optics and laser physics represent fields of study with great depth and history. However, a solid foundation of theoretical understanding is necessary both to understand the goals of the experimental efforts, and to frame the discussion of their results.

3.1 Optical fibres

Our focus throughout this work revolves centrally around the development of lasers, a technology with dramatic impact on our modern world as discussed in chapter 1. Yet the technology of optical fibre itself could certainly be argued to be one of the most impactful technological advancements of this “digital” age. Throughout the world, optical fibre is omnipresent, and in most of the developed world, fibre optic networks could be considered basic infrastructure, topped only by the likes of plumbing and electricity.

There is certainly no shortage of texts covering theoretical aspects of optical fibres and fibre lasers [4, 95–97]. The depth and rigour in many of these exceeds the scope of this thesis. A rather concise treatment with sufficient focus on application is provided by France et. al [98] which we loosely follow here. Specifically we will restrict ourselves to the single (but widely applicable) case of step index fibres.

3.1.1 Step index fibre

At its simplest, confinement of light in an optical fibre or waveguide is achieved by the interface of two materials with differing indices of refraction n

$$n = \frac{c}{v_p} \tag{3.1}$$

where here v_p is the phase velocity of light in the given medium and c is the speed of light in vacuum. Note also that this quantity is dependent both on material, and optical frequency ν. Frequency (alternatively *wavelength*) dependence of the refractive index has an important influence on the guidance properties of optical fibre and is most commonly described by the empirical Sellmeier relation [99]

$$n(\lambda) = \sqrt{1 + \sum_i \frac{A_i \lambda^2}{\lambda^2 - B_i}} \tag{3.2}$$

where A_i and B_i are material dependent coefficients. Using values for the coefficients taken from the literature [38], the refractive index for typical ZBLAN is calculated and plotted over our spectral region of interest in figure 3.1.

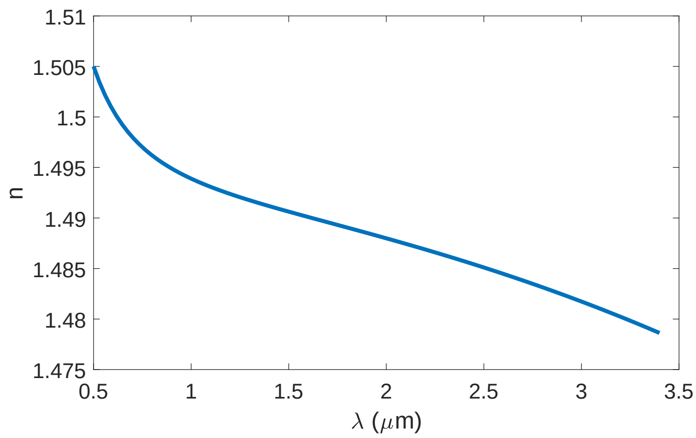

FIGURE 3.1: Index of refraction of a typical ZBLAN composition calculated from a two term Sellmeier relation.

The most common implementation of index contrast in a fibre geometry is to surround a centre core with a cladding of lower index in a step-function fashion:

$$n(r) = \left(\begin{array}{ccc} n_{core} & : & r < a \\ n_{clad} & : & r > a \end{array} \right. \tag{3.3}$$

where r is radial distance and a is the diameter of the core region. The sets of electromagnetic fields which can propagate in such a structure are referred to as *modes*. If the fibre supports many modes (*multimode fibre*) then the physical description of light confinement reduces to a simple form relying on a geometrical ray optics picture.

Consider the situation illustrated in figure 3.2. Inside the fibre, rays will be confined by total internal reflection provided they make an angle with the centre axis of the fibre less than or equal to some critical angle θ_c. We would like to know the maximum angle θ_{max} of rays entering the fibre which will meet this guiding criteria, and this can be derived directly from Snell's law.

$$n_{core}\cos(\theta_c) = n_{clad} \tag{3.4}$$

$$n_{core}\sin(\theta_c) = \sin(\theta_{max}) \tag{3.5}$$

Squaring both (3.4) and (3.5) allows for definition of a quantity known as numerical aperture NA

$$NA = \sin(\theta_{max}) = \sqrt{n_{core}^2 - n_{clad}^2} \tag{3.6}$$

Numerical aperture is a very useful parameter, as it is easily known, and completely char-

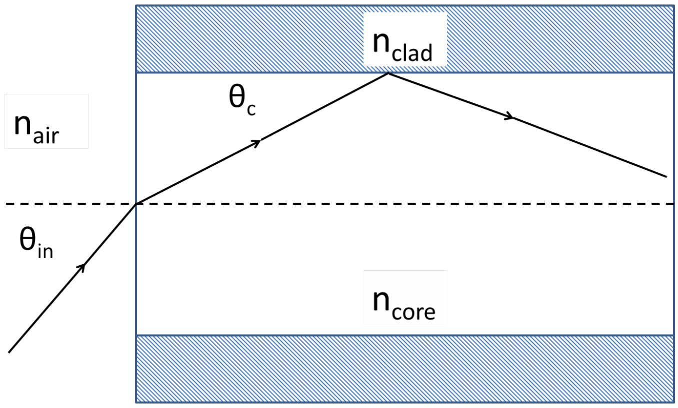

Figure 3.2: Total internal reflection in a multimode step index fibre; numerical aperture $NA = \sin\theta_{in}$.

acterizes the condition for guidance in a multimode fibre. However, while useful for several applications, lasers based on multimode fibre have inherently poor beam quality, in some sense defeating a key advantage of fibre lasers i.e. diffraction-limited output. The same index profile is capable of guiding only one mode as well (*single mode fibre*), but the physical description of guidance becomes more complicated as ray optics are no longer valid.

To accurately describe the modes of a fibre when the ray optics approach fails requires a full electromagnetic treatment by the application of Maxwell's equations. In any medium with a dielectric constant ε, Maxwell's equations yield vector wave equations governing the electric and magnetic fields, **E** and **H**.

$$\nabla^2\mathbf{E} + \nabla\left(\frac{\mathbf{E}\cdot\nabla\varepsilon}{\varepsilon}\right) = \frac{\varepsilon}{c^2}\frac{\partial^2\mathbf{E}}{\partial t^2} \tag{3.7}$$

$$\nabla^2\mathbf{H} + \frac{(\nabla\varepsilon)\times(\nabla\times\mathbf{H})}{\varepsilon} = \frac{\varepsilon}{c^2}\frac{\partial^2\mathbf{H}}{\partial t^2} \tag{3.8}$$

Exact solutions to these equations in a step index dielectric cylinder (fibre) are provided by Snitzer [100], but involve all six field components and are mathematically rather complex. We can however summarize some of the key points by noting that the fields are different for the core and cladding regions, and must be matched at the interface to find solutions. To do this, normalized parameters u and w are introduced which relate to solutions in the core and cladding respectively.

$$u^2 = a^2(k^2 n_{core}^2 - \beta^2) \tag{3.9}$$

$$w^2 = a^2(\beta^2 - k^2 n_{clad}^2) \tag{3.10}$$

In these equations a is the fibre core radius, β is the propagation constant of the given mode, and $k = 2\pi/\lambda$ is the vacuum wavenumber. With these parameters, solutions for the z component (along the fibre propagation axis) take the general form

$$\mathbf{\Psi_z} = A_1 J_m(ur/a)\cos(m\phi + B) \tag{3.11}$$

$$\mathbf{\Psi_z} = A_2 K_m(wr/a)\cos(m\phi + B) \tag{3.12}$$

where $A_{1,2}$ and $B_{1,2}$ are arbitrary constants, m is an integer value, and perhaps unsurprisingly due to the cylindrical symmetry, J_m and K_m are ordinary and modified Bessel functions of the first and second kind respectively, while m indicates their order. An additional normalized parameter known as the *V-number* defines the relationship between u, w and the previously defined quantity of numerical aperture

$$V = \sqrt{u^2 + w^2} = akNA \tag{3.13}$$

For guided modes, both u and w must be non-zero, and if we introduce the useful concept of *effective index*

$$n_{eff} = \frac{\beta}{k} \tag{3.14}$$

inspection of equations (3.9) and (3.10) reveals that the effective index of a guided mode must fall between that of the core and the cladding.

Fortunately, the complexity of the situation can be substantially reduced if we apply the *weakly guiding approximation* [101]

$$\Delta = (n_{core} - n_{clad})/n \ll 1 \tag{3.15}$$

a condition which is met in most step-index fibres of concern. With this approximation, we can define a set of linearly polarized LP_{lm} modes (l and m are azimuthal and radial mode index) which follow from an eigenvalue equation:

$$\frac{uJ_{l+1}(u)}{J_l(u)} = \frac{wK_{l+1}(w)}{K_l(w)} \tag{3.16}$$

Equation (3.16) is transcendental and can be solved numerically by root finding. However, simple inspection reveals that the left hand side will only have solution regions between the zeros of the ordinary Bessel function. Each of these solution regions represents a particular mode. As we have previously stated, the effective index of a mode must lie between the core and cladding to be guided, when $n_{eff} = n_{clad}$, w goes to zero, $V = u$ and the mode is considered *cut-off*. Thus the condition that fibres with a V number less than the first zero of the ordinary Bessel function ≈ 2.405 support only a single fundamental LP_{01} mode.

The intensity profiles of each mode can be given by [95]

$$I_{core} = J_l^2(ur/a)\cos^2(l\phi) \tag{3.17}$$

$$I_{clad} = \left(J_l(u)/K_l(w)\right)^2 K_l^2(wr/a)\cos^2(l\phi) \tag{3.18}$$

Profiles for the first few low order fibre modes are presented in figure 3.3. We can make one

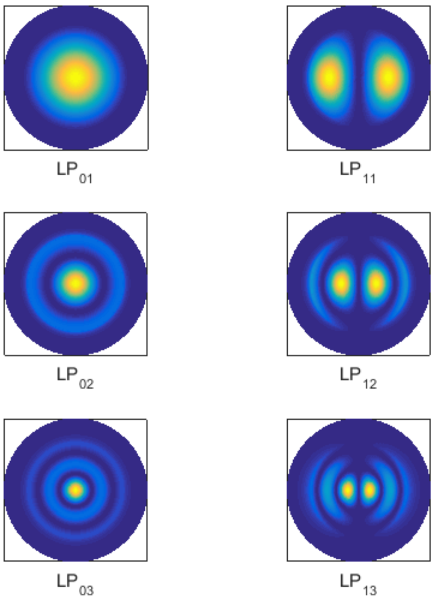

FIGURE 3.3: Intensity distributions of low order fibre modes.

more important simplification by noting that the intensity distribution of the fundamental LP_{01} mode is approximately Gaussian. The fundamental mode radius (w_{mode}) of a step index fibre can then be represented with fair accuracy by a Gaussian beam with a $1/e^2$ intensity width given by Marcuse [102].

$$\frac{w_{mode}}{a} \approx 0.65 + \frac{1.619}{V^{3/2}} + \frac{2.879}{V^6} - (0.016 + 1.561V^{-7}) \tag{3.19}$$

This is a very convenient approximation as it allows direct translation between fibre modes and the Gaussian modes typically encountered in free-space optics.

3.1.2 Double clad fibre

When implemented as a laser, a single mode fibre will generally have near diffraction limited output. However, to pump a purely single mode fibre requires that the pump light is also confined closely to the fibre core. To efficiently couple pump light into the fibre core requires a pump source which itself has near diffraction limited output, which in practice can be a sizeable constraint. A solution to this issue is to add a second cladding, as seen in figure 3.4. Essentially, this operates like a single mode fibre contained inside a multimode fibre,

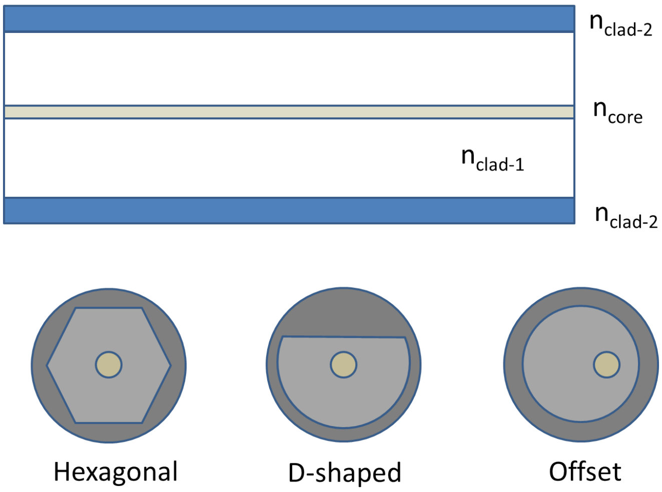

FIGURE 3.4: Double clad fibre geometry and some common cladding designs.

allowing for lower brightness (beam quality) pump sources such as diode stacks. This has proven to be a key advancement in high power fibre laser design [103], as it opens up much more possibility for power scaling [5]. And specifically in the field of mid-IR fibre lasers, double-clad diode-pumped systems represent some of the highest powers yet achieved [104].

We note also from figure 3.4 that the common cladding configurations shown are not purely circular as perhaps one may expect. From a ray optics perspective this is because a purely circular configuration allows helical rays which may never interact with the absorbing core region. This can be mitigated by designs such as those shown which have less circular symmetry, breaking up the ray paths to be more chaotic, thus interacting more effectively with the core.

Discussion of double clad fibre is largely included here in the interest of completeness, as the majority of the experimental efforts to follow focus on pumping the core of single or few-mode fibres. Reasons for this will be variously discussed in both chapters 4 and 5 but can be summarized generally in that the electronic structure of dysprosium and the availability of sources precludes effective diode pumping at present.

3.2 Basic laser theory

Just as in section 3.1, texts covering the subject of laser physics and theory are too numerous to name, though texts by Svelto and Hanna, and of course Siegman are excellent resources [105, 106]. While many advanced concepts necessary for a full treatment of laser theory are beyond the scope of this thesis, a basic understanding of the formalism will prove useful if not necessary. We aim to cover the fundamental concepts applicable to lasers generally, then apply those specifically to fibre systems, then introducing a rate equation numerical approach that will be applied at points to experimental results analysis.

3.2.1 Population inversion, gain, and oscillation

We have previously introduced in section 2.1.2 the concepts of absorption, spontaneous, and stimulated emission from an atomic system interacting with photons. Specifically, the concepts of absorption (2.10) and emission cross section (2.11) will now become quite useful.

We begin by posing the question of how can gain, g, be realized? First we define the *effective gain*:

$$g_{eff} = g_0 - \alpha_0 = \sigma_e N_2 - \sigma_a N_1 - \rho \tag{3.20}$$

where ρ is a term combining all other loss mechanisms. This is useful as it allows combination of two equations (2.8) and (2.9) into a single relation governing the evolution of the optical beam interacting with the atomic system.

$$I_{out} = I_{in} e^{g_{eff} L} \tag{3.21}$$

Relative population of any two energy levels will, at thermal equilibrium, follow from Boltzmann's Principle

$$\frac{N_2}{N_1} = \exp\left(-\frac{\Delta E}{k_b T}\right) \tag{3.22}$$

where ΔE is the separation in energy of the two levels. This quantity is always positive if N_2 is a higher energy level, meaning that at thermal equilibrium, there will always be more population in N_1 and the effective gain g_{eff} will be negative (absorption).

To achieve a net positive effective gain, a *population inversion* needs to be created. Here is where the simplified two level system under consideration is not sufficient. In a purely two level system, a pump beam will be absorbed following (3.21), increasing the population N_2, but also depleting the population N_1 as total population must be conserved $N_{tot} = N_1 + N_2$. Thus when exactly half of the ions are excited, the populations in each level are equal, rendering the system transparent (*pump transparency*) and prohibiting population inversion. If we expand the atomic system to include additional energy levels, the situation is much different.

Virtually every laser can be represented as either a three or four-level system. A general energy level diagram of a four-level system is seen in figure 3.5. Here pump radiation will excite ions from the ground state to level 4 which undergoes fast (generally non-radiative) relaxation to level 3. Since there is little to no thermal population N_2 this process immediately represents population inversion. Two additional points merit consideration however: the lifetime of level 3 should be long as compared to that of levels 4, or 2. If the first criteria is not met, the upper laser level will be de-populated spontaneously faster than it can be replenished by the pump level, and if the second is not met, a bottleneck of population N_2 will build, leading to a *self termination*.

The four-level system is almost always preferable to a three-level system, but nature will not always allow this. There are variants of three level systems in which the targeted emission transition does not terminate on the ground state (via cascade lasing or cooperative

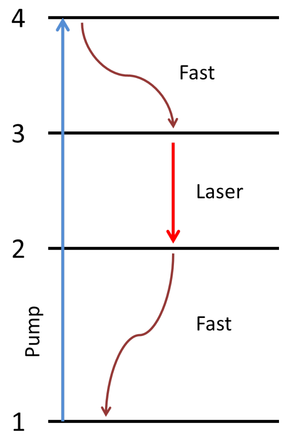

FIGURE 3.5: Simplified energy level diagram of a four-level system.

up-conversion for example) but the general layout of a three-level system, as it applies directly to the $^6H_{13/2} \rightarrow {}^6H_{15/2}$ dysprosium transition, is presented in figure 3.6. Absorbed

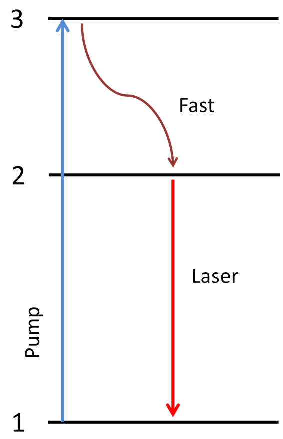

FIGURE 3.6: Simplified energy level diagram of a three-level system.

pump radiation excites ions to level 3, which rapidly (again non-radiatively) relax to the upper laser level 2. The active optical transition then is from level 2 back to the ground state. Involving the ground state directly in the lasing transition is quite a disadvantage, as to achieve population inversion requires excitation of a substantial fraction of the total population. This is mitigated somewhat if we recall that each level in general consists of several sub-levels, so if we target a transition from level 2 to a higher lying sub-level of the ground state with a reduced thermal population, inversion can be achieved with smaller fractional excitation.

So far the theory presented is sufficient to simplistically describe an optical amplifier, i.e. we can create positive gain by creating a population inversion via absorption of pump radiation, and we could then extract power from the atomic system with an optical beam of the same frequency as the laser transition, which will then be amplified according to (3.21). This is relevant, but we are ultimately interested in a laser, which requires oscillation.

Before discussing oscillation we must also introduce the concept of saturation, which will be particularly relevant to the three level dysprosium transition under consideration. We have previously mentioned pump transparency in the context of a purely two level system, and though we have included a third level to physically allow for population inversion, this effect remains and falls under the general term *saturation*. If ions are excited to upper energy levels at a faster rate than they relax back down, the population in the ground state will be depleted, thus reducing the $\sigma_a N_1$ term in (3.20) and reducing the absorption. This will be defined analytically in section 3.2.2.

To achieve this we put the whole picture of optical beams interacting with atomic systems inside of a resonant cavity closed with mirrors. At the most basic, this could be simply a Fabry-Pérot interferometer with an active medium (rare earth-doped glass or crystal for example) between the mirrors as seen in figure 3.7a. As real laser beams diverge, a more

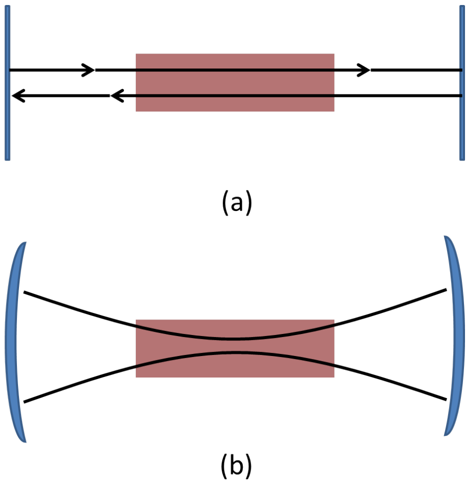

Figure 3.7: Basic laser cavity designs; (a) a Fabry-Pérot design and (b) a curved mirror cavity.

general cavity is figure 3.7b, where one or both mirrors are curved to create a reproducible beam size over the active medium. A cavity such as this can support any number of transverse modes, depending on the curvature of the cavity mirrors, and possibly physical characteristics of the active medium.

In a fibre laser, the concept of resonant cavity is replaced by the optical fibre itself. Cavity mirrors are, in the vast majority of cases, either the Fresnel reflections from perpendicularly cleaved fibre ends, or a fibre Bragg grating (FBG) inscribed into the fibre core, or a combination of both. Occasionally, and as we will make use of in some of the experimental work to follow, *extended cavities* are employed where lenses are used to collimate laser light and cavity mirrors are placed externally. This approach can be advantageous in developmental laboratory work, as it allows some increase in flexibility in terms of cavity design and experimental layout. The transverse cavity modes supported in any of these fibre cavities are simply the modes supported by the fibre that we derived in section 3.1.1. This is an advantage of fibre lasers over many solid state lasers based on cavities such as in figure 3.7b; single transverse mode operation is virtually assured if we simply use fibre designed as single mode.

Finally we consider the reflectivity of cavity mirrors. Obviously reflectivity of 100%, makes for an excellent resonant cavity, but its rather useless in practice as no laser light will escape. At the opposite extreme is 0%, which is not a resonant cavity. We can derive a very useful relation considering figure 3.8. During steady-state (*continuous wave* or *CW*)

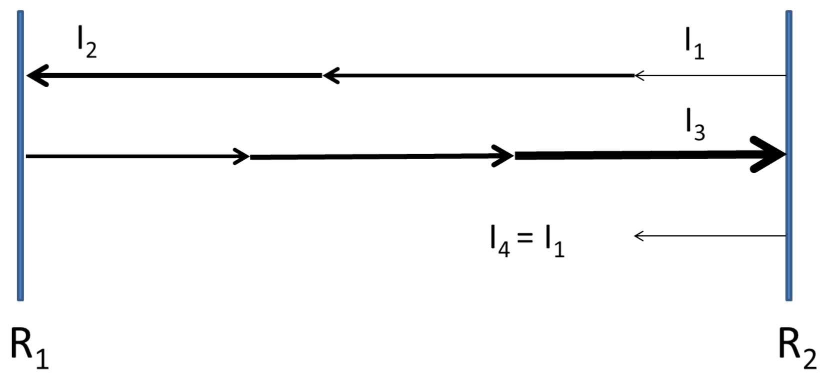

FIGURE 3.8: Selecting cavity mirrors R_1 and R_2 based on requirement that the round-trip intensity I is reproduced.

the optical intensity must be reproducible for each round trip of the laser cavity. Consider that I_1 is the laser intensity just after being partially reflected by mirror R_2. After one pass of the cavity, this intensity is amplified to an intensity I_2 just before mirror R_1 just as in (3.21)

$$I_2 = I_1 e^{g_{eff} L} \tag{3.23}$$

Reflection from mirror R_1 reduces the intensity, which then is amplified through traversal of the cavity in the opposite direction, producing a new intensity just before R_2

$$I_3 = I_2 R_1 e^{g_{eff} L} \tag{3.24}$$

Finally, reflection at R_2 must produce an intensity equal to what we started with

$$I_4 = R_2 I_3 = I_1 \tag{3.25}$$

Combining (3.23), (3.24), and (3.25) leads to the *oscillation condition* [107]

$$1 = R_1 R_2 e^{2 g_{th}} \tag{3.26}$$

Where we have now introduced a new quantity $g_{th} = \ln(1/R_1R_2)/2$, which is the gain (now integrated over length, $g_{th} = g_{eff}L$) required to reach oscillation threshold. This is obviously an important quantity in laser design, and is often considered more practically in terms of threshold power, P_{th}, which is the pump power required to achieve said gain. At this point the gain is said to be clamped, as any further increase in gain would allow for exponential increase in laser output with pump power. Beyond this power, increase in pump power absorbed by the system, P_{abs}, produces a linear increase in laser signal power P_{out} (ignoring higher order effects) following

$$P_{out} = \eta(P_{abs} - P_{th}) \tag{3.27}$$

where η is the *slope efficiency*. From a laser system engineering point of view this is one of the most important characteristics of any laser.

One may observe in the above analysis that the ρ term representing other loss mechanisms is neglected. In most fibre lasers this is a reasonable assumption as the cavity mirrors are often the dominant loss. It will be important to remember this simplification, as developmental fibre such as that used in the experiments presented in this work can have background loss which ranges from non-negligible to substantial.

3.2.2 Analytical treatment

While the treatment above is useful in abstract understanding of the basic concepts of laser operation in general, it does not provide the ability to actually calculate any of the relevant quantities. For that we must turn to a much more rigorous analysis of specifically fibre lasers.

Driven in part by the increase in telecommunications, and the relative lack of strong computing power, in previous decades there was considerable effort placed on deriving closed-from analytical expressions for the operating parameters of fibre lasers and amplifiers [108–110]. Pask et. al provide a particularly useful approach which we will summarize briefly here [111].

Consider both the pump P_p and signal (*laser*) P_s powers are contained within the core of a fibre. The evolution of the pump power along the fibre length L follows the following differential equations:

$$\frac{dP_p(z)}{dz} = (\sigma_{ep}N_2 - \sigma_{ap}N_1)P_p(z) \tag{3.28}$$

$$\frac{dP_p(z)}{dz} = -\frac{Ahv_p}{\tau}N_2(z) \tag{3.29}$$

which involves the population densities $N_{1,2}$ and cross sections $\sigma_{e,a}$, but now also the fibre core area A and the upper state lifetime τ. These two equations then generate the result

$$\ln\left(\frac{P_p(z)}{P_p(0)}\right) + \frac{P_p(z) - P_p(0)}{P_{sat}} = -N_{tot}\sigma_{ap}L \tag{3.30}$$

where we have now formally quantified *saturation power* as

$$P_{sat} = \frac{hv_pA}{(\sigma_{ep} + \sigma_{ap})\tau} \tag{3.31}$$

this power defines the power at which the absorption coefficient is reduced by half. We can then calculate the pump power at the fibre output $P_p(L)$ and consequently the power absorbed $P_{abs} = P_p(0) - P_p(L)$ allowing definition of the integrated gain over the fibre as

$$g = \frac{(\sigma_{es} + \sigma_{as})\tau P_{abs}}{Ahv_p} - N_{tot}\sigma_{as}L \tag{3.32}$$

Recall that for laser oscillation the gain is clamped once threshold is achieved. Thus we can use known cavity mirror reflectivity $R_{1,2}$ and calculate the threshold gain g_{th} from (3.26);

substitution into (3.32) then directly allows calculation of absorbed pump power threshold to reach the necessary gain. This method assumes no background loss, but is very useful in determining sensible operating regimes when designing fibre laser cavities.

While the above analysis and (3.32) is fairly accurate in many cases, it does make a simplification in not explicitly accounting for the overlaps of the pump or signal mode with the active fibre core. In purely single mode operation reasonably above cut-off this is not overly detrimental, and even in the limit of cladding pumping where the pump mode overlaps poorly with the core, the technique still holds well provided the pump cross sections are scaled by the cladding area ($\sigma_{p,clad} = \sigma_p/A_{clad}$). However, in slightly multi-mode cases, or single mode operated far from cut-off, mode overlap becomes increasingly significant. Digonnet addresses this issue by introducing overlap factors η_p, η_s, and F which represent the overlaps between pump and core, signal and core, and pump and signal respectively. These lead to a slightly modified equation for fibre gain [112]

$$g = -\sigma_{as}N_{tot}\eta_s L + \frac{(\sigma_{as} + \sigma_{es})\tau P_{abs}F}{Ahv_p\eta_p} \tag{3.33}$$

Inspection of (3.33) shows that the factor F/η_p will have a direct influence on proportionality of absorbed pump power to gain. Though exact calculation of this ratio is possible, it can be approximated as [113]

$$\frac{F}{\eta_p} \approx \frac{a^2}{w_s^2 + w_p^2}\frac{1}{1 - \exp(-(a/w_p)^2)} \tag{3.34}$$

where a is fibre core, and $w_{s,p}$ are Gaussian waist radii of the signal and pump modes calculated from (3.19). This approximation is very accurate for the fundamental LP_{01} mode over a range $1.3 < V < 2.4$, and in general is close to unity. Applying a Gaussian mode approximation to η_s can also be done by equating it to the relation for power through an aperture for a Gaussian beam.

$$\eta_s \approx 1 - \exp(-2a^2/w_s^2) \tag{3.35}$$

While all of the above is certainly useful, many real-world applications, particularly those where saturation effects are prominent, still require a numerical solution approach.

3.2.3 Rate equation modelling

The analytical expressions presented in 3.2.2, while rigorous in their derivation, struggle to account for many higher order effects which are common in fibre lasers and amplifiers. While a correction term can be added to (3.33) to account for depletion of the ground state (pump absorption saturation) or excited state absorption (ESA) [112], if either of these effects a prominent, it is generally preferable to seek a numerical solution. Additionally, these expression do not address energy transfer processes, such as upconversion or cross-relaxation, which may be so significant as to have been introduced intentionally through large ion concentration or co-doping. These points combined with the fact that even a modern personal computer possesses enough computational power to handle rather complex numerical computation has led to numerical solutions being the widely preferred method of fibre laser design and analysis. This is where we turn to rate equation analysis.

Any rate equation model consists basically of a system of coupled differential equations, each governing the temporal evolution of population in a particular energy level. Perhaps more so than any other theoretical concern, basic treatment of rate equations is a commonality across virtually every text covering lasers, but here we have adopted the notation of Morin et. al [114].

We have seen the three-level system before (figure 3.6), but it is presented here in figure 3.9 specifically for the 3 µm dysprosium transition pumped at 1700 nm, and with the relevant transition rates indicated. The three differential equations governing the evolution of level

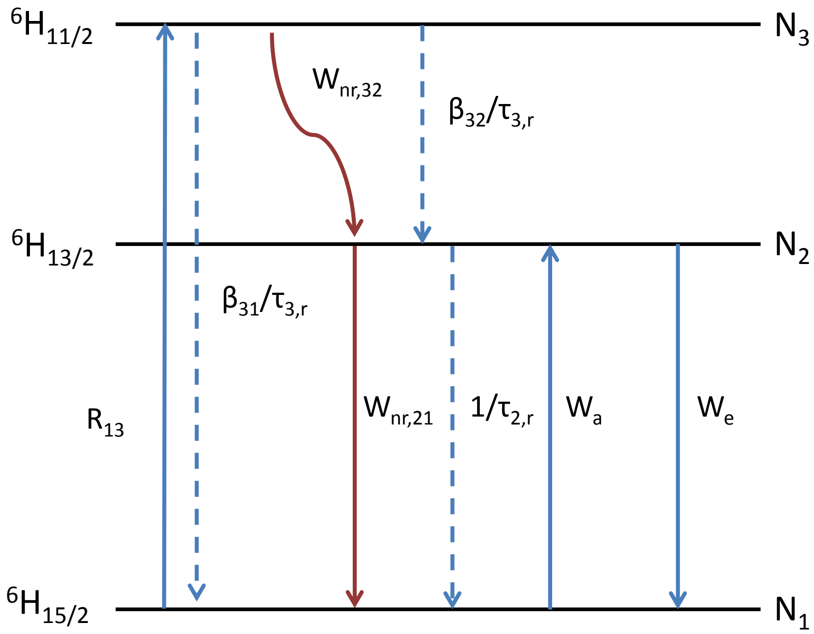

Figure 3.9: Energy level diagram of dysprosium pumped at 1700 nm with the transitions relevant for rate equation modelling indicated.

populations here are as follows:

$$\frac{dN_3}{dt} = R_{13}N_1 - \left[W_{nr,32} + \frac{\beta_{3,1}}{\tau_{3,r}} + \frac{\beta_{3,2}}{\tau_{3,r}}\right] N_3 \tag{3.36}$$

$$\frac{dN_2}{dt} = W_aN_1 - \left[W_e + W_{nr,21} + \frac{1}{\tau_{2,r}}\right] N_2 + \left[W_{nr,32} + \frac{\beta_{3,2}}{\tau_{3,r}}\right] N_3 \tag{3.37}$$

$$\frac{dN_1}{dt} = \frac{\beta_{3,1}}{\tau_{3,r}}N_3 + \left[W_e + W_{nr,21} + \frac{1}{\tau_{2,r}}\right] N_2 - \left[R_{13} + W_a\right] N_1 \tag{3.38}$$

where it is important to note that $\tau_{i,r}$ is the *radiative* lifetime as calculated say from Judd-Ofelt analysis, and W_{nr} is the non-radiative transition rate considered down only to the next closest level. Also notice that the branching ratio $\beta_{2,1}$ is unity, and is not explicitly considered in (3.37) and (3.38).

Before further consideration of this system, we can quickly make some key simplifications. First the non-radiative term in (3.36) is considered to dominate the population dynamics of the $^6H_{11/2}$ level, effectively eliminating this level from the system and allowing us to move the pumping term $R_{13}N_1$ to the equation governing $^6H_{13/2}$. Second, as we have defined the non-radiative rate W_{nr} as (2.18) we can combine the contributions of radiative and non-radiative transitions into simply the observed lifetime τ. This reduces the system to one differential equation and one constraint

$$\frac{dN_2}{dt} = [R_{13} + W_a]\, N_1 - \left[W_e + \frac{1}{\tau}\right] N_2 \tag{3.39}$$

$$N_1 = N_{tot} - N_2 \tag{3.40}$$

Where the relevant rates are defined as

$$R_{13} = \frac{\sigma_{a,p} I_p}{h v_p} \tag{3.41}$$

$$W_a = \frac{\sigma_{a,s} I_s}{h v_s} \tag{3.42}$$

$$W_e = \frac{\sigma_{e,s} I_s}{h v_s} \tag{3.43}$$

In the steady state, (3.39) is set equal to zero and can be solved simply algebraically provided the relevant rates are known. For the in-band pumped system investigated in chapter 4, only two levels are involved, thus the assumption of non-radiative decay of the pump level is further justified, though an additional term R_{31} must be included to account for stimulated emission of the pump.

To calculate the transition rates requires knowledge of the pump and signal intensities, which will vary along the length of the fibre, as well as with the temporal evolution of level population according to

$$\left[\frac{1}{c}\frac{\partial}{\partial t} + \frac{\partial}{\partial z}\right] I_p(z,t) = -\sigma_p I_p(z,t) N_1(z,t) \tag{3.44}$$

$$\left[\frac{1}{c}\frac{\partial}{\partial t} + \frac{\partial}{\partial z}\right] I_s(z,t) = [\sigma_e N_2(z,t) - \sigma_a N_1(z,t)]\, I_s(z,t) \tag{3.45}$$

Additionally, both field intensities have a forward and backward propagating component. Thus to solve the full spatio-temporal dynamics will require numerical solution of coupled partial differential equations (PDE's). We are however largely concerned with CW operation, thus we can drop the $\partial/\partial t$ term in the intensity equations and set (3.37) equal to zero. Further, though (3.44) and (3.45) do not account for transverse (modal) aspects, we can incorporate the concept of overlap factor (3.35) for both pump and signal intensity and insert these as multiplicative factors. Alternatively, as we discuss in chapter 4 one could integrate the effective gain or absorption over the core area.

These simplifications allow for implementation of a *relaxation algorithm*, where we make (educated) estimates of excitation level, and then propagate all of the fields, re-calculate algebraically level populations, and propagate the fields again and repeat the process. With careful selection of starting values, this process converges on a steady state answer. And this is precisely where the approximate analytical expressions from section 3.2.2 are helpful, as they generally inform a region of convergence.

3.2.4 Additional considerations

The theory presented thus far may be sufficient for model, design, and analysis of CW fibre lasers or amplifiers based on rare earths with simple energy level structure, a condition that is actually well met for the ${}^6H_{13/2} \rightarrow {}^6H_{15/2}$ transition of dysprosium. However, there are additional aspects which play varying degrees of importance in lasers in general, and specifically mid-IR fibre lasers. We will endeavour to cover some of the most prominent in brief here.

First is the concept of amplified spontaneous emission (ASE). Consider again equation (3.39), during laser operation the expectation is that stimulated transitions (W_e) will dramatically outweigh spontaneous transitions. While this is true, spontaneous transitions will still occur, and light emitted from these transitions, if it propagates through the inverted medium, will be amplified. Spontaneous emission will not have the same directionality of stimulated emission, rather emitting in all directions. In a solid state laser such as a rod or slab based system, ASE can be regeneratively amplified by reflection of a crystal facet for example, leading to parasitic lasing. In a fibre this is mitigated somewhat by the fact that only a small fraction of spontaneous emission will fall along the fibre propagation axis, but that which does will be well confined and can undergo significant amplification. ASE has several impacts, but of particular note it can reduce the total system gain, thus reducing the output power. Additionally, ASE is possible across the entire gain bandwidth of the given system, and will be strongest at the wavelength around peak gain. When operating a laser off of the natural gain peak (a diffraction grating tuned cavity for example) ASE can be well removed in wavelength from the laser signal. This can be detrimental for example if the application of the laser system is emission frequency specific.

Though a key advantage of most fibre lasers is diffraction limited output, we must also make mention of beam quality. There are many ways to define and measure beam quality [115], but one of the most widely used is the M^2 factor. This factor is defined as the beam parameter product (BPP - product of beam radius w and divergence half-angle θ) divided by that of an ideal Gaussian beam. As the BPP of a Gaussian beam is equal to λ/π this results in

$$M^2 = \frac{\theta \pi w}{\lambda} \tag{3.46}$$

This is quite useful, as an arbitrary beam can be represented by simple Gaussian optics with accuracy provided λ is replaced by $M^2\lambda$ in the relevant equations.Beam quality is relevant in fibre optics when dealing with multimode fibres, and also as we may see in the experimental work here, when coupling free space laser sources into a fibre.

Finally, though we have considered transverse modes of a laser (specifically fibre), longitudinal modal properties have been neglected. Consider again the simple Fabry-Pérot cavity in figure 3.7(a). This cavity will support any number of electric field configurations that follow $E(z) = E_0 \sin(mz)$ where m is a positive integer. Each one of these is a *longitudinal mode* of the cavity of a particular frequency, equally spaced according to $c/2nL$ where n is the refractive index of the medium and L is the cavity length. The number of modes actually oscillating in a laser cavity then can be determined by the linewidth of the emission and the known spacing of cavity modes. In a typical fibre laser, L can be rather long, leading to a large number of longitudinal modes oscillating even in a relatively narrow emission linewidth. The concept of longitudinal modes is necessary for an understanding of *mode-locking*.

3.3 Summary

In this chapter we have discussed basic fundamental principles of optical propagation in a fibre, as well as several key aspects of laser physics. These concepts will prove not only useful but necessary in discussion of the experimental work to follow. Fibre modal properties must be considered in both pumping schemes investigated in chapters 4 and 5, and the concepts of gain, threshold and efficiency are paramount to the experimental goals. In particular, modelling based on systems of rate equations will be referred to repeatedly. All of this material, in conjunction with that of chapter 2 allows this thesis to progress to the experimental work.

4

In-band pumping at 2.8µm

To this point in the thesis, we have addressed the relevant theoretical considerations, as well as hopefully providing a compelling motivation for the effort to further development of mid-infrared dysprosium fibre lasers. This chapter now represents our introduction in earnest to the actual experimental work carried out, which will be continued in chapters 5 and 6.

The overall aims of the work presented in this chapter can be summarized succinctly in two key points.

1. Leverage existing maturity of 3µm erbium-doped ZBLAN fibre lasers
2. Realize conversion efficiency greater than all previous 3µm fibre sources via an in-band optical pumping scheme

While this chapter is intended as a more in depth discussion provided with greater detail, the critical experimental results can be found published in both [116] and [117].

4.1 In-band pumping overview

In-band (alternatively *resonant*) pumping describes the situation where pump light excites a laser-active ion from the ground state, which then radiatively emits directly back down to the ground state, i.e. there are only two Stark level manifolds involved in the entire laser process. Occasionally one may find references to *in-band pumping* in cases where there are three manifolds involved and pump light excites ions directly to the upper laser level. The author finds this somewhat misleading and might otherwise suggest this situation referred to as *direct excitation*. For example this is the case for the $^6H_{11/2} \rightarrow {}^6H_{13/2}$ transition of the Dy^{3+} ion, which is capable of emission in the 4.5µm spectral region when pumped directly to the upper level by light around 1.7µm [86, 87].

Occasionally, in-band pumping is employed due to necessity, for example in ytterbium-doped gain media, in which there is only one excited state manifold which is reasonably accessible from the ground state [118]. However, in the majority of cases, this method of pumping is chosen due to the advantage that it offers, namely, *efficiency.* With only two level manifolds involved in the radiative transition, the quantum defect can be as small as a few percent, with theoretical pump-to-signal conversion efficiencies approaching unity. Indeed this has been realized most notably in the field of erbium-doped fibre amplifiers (EDFA's) emitting in the 1.5 µm telecommunications band [119].

This approach is not without its drawbacks however, as there are clear physical limitations due to the pump and signal falling under the same gain bandwidth. The pump field can also stimulate transitions of the excited medium back to the ground state, thus reducing the available gain by a factor of [120]

$$\eta = \left(\frac{\sigma_{a,s}}{\sigma_{e,s}}\right)\left(\frac{\sigma_{e,p}}{\sigma_{a,p}}\right) \tag{4.1}$$

where $\sigma_{a,(sp)}$ and $\sigma_{e,(sp)}$ are the absorption and emission cross sections at the signal and pump frequency respectively. If the pump and signal wavelength are equal, then the gain reduction factor, (4.1) is unity, meaning complete gain reduction, thus no gain is possible.

A complementary view of this in-band effect takes into consideration the maximum possible population inversion when only two manifolds are involved. We can derive this directly by simple examination of the equations governing pump absorption. For a single pass through a length of fibre (unidirectional pumping - a commonality for the bulk of this work), the pump field can be written as

$$P(L) = P_0 e^{-\alpha_p L} \tag{4.2}$$

where α_p defines the effective absorption coefficient, defined in terms of the pump emission and absorption cross sections and the populations $N_{0,1}$ in the ground state and upper state respectively.

$$\alpha_p = \sigma_{a,p} N_0 - \sigma_{e,p} N_1 \tag{4.3}$$

$$N_{tot} = N_1 + N_0 \tag{4.4}$$

Combining (4.3) and the additional constraint that total population is conserved (4.4) allows us to equate the *pump transparency condition* ($\alpha_p = 0$) with the maximum upper state population.

$$\frac{N_{1,max}}{N_{tot}} = \frac{\sigma_{a,p}}{\sigma_{e,p} + \sigma_{a,p}} \tag{4.5}$$

For *lasing* to be a possibility, the effective absorption coefficient α_s for the signal wavelength must be less than zero (gain must exist).

$$0 > \alpha_s = \sigma_{a,s} N_0 - \sigma_{e,s} N_1 \tag{4.6}$$

Combination of (4.4), (4.5), and (4.6), along with algebraic manipulation leads to the lasing condition

$$\frac{\sigma_{a,p}\sigma_{e,s} + \sigma_{e,p}\sigma_{a,s}}{\sigma_{e,p} + \sigma_{a,p}} > 1 \tag{4.7}$$

As the cross sections are always non-negative values, the numerator on the left hand side of (4.7) must be positive, requiring that

$$\frac{\sigma_{a,p}\sigma_{e,s}}{\sigma_{e,p}\sigma_{a,s}} > 1 \tag{4.8}$$

which we see from (4.1) is equivalent to $\eta < 1$; gain reduction factor must be less than unity.

4.2 Dysprosium considerations

4.2.1 In-band benefits and existing technology

We've seen in chapter 1 that the field of mid infrared fluoride fibre lasers has advanced tremendously in recent years. Though it would be fair to assess the field as still in a research and developmental phase, it is significant that commercial products are beginning to emerge [121]. Of the rare earths capable of emission in the 3µm spectral region, fibre lasers based on Er^{3+} are clearly leading the way both in terms of the volume of work focused on their development, and the output powers achieved. Lasers based on Ho^{3+} have also shown promise, though to this point there has been comparatively less collective effort to develop these sources. Currently, the combined efforts at these two ions has nearly overshadowed the possible advantages of Dy^{3+}.

As discussed in chapter 2, there are four possible ground state absorption transitions one can reasonably target to generate emission in the 3µm region from the ${}^6H_{13/2} \rightarrow {}^6H_{15/2}$ transition of Dy^{3+}. The magnitude and spectral locations of these transitions effectively disallow pumping with low cost commercially available diode lasers (which we will consider in more detail in chapter 5), something which has been the major driver for the relative success of Er^{3+} and Ho^{3+} systems.

However, what on the one hand is a technological advantage, on the other is a limitation. While pumping with near infrared diodes has made for fairly robust and high power systems, as we have seen in chapter 1 that historical progress in power scaling fibre systems at 3µm appears to be asymptotically approaching a limit. One clear possibility for this is that near infrared pumping dictates an inherently large quantum defect. While recently some clever cascading techniques have been applied to exceed the Stokes limit of an Er^{3+} system [47], for the majority of systems this is a fundamental upper limit.

In contrast to these two ions, the 3µm transition in dysprosium terminates at the ground state (as emphasized in the simplified energy level shown in figure 4.1), offering the possibility of an inherently efficient in-band pumping scheme. Obviously, to exploit this efficiency in practice requires a reliable pump source in the 3µm band. This is where we hope to build on existing technology by employing an Er^{3+} fibre laser as a pump source. The immediate utility of this approach should be clear in the experiment and results that follow. Having proved the principal in practice, one could begin to see the potential of applying well known near IR beam combining techniques to the mid-IR, i.e. combining several inefficient multi-watt output Er^{3+} lasers to then efficiently pump a Dy^{3+} laser [122, 123]. Such multi-stage efforts may be exactly what is required to continue advancement of the output power in mid-IR fibre lasers.

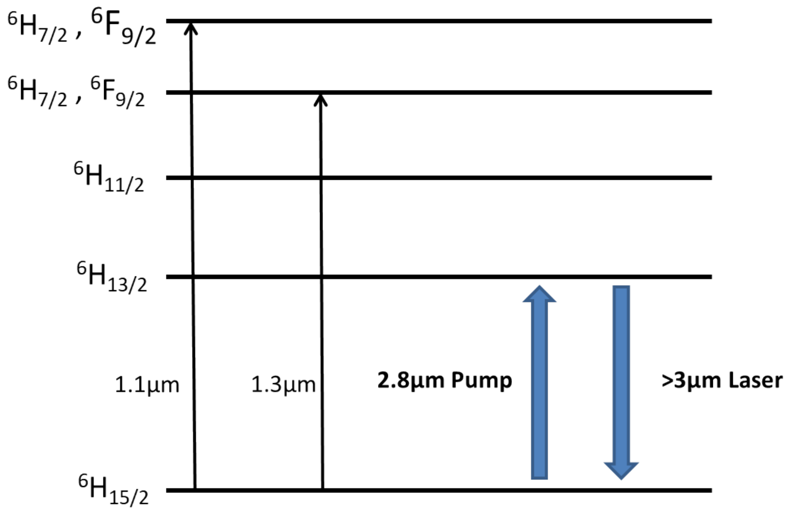

FIGURE 4.1: Simplified energy levels of the dysprosium ion, indicating previous near infrared pumping schemes.

4.2.2 Gain reduction effects

Before moving on to the experimental efforts, it is important to address the in-band effects on gain reduction and population inversion introduced in 4.1 in regards to dysprosium specifically. We can calculate the relevant effects using the spectroscopic data [80] which we've seen in greater detail in chapter 2, specifically, the absorption and emission cross sections of the $^6H_{13/2} \rightarrow {}^6H_{15/2}$ transition seen in figure 4.2. The gain reduction factor described

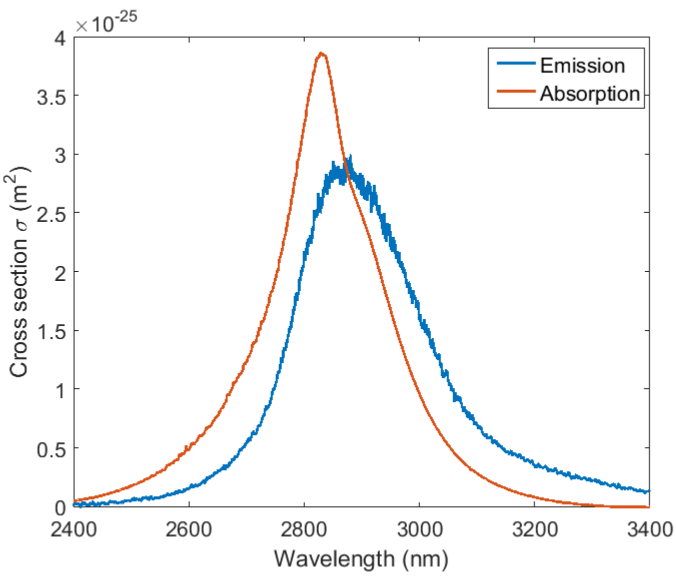

FIGURE 4.2: Absorption and emission cross sections of the $^6H_{13/2} \rightarrow {}^6H_{15/2}$ 3µm transition.

in (4.1) is calculated as a function of emission wavelength for a pump wavelength of 2.8µm in figure 4.3. It is clear, as expected, that the gain reduction factor increases for shorter emission wavelengths that approach the pump. This factor is reduced at longer emission wavelengths, and though it remains non-negligible it will prove to not be the limiting factor in system performance. The maximum achievable population inversion as defined in (4.5)

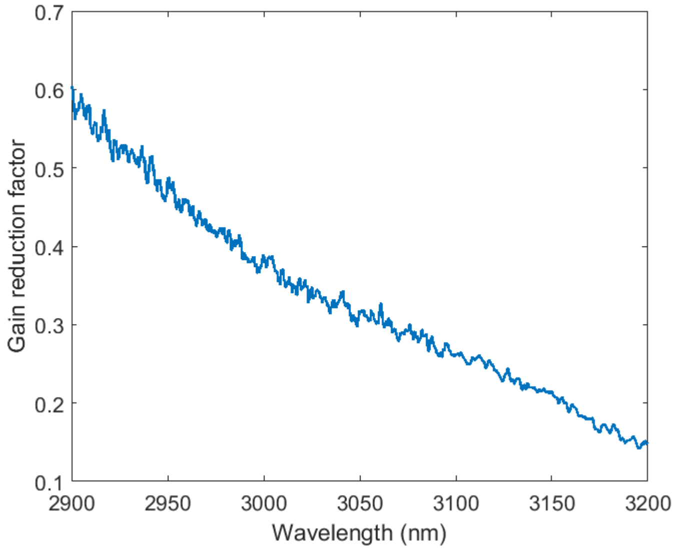

Figure 4.3: Gain reduction factor calculated as a function of emission wavelength at a fixed pump wavelength of 2.8 µm.

is dependent only on the choice of pump wavelength and is presented in figure 4.4. We

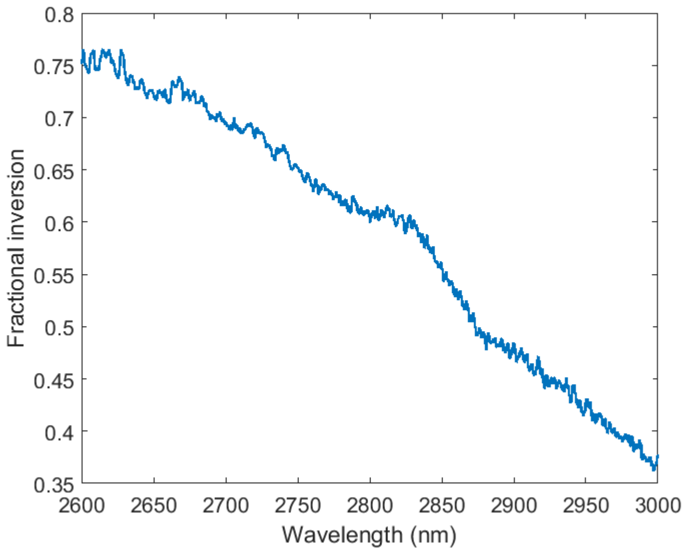

Figure 4.4: Calculated fractional inversion (N_1/N_{tot}) as a function of pump wavelength.

see that the pump wavelength must be shorter than 2900nm to exceed 50% population inversion. While shorter pump wavelength allow for a larger theoretical population inversion, recall from figure 4.2 that the absorption cross section decreases at shorter wavelengths as well. To properly design an efficient system, these two effects must reasonably balance.

4.3 Experimental overview

We have previously observed that the available ground state absorption peaks of dysprosium effectively disallow pumping with low cost diodes. Further, the nature of $^6H_{13/2} \rightarrow {}^6H_{15/2}$ being a ground terminated transition dictates that even should diodes be readily available, cladding pumping would be inherently high in oscillation threshold. This is because effective cladding pumping requires a rather large intrinsic absorption per unit length, as the cladding pump field generally has a small overlap with the active core region. To accomplish this one would generally increase the dopant concentration, fibre length, or a combination of both. However, with a ground state terminated transition both of these actions result in an increase in re-absorption of the signal field, directly increasing threshold, which we will see in greater detail in chapter 5.

When considering in-band pumping the 3µm transition, in addition to the constraints above, one must understand that producing diodes at these wavelengths is a technological difficulty unto itself. While it is true that diode lasers in this spectral region have been demonstrated [124], they are limited in output power to well less than 1W and remain a developmental technology. However, as we have seen, Er^{3+} fibre lasers have reached a level of maturity where employing one as a tool to core pump a dysprosium fibre is a viable path. Additionally, though there are commercial options, our group has an established history in the development of Er^{3+} fibre lasers [125, 126], thus constructing one in house was deemed the best option.

4.3.1 Laboratory setup

Implementation of the experimental work begins with the construction of the Er^{3+} pump laser. This consisted of a length of octagonal double clad Er^{3+}-doped ZBLAN fibre (Le Verre Fluoré) pumped by a high power commercial diode laser emitting at 976nm. The laser cavity was closed at the pump input end by a butt-coupled dichroic mirror exhibiting high reflectivity across the 3µm band. The nominally 4% Fresnel reflection from the distal end of the fibre served as the output coupler. Without a means to force a specific oscillation frequency, we are reliant on the free-running output of the system, the spectrum of which is seen in figure 4.5. Though this emission wavelength is slightly shifted from the absorption peak, inspection of figure 4.2 shows that it is still well within the strong absorption region with a cross section of 3.1×10^{-25} m^2 (i.e., α_{abs} =11.5 m^{-1}).

As we have seen, Er^{3+} fibre lasers have succeeded thus far in scaling output powers to the 10's of W level, in part due to the benefits provided both by fibre Bragg grating (FBG) stabilization [104] and spliced AlF_3 end caps [46] which protect potentially vulnerable fibre tips from environmental contamination and reduce the laser intensity at the glass/air interface. Due to in-house glass processing limitations at the time, our pump source employs neither advantage, limiting the output powers accessible to <3W.

With an operational pump source, we move on to complete the laboratory setup as seen in figure 4.6. The particular Dy^{3+} fibre (Le Verre Fluoré) used for this set of experiments was doped to a concentration of 2000 ppm (3.63×10^{25}m$^-3$) with a core diameter of 12.5 µm and a numerical aperture of 0.16, thus supporting single transverse mode operation down to 2.6 µm. The background loss of this fibre was measured by the manufacturer as 20 dB/km

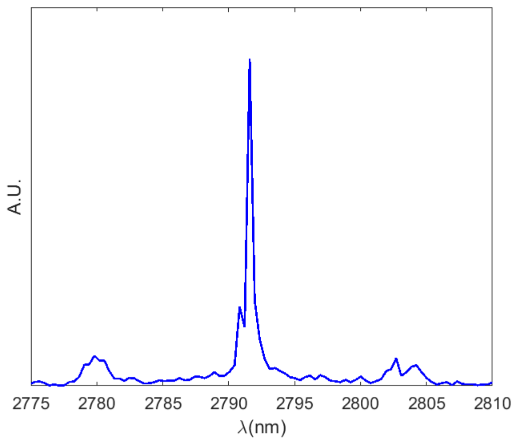

Figure 4.5: Measured output spectrum of the Er^{3+} ZBLAN pump laser.

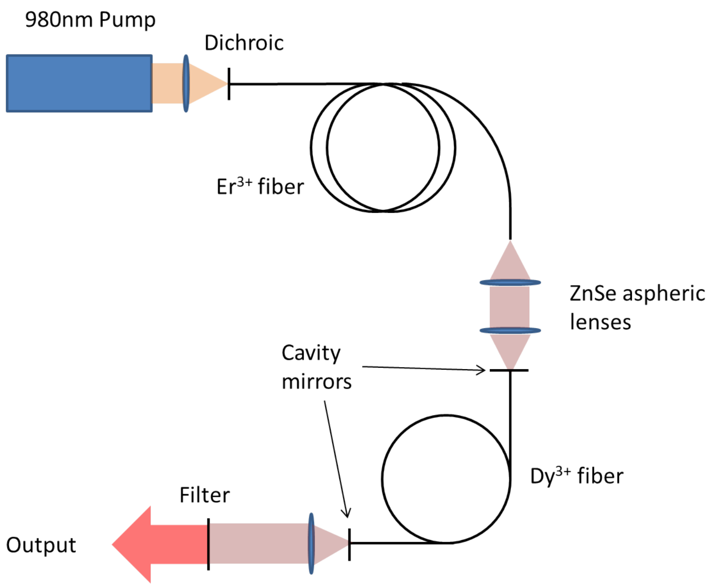

Figure 4.6: Laboratory setup for an in-band pumped dysprosium fibre laser. The laser cavity consists of butt-coupled mirrors, and following collimation the output is filtered to remove residual pump light.

at a wavelength of 2.11 µm, though the loss at pump and laser wavelengths is currently not exactly known, which we will see as an important consideration later. Coupling free space light into the core of a single mode fibre can be a challenging task which requires careful selection of optics. To accomplish this task in this experiment a pair of anti-reflection coated ZnSe aspheric lenses were used. Due to a mismatch in fibre core sizes between the pump and dysprosium laser, these lenses were chosen such that they effectively served as a telescope with 1:2 de-magnification. This results in a nominal coupling efficiency of pump light to the Dy^{3+} fibre core of 70%. The dysprosium fibre laser cavity itself was also a linear cavity, with the input mirror a butt-coupled dichroic mirror transmitting 90% of the incident pump light and reflecting >95% at wavelengths longer than 3 µm. The output coupler was another butt-coupled dichroic mirror, with broadband reflectivity of nominally 50% across the 3 µm band (thus partially reflecting any residual pump light as well). Output at the distal end of the fibre was collimated with a CaF_2 plano-convex spherical singlet lens. A bandpass filter with a transmission window of 2.9 - 3.5 µm was then used to reject any residual pump light; the transmission of both the un-coated collimation lens and the bandpass filter are taken into account for measurement of output power. Output diagnostics consisted of a thermopile laser power detector, an FTIR optical spectrum analyser, and a Si microbolometer array to image the output mode profile.

4.4 Results

4.4.1 Free running emission and the efficiency record

We achieve successful laser emission from the Dy^{3+} system for a fibre length of 92 cm, with an emission centred around 3.04 µm. This emission wavelength is slightly longer than the previous efforts [51, 52] due both to the in-band effects we have discussed and the filtering effect of the input dichroic mirror (RMI Co.), the spectral transmission/reflection characteristics of which are shown in fig 4.7. Output power characteristic as a function of the launched pump power is presented in figure 4.8 (note that residual pump power is essentially negligible, thus launched = absorbed). Based on the linear fit to measured data, the slope

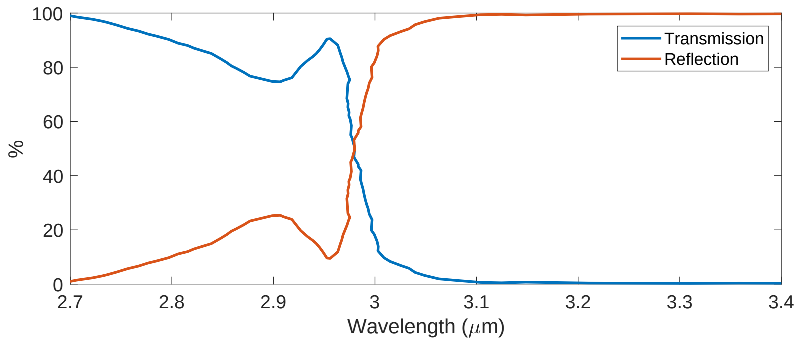

FIGURE 4.7: Spectral transmission and reflection data for the input dichroic mirror (RMI Co.). Mirror is highly reflective beyond 3 microns.

efficiency with respect to launched power is 51%, representing a current record in terms of pump conversion for all 3 µm class fibre lasers, clearly demonstrating the potential of this pumping scheme.

Though this configuration lacks a cavity element (aside from the short wavelength filtering effect of the input dichroic) to fix the oscillation wavelength, given the three level ground state terminated nature of the transition coupled with unidirectional pumping allows for a degree of wavelength tuning by increasing fibre length. Inversion factor decreases with fibre length, amplifying the effect of signal re-absorption, which from figure 4.2 is a weaker effect at longer wavelengths, thus red-shifting the emission.

We exploit this effect by increasing the fibre length to 140 cm, which results in emission centred around 3.26 µm as shown in figure 4.9. This was, until the work in section 4.4.2,

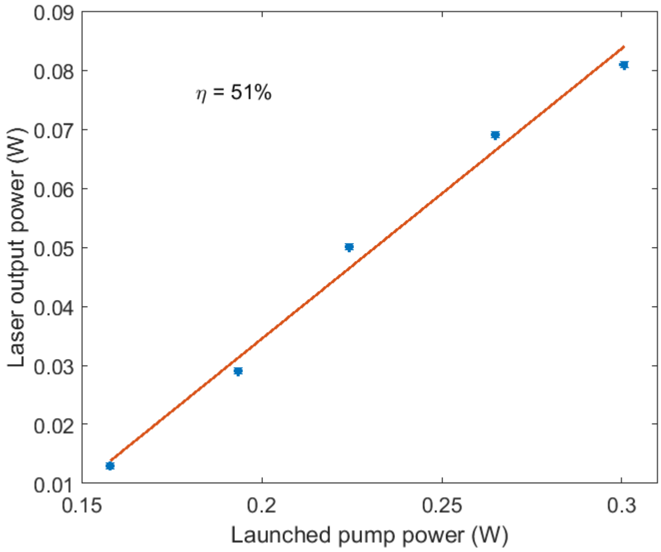

FIGURE 4.8: Measured output as a function of the launched pump power for L = 92 cm fibre. Slope efficiency with respect to launched power is 51% with an oscillation threshold of 130 mW.

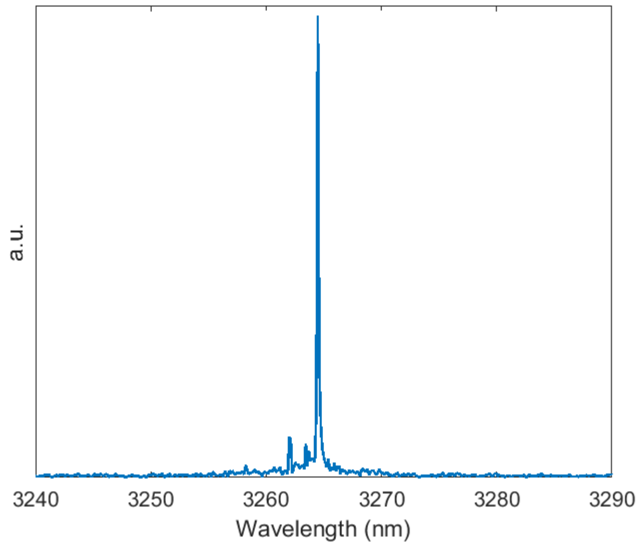

FIGURE 4.9: Measured optical spectrum for the output of a L = 140 cm length of dysprosium fibre.

the longest infrared emission from a Dy^{3+} ZBLAN fibre laser. However, tuning simply by fibre length is not particularly efficient, and this increased length exhibited an increase in oscillation threshold to 170 mW and a corollary decrease in slope efficiency to 37%. It is important to note though, that aside from comparatively more complex cascading techniques [47], this pump conversion efficiency would be greater or at least equal to the best alternative 3 µm fibre laser system.

4.4.2 Diffraction grating tuning

Discrete tuning of emission wavelength by control of fibre length demonstrated in section 4.4.1 has the drawbacks as discussed, but also clearly offers the potential of continuous tuning across a wide band. We can achieve this by the rather simple extension of the previous cavity setup by removing the butt-coupled output coupler and implementing an extended cavity segment employing a diffraction grating as the retro-reflector. A particular solution of the diffraction grating equation (4.9)

$$d(\sin\alpha + \sin\beta) = m\lambda \tag{4.9}$$

where $\alpha = \beta$ termed *Littrow configuration*, allows us to employ a grating as the retro-reflector, with angle adjustment providing frequency selectivity. A 300 l/mm plane ruled diffraction grating with an nominal efficiency of 60% reflection to the first order in Littrow configuration was used, while output is taken from the zero-order specular reflection.

For a fibre length of 1.1 m we achieve output continuously over a range greater than 300 nm. The measured tuning range is presented in figure 4.10.

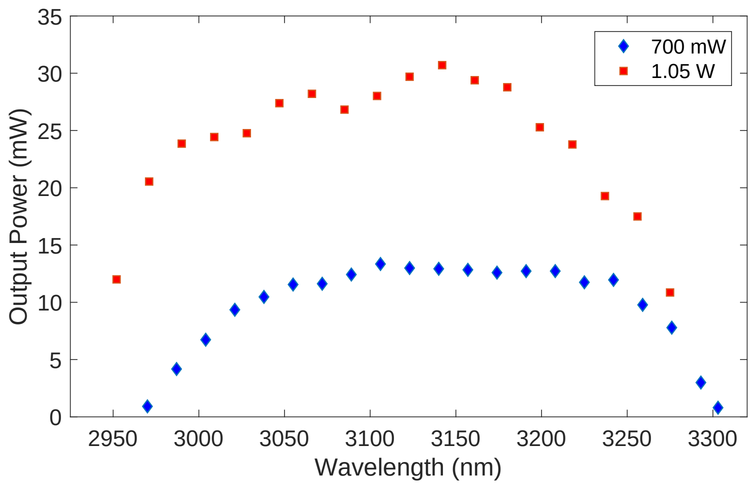

FIGURE 4.10: Measured tuning range of a 1.1 m length of Dy^{3+} fibre for two values of launched pump power.

The observed fall in output power that defines the short wavelength tuning limit of 2.95 µm is due to the discussed in-band effects and filtering provided by the input dichroic mirror. The measured limit of 3.303 µm on the long wavelength side of the range needs to be explained differently.

If we consider the oscillation condition (3.26), we can define a minimum fibre length

$$L_{min,\lambda} = \frac{\ln(1/R_1R_2)}{2g_{max}} \tag{4.10}$$

$$g_{max,\lambda} = \sigma_e N_{2,max} \tag{4.11}$$

in terms of the reflectivity of the cavity mirrors ($R_{1,2}$) and the maximum possible gain. Maximum gain (4.11) is in turn defined by the product of the emission cross section and the maximum population in the upper state, which recall for this inband scheme is capped near 60%. As the emission cross sections are reduced at increasingly long wavelength, the length of fibre required to achieve oscillation increases. With this in mind, we can increase the achievable tuning range by employing a substantially longer 1.8 m length of fibre. This length of fibre extends the long wavelength emission limit to 3.35 µm as seen in fig 4.11. The

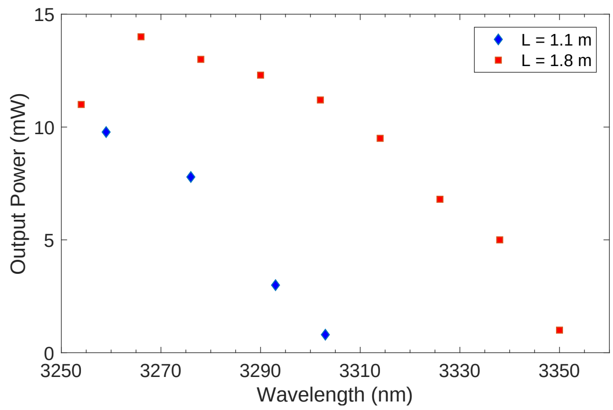

Figure 4.11: Increase in infrared tuning limit using a 1.8 m length of fibre vs. 1.1 m. The injected pump power in both cases is nominally 1 W.

emission cross sections in figure 4.12 for this long wavelength region show modest decrease beyond the observed tuning limit, indicating the strong possibility of further tuning with the design of lower loss cavities.

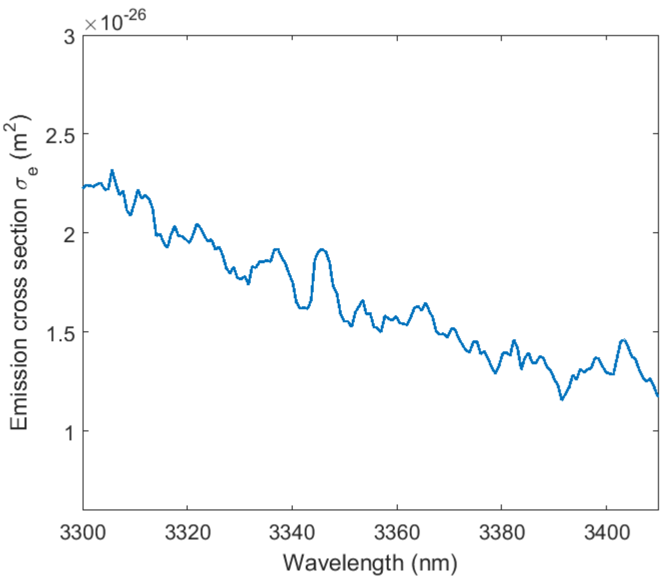

Figure 4.12: Emission cross sections in the region of maximum wavelength output.

4.5 Results analysis and fibre loss

The results presented above are encouraging, yet they certainly merit some additional analysis, specifically the conversion efficiency achieved. While efficiency of 51% is currently a record for fibre lasers in this spectral region, for this particular in-band scheme it actually represents a sizeable reduction from the quantum limit of 90%. Both previous efforts [51, 52] also exhibited efficiency well below the Stokes limit, though this was attributed at least in part to the influence of pump excited state absorption (ESA). For this in-band pumped system this effect is expected to be minimal if not negligible, so we must find another possible explanation. Given that the Dy^{3+} fibre used throughout this thesis is developmental (no standard commercial Dy^{3+} doped fibre yet exists) it is possible that the background loss of this fibre exceeds that of well characterized passive ZBLAN fibre. Recall also from chapter 1, that while there has been much improvement in ZBLAN fibre quality, the potential of contamination with OH^- is a well known issue for background loss around 3 µm [127]. For the particular in-band pumped systems presented in this chapter, the influence of loss at 3 µm would be amplified in that it would apply to both pump and signal fields. To explore this possibility, we employ numerical methods coupled with some additional experimental work based solely on pump absorption.

4.5.1 Numerical model overview

Before we attempt to quantify fibre loss using pump absorption it is important to consider the saturation effects introduced in chapter 3. We have seen there that the absorption coefficient is effectively reduced as the ground state population is depleted. Given that we are pumping unidirectionally, ground state depletion and thus the magnitude of absorption saturation will also have a length dependence. While in some instances it may be sufficient to take an average value to account for this, in our case of unidirectional core pumping the dependence on absorption with length will be strong, i.e. the input end will essentially be bleached (*pump transparency*) while the exit end may exhibit absorption near the small signal limit. Because of this we implement a full rate equation approach that while computationally more demanding, provides much greater accuracy when dealing with length dependent effects.

The rate equations governing absorption and emission have already been covered generally in chapter 3 but we need to include some additional detail for this particular case. Specifically because both pump and signal fields are contained in the fibre core, an explicit account of the mode overlap with the core is required.

$$I(r)_{p,l} = \left(\frac{2}{\pi\omega_{p,l}^2}\right)\exp\left(\frac{-2r^2}{\omega_{p,l}^2}\right) \tag{4.12}$$

$$g_{eff} = \int_0^a \left[\sigma_{e,p,l}N_2 - \sigma_{a,p,l}N_1\right] I_{p,l}(r) 2\pi r dr \tag{4.13}$$

Variation in field intensity across the fibre core for the single fundamental mode (of both pump and laser) can be represented by a normalized Gaussian intensity distribution (4.12) in cylindrical coordinates. This then serves as a weighting function for the calculation of effective gain (or absorption if g_{eff} is negative) which now needs to be integrated over the fibre radius a. This integrated effective gain is then inserted directly into the equation governing propagation of either pump or laser power (4.14) now with the inclusion of a loss term δ_{pump} as a free parameter.

$$\frac{dP_{p,l}}{dz} = (g_{eff} - \delta_{pump})P_{p,l} \tag{4.14}$$

4.5.2 Application to experiment

Using oscillation performance alone as an indicator of background fibre loss may not be adequate as the dynamics of laser performance can be affected by a multitude of factors. Single pass absorption of pump light on the other hand, is theoretically more straightforward. Therefore to try to assess possible background loss in our fibre we carry out two separate experiments looking solely at pump absorption characteristics. The laboratory setup is the same as in laser experiments with exclusion of cavity mirrors, which increases oscillation threshold well above the pump power levels used for investigation.

First we use a fixed length of fibre and monitor the residual (unabsorbed) pump light as a function of increasing launched pump power. The results of this experiment in figure 4.13 show clearly that an additional loss term is necessary for a better fit of model to measurement. Secondly, we use a fixed launched pump power and measure unabsorbed pump as a

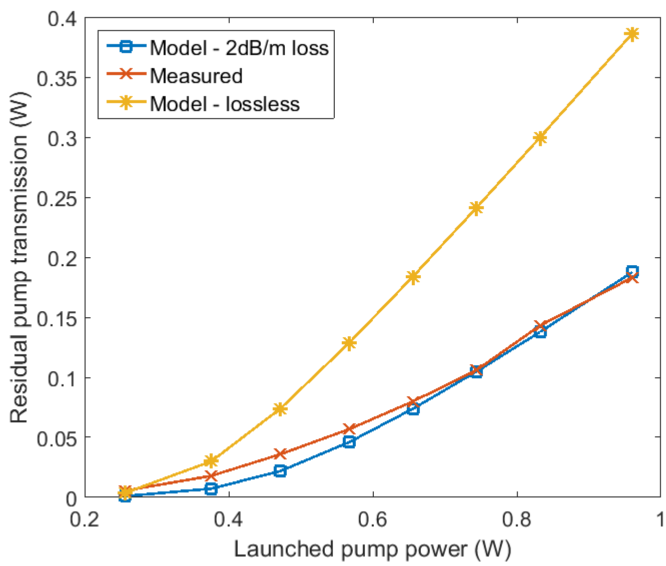

Figure 4.13: Residual pump transmission as a function of launched pump power; measured and modelled with and without additional loss term.

function of fibre length (cut back method). Again as seen in figure 4.14, without an additional loss term there is not good agreement between model and measurement. Additionally, good agreement is achieved in both experiments for the same value of the loss parameter.

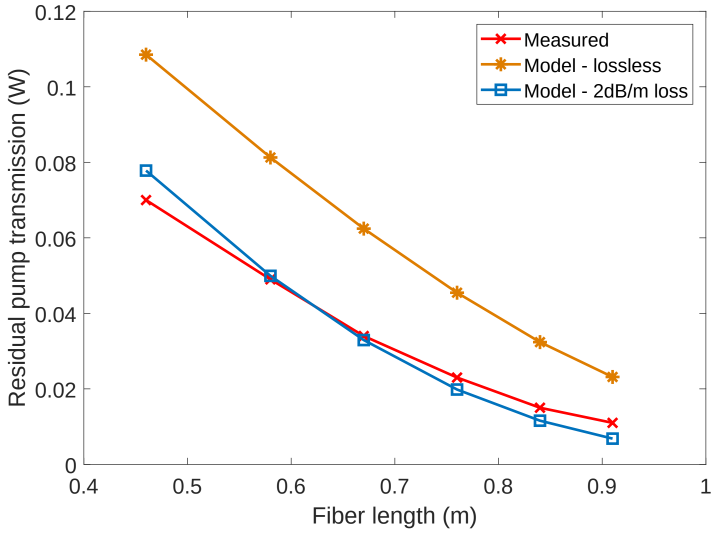

FIGURE 4.14: Residual pump transmission for a fixed input as a function of fibre length (cut back method); measured and modelled with and without additional loss term.

Having established an estimate of fibre loss grounded in experimental measurement, we can apply this loss parameter to a full rate equation treatment of laser oscillation, with the results for various test cases presented in table 4.1. Case 1 is lossless, producing efficiency

Case	δ_{pump}	δ_{signal}	Slope efficiency - η	Threshold - P_{th}
1	0	0	85%	190 mW
2	2	0	71%	227 mW
3	2	2	23%	340 mW
4	1.3	0.43	58%	230 mW

TABLE 4.1: Rate equation modelling of a $L = 92$ cm dysprosium fibre laser emitting at 3.04 µm for various values of pump and signal loss in dB m^{-1}. Experimentally measured values for η and P_{th} were 51% and 130 mW respectively.

near the Stokes limit as expected, ensuring the model performs to reasonable theoretical accuracy. The injected pump power threshold for oscillation here is somewhat larger than measured experimentally, though this can likely be explained by the fact that the experimental measurement of injected pump power relies on an estimate of fibre launch efficiency. Though this introduces some error, if the calibration factor is kept constant, efficiency measurements are unaffected. Case number 2 represents the loss estimate as applied only to the pump power, and we see that oscillation threshold is increased, and conversion efficiency is reduced, though still is larger than measured. The third case applies the same loss to both pump and signal fields, and it is clear that this is exceedingly lossy, with efficiency much lower than measured and threshold well beyond reasonable measurement error.

The last case takes both loss terms as free parameters to generate the best fit to experimental data. However, starting values for this process were based on the shape of the OH^{-1} loss peak seen in the attenuation data in figure 1.3. As previously discussed, OH^{-1} is a common impurity in ZBLAN glass, making this approach to assigning parameter values motivated by a physical reasoning, and also provides the best fit to laboratory observation. This would at least circumstantially indicate that there is a negative impact from background loss due to glass impurity, though to more conclusively attribute it specifically to hydroxyl would require direct loss measurements across a spectrum, as opposed to the single point pump measurements the approach here relies on.

4.5.3 Independent validation

Fortunately, we can also add a degree of independent validation of these loss estimates. A group led by Galzerano from Politecnico di Milano has also been conducting experimental work with Dy^{3+} doped ZBLAN fibre [128]. We have provided their group with a sample length of our experimental dysprosium fibre for characterization, affording a unique opportunity for direct comparison of independent results. With the benefit of a Cr:ZnSe laser source tunable from 2.3 to 2.9 µm they are able to probe fibre loss away from the strong absorption our Er^{3+} laser experiences. With permission, the results they obtain are presented in table 4.2.

Wavelength (µm)	P_{out}/P_{in} (%)	Measured total loss (m^{-1})	Dy absorption (m^{-1})
2.5	39.0	1.04	0.51
2.6	30.6	1.32	1.63
2.65	25.1	1.54	2.46

Table 4.2: Galzerano fibre absorption measurements

From the difference between the calculated intrinsic Dy^{3+} absorption and the total measured loss they extrapolate a propagation loss of $1.74 \pm 0.4\text{dB}\,\text{m}^{-1}$ across the 3 µm band. This reasonably concurs with our estimates, and leads to the conclusion that background loss in this fibre clearly exceeds that of un-doped ZBLAN as seen in figure 1.3. It should be noted however that though these measurements are further removed from the intrinsic absorption peak than those presented in section 4.5.2, the effect of absorption by Dy^{3+} is not negligible at these wavelengths, likely contributing to the uncertainty they estimate. Further, though the conclusion that the background loss is a static number would appear to directly contradict our circumstantial conclusion regarding hydroxyl, to make this claim more conclusively would require similar measurements done both beyond the OH^{-1} peak and the intrinsic dysprosium absorption, for example at 3.3 µm or beyond. This measurement is currently beyond our capabilities, though a further optimized version of the dysprosium laser presented in this chapter would itself make for a useful probe in loss measurements .

4.6 Summary

In this chapter we have introduced the first truly experimental work on Dy^{3+} fibre lasers presented in this thesis. By exploitation of an inherently efficient in-band pumping scheme, we are able to achieve conversion efficiency that at the time of this writing is a world record for 3 µm class fibre lasers. Increased fibre length leads to the creation of a fibre oscillator which at 3.26 µm is a penetration into a gap in the mid-IR spectrum not covered directly by any other rare earth fibre laser [129], while still retaining efficiency comparable or greater than more established Er^{3+} and Ho^{3+} based systems. To achieve continuous tuning in this particular system required a free space extended cavity arrangement with a diffraction grating, which unavoidably introduces additional loss. However, at peak output power, this arrangement achieves a spectral brightness of 155 $\mathrm{mW\,nm^{-1}}$ which may still be comparable to alternative supercontinuum sources in this region [130]. Additionally, the entirety of the tuning range effectively bridges the full gap between existing 3 µm fibre lasers and recently demonstrated room temperature emission from the Er^{3+} $^4F_{9/2} \rightarrow {}^4I_{9/2}$ transition tunable to 3.78 µm. Thus emission from ZBLAN rare earth fibre lasers alone can cover greater than 1000 nm of the mid-IR spectrum.

There remains much to be done however. For example, we know that room-temperature laser emission has been achieved at 3.4 µm in a solid state host [90]. This wavelength has high impact potential in polymer processing [131]. Following the argument presented in section 4.4.2, with further optimization, emission at this wavelength or perhaps even longer should be readily achievable from a Dy^{3+} fibre laser.

There are also some limitations to this approach which bear consideration. For instance, the requirement of a fluoride fibre laser as a pump source, while novel and effective, at the current state of the field likely represents a sizeable impact on overall system cost, as ZBLAN systems still are exceptionally more expensive than those based on silica. Further, the in-band nature of pumping restricts the full gain bandwidth. If we inspect figure 4.2 and simply compare the magnitude of the emission cross section at the achieved long wavelength to the short wavelength side, one might infer emission down to 2.6 µm may be possible. Given the increase in absorption cross section at the shorter wavelengths, emission would require much higher inversion levels, something in-band pumping cannot provide. Finally, the issue of fibre loss is perhaps a constant throughout this work, as we are only able to work with one particular fibre draw. As with other dopants, and the evolution of fibre technology in general, it may be a matter of allowing for further maturation of doping and fabrication methods specific to dysprosium.

5

Pumping at 1.7μm - source development

Having demonstrated a dysprosium fibre laser based on inband pumping in chapter 4, we are left to consider the only remaining infrared absorption yet to be investigated: 1700 nm. Aside from the simple novelty of pumping dysprosium at this wavelength, there are specific potential benefits as compared to the previous pumping schemes, inband included. Despite falling short of the Stokes limit, inband pumping still achieved conversion efficiency superior to all previous 3 µm lasers, yet this required the use of a ZBLAN fibre pump laser. While promising for future development, currently this means that the pump laser itself is still in an early stage of technological development, i.e. few commercial sources are available, and those that are available have limited output power and carry a substantial price tag. Additionally, as discussed in detail in chapter 4, the inband scheme sets a fundamental limit on the achievable gain, both in magnitude and in bandwidth. Thus it is highly desirable to investigate near infrared (NIR) pumping at 1700 nm. This should allow for access to the full gain bandwidth inherent to dysprosium, while also representing an improvement in quantum defect over previous dysprosium systems. Further, a NIR scheme allows for greater use of standard commercial optical components (lenses etc.) allowing for a greater degree of flexibility and likely a reduction in system cost, as components for the mid-IR are often costly, or in some cases simply do not yet exist. However, before embarking on any experimental work based on a NIR pumping scheme at 1700 nm, we must first identify an appropriate pump laser source.

5.1 Diode laser

As we are considering NIR pumping, we may be tempted to consider diode laser pumping, as diode lasers emitting multiple watts at 1700 nm are available and are not prohibitively costly. Diode lasers, particularly higher power variants, generally have very poor beam quality, with M^2 values exceeding 100 being common. This means that we cannot effectively couple high power diode laser light into the core of a single mode fibre. As discussed in section 3.1, this issue is solved by employing double clad fibre, where the diode pump light is coupled into a much larger diameter cladding. This is exactly the scheme employed by the most recent examples of holmium and erbium mid-IR fibre lasers discussed in chapter 1.

Direct application of a diode pumping scheme to a dysprosium system however requires some additional consideration. With a cladding pumping scheme, the overlap of the pump field with the absorbing core is small, which we can represent simply as the ratio of the core cross sectional area to that of the cladding $x = A_{core}/A_{clad}$. The fractional pump power absorbed in a single pass through a double clad fibre will then be described by

$$\frac{P_{abs}}{P_0} = \left[1 - \exp(-x\sigma_{a,p}N_{tot}L)\right] bs \tag{5.1}$$

where $x \leq 0.01$ in almost every case. Thus, to achieve even moderate absorption of pump light requires fairly large doping concentration N_{tot}. This is not a particularly negative issue in either holmium or erbium three micron systems as both laser transitions terminate on an excited state which is then rapidly de-populated. This means that signal re-absorption by the ion is not highly probable. The three micron transition of dysprosium on the other hand is a true 3-level system, with the laser transition terminating on the ground level. As there is significant population in the ground state, even under strong pumping conditions, signal re-absorption is a serious design concern. We can consider this analytically by re-arranging (3.32) to solve for absorbed power at oscillation threshold P_{th}

$$P_{th} = \frac{hv_p A\left(g_{th} + N_{tot}\sigma_a L\right)}{\tau\left(\sigma_e + \sigma_a\right)} \tag{5.2}$$

These quantities are plotted in figure 5.1 as a function of doping concentration for a representative Dy^{3+} fibre laser pumped at 1700 nm. We notice to achieve reasonable pump power absorption, requires an increasing threshold. An empirical rule of thumb for fibre laser design generally calls for single pass pump absorption of 80-90%, and we see from figure 5.1 that to achieve this would dictate a threshold in excess of 10 watts, which is beyond the output power of available diode laser systems at this wavelength. Thus we conclude that cladding pumping with NIR diode lasers is not viable at this stage, and also note how valuable the simple analytical expressions introduced in chapter 3 can be in shaping laser design. To continue with efforts at NIR pumping at 1700 nm we rather shift focus to pumping the core directly with a high beam quality laser source.

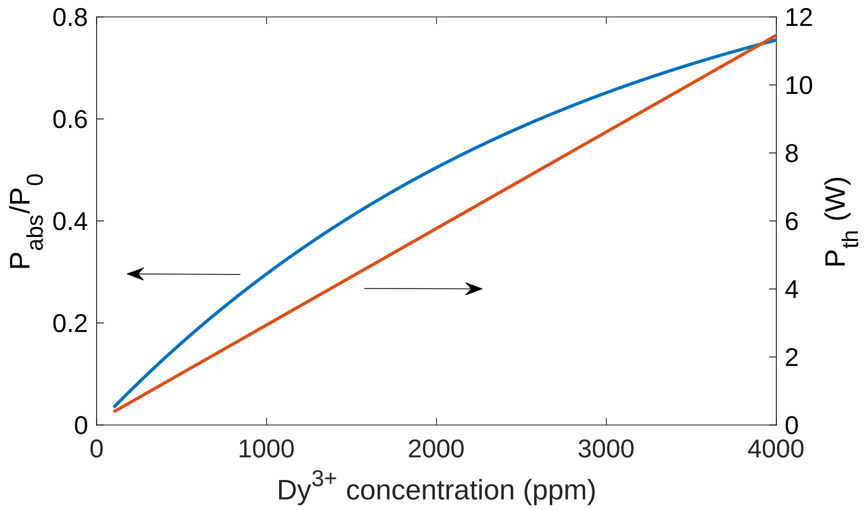

Figure 5.1: Pump absorption and threshold power calculations for a 1-m length of dysprosium fibre as a function of dopant concentration. The fibre diameter used is 12.5 µm and emission is assumed at the gain peak of 2.9 µm. Cavity mirror reflectivities used in the calculations were 100% and 4% - a common cladding pumped arrangement.

5.2 Fibre sources

To effectively couple pump light into the fibre laser core, we desire a high beam quality source, preferably one that operates on a single transverse mode. Keeping with a theme of this thesis, a fibre laser pump source would be ideal. Fortunately, there are applications beyond pumping of dysprosium which have recently motivated effort towards development of 1700 nm fibre laser sources. For example, the low loss window of silica fibre extends beyond the reach of the erbium doped fibre amplifiers (EDFAs) commonly used in optical communication, meaning that new sources around 1700 nm could open the possibility of increased data transmission over existing fibre networks. Additionally, the C-H bond exhibits a strong overtone stretching resonance in this wavelength range, indicating promising applications in processing of a variety of polymers [132], as well medical applications targeting lipid-rich tissue [133].

5.2.1 Bismuth

Bismuth (Bi) as a dopant for radiative emission is relatively new, having only been shown to emit luminescence when doped into aluminosilicate glass in 2001 [134]. Emission from Bi-doped glass emits over a quite broad range from 800 to 1700 nm, which has attracted a fair amount of interest for laser and amplifier applications. The first CW Bi fibre laser was demonstrated in 2005 [135] but was limited in emission from 1150 to 1300 nm. Since then however, several Bi-doped fibre lasers have been demonstrated across a range of wavelengths, with output powers at select wavelengths exceeding 10 W (see figure 5.2). Bismuth fibre lasers emitting at the desired wavelength of 1700 nm have been demonstrated [136], but despite recent improvement of nearly 50% in both maximum output power and slope efficiency [137], they are currently limited to 1 W of output power. Therefore we conclude that though

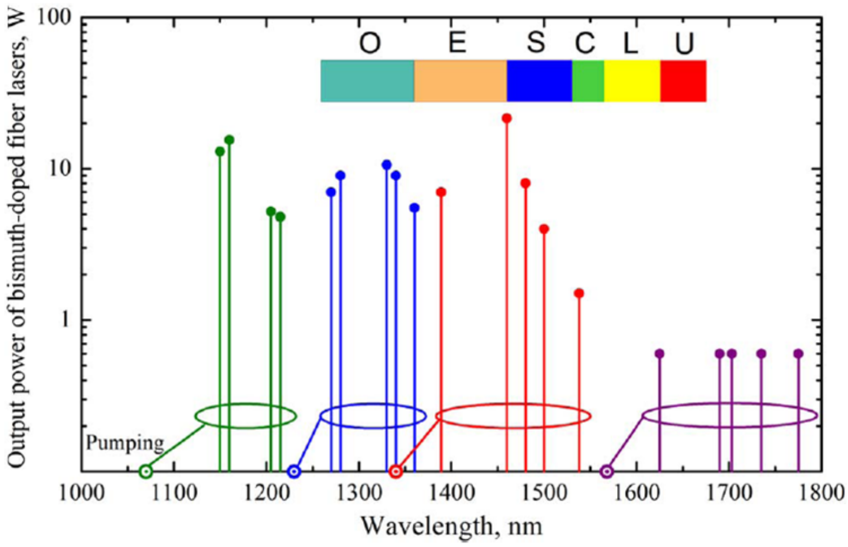

FIGURE 5.2: Bismuth doped fibre laser performance across the spectrum. Image adapted from [135].

promising for future efforts, Bi doped fibre lasers are not well suited to the present work.

5.2.2 Thulium

Thulium as a rare earth ion for laser emission has seen substantial commercial success as a 2 micron laser source [138], yet the transition it operates on is actually quite broad, with lasers tunable to nearly 1800 nm having been demonstrated [139, 140]. Further, short wavelength tuning should be possible provided a high level of population inversion is achieved, as we can see from figure 5.3 that a fully inverted system shows net positive gain shorter than 1600 nm. Indeed recently, watt-level emission from a thulium fibre has been achieved down to 1660 nm [141] by utilizing a fibre with low dopant concentration and single mode core design. This system is attractive for our purposes for multiple reasons, one that the slope efficiency achieved at 1700 nm was 50%. Secondly, the pump source was a commercial Er:Yb laser emitting at 1565 nm, ensuring a higher level of robustness than most in-house built laser systems. Finally, a high power variant of the tunable system was demonstrated at 1726 nm which exhibited a high slope efficiency of 67% and importantly a peak output power of 12.6 W, indicating that high power emission at 1700 nm should be readily achieved. Though this thulium system should certainly by viable for pumping of dysprosium, there is perhaps a more convenient approach.

5.2.3 Raman fibre

Before fully introducing the concept of a Raman fibre laser, it should be necessary to briefly discuss the Raman effect itself. C.V. Raman discovered his namesake scattering effect in 1928 [142], and though full explanation of it requires a quantum mechanical treatment, we can understand it qualitatively by the energy diagram in figure 5.4. Here light incident on

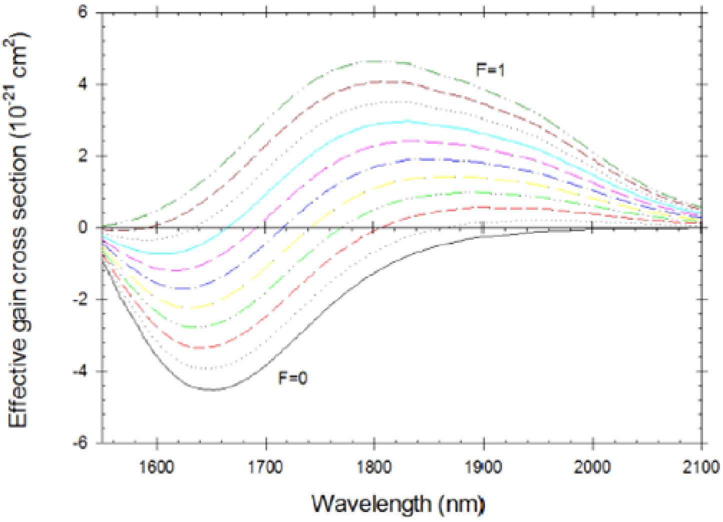

Figure 5.3: Effective gain cross section of Tm^{3+} for increasing levels of fractional population inversion F. Image adapted from [141].

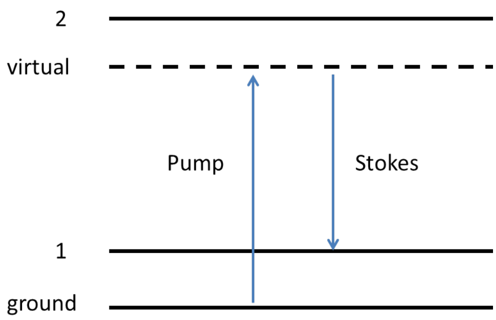

Figure 5.4: Energy level diagram depicting Raman Stokes scattering as an interaction with a virtual state (dashed line).

a medium will be scattered in part to light of a reduced frequency (longer wavelength) by excitation from the ground state to a so-called *virtual state* of the medium, which is associated with the excited level 2, followed by radiative relaxation to level 1. The difference in frequency of the incident and scattered light is called the Raman shift, and is medium dependent, varying greatly over many studied materials. The inverse process is also possible whereby the scattered light is of larger frequency, and is termed anti-Stokes Raman scattering, though this effect is substantially weaker, and is not considered further here.

While the scattering process described above is spontaneous, and often rather weak, if the incident light is sufficiently intense, and/or the interaction length with the scattering medium is long, stimulated Raman scattering (SRS) can occur. This process can actually be very efficient, and in contrast to the spontaneous process, results in highly directional forward and backward scattered light [143]. Considering the small core diameters and long lengths typically encountered in fibre optics, it should not be surprising then that SRS in optical fibres has been studied extensively.

Conversion of pump to Stokes light in an optical fibre can occur in a single pass, a fact which can have significant detrimental impact on optical communication based on multiple wavelengths in that if signal intensity is too large, the Raman effect induces cross-talk as power in one channel can be scattered to another. However, this can also be exploited intentionally in the form of a Raman fibre amplifier, where one injects a weak signal along with a strong pump beam. If the frequency separation of these two fields is within the Raman bandwidth (discussed in more detail in section 5.3) then the signal will be effectively amplified by the transfer of energy from the pump beam. The concept can be extended to oscillation if we place the fibre in a resonant cavity, creating a Raman fibre laser (RFL) [144]. Similar to traditional laser radiation beginning from noise, spontaneous scattering here is resonated in the fibre, reaching high enough intensity to become an efficient stimulated process. RFLs have allowed for the creation of fibre lasers at wavelengths not directly covered by actively doped lasers. We choose to pursue this route to realize a 1700 nm fibre laser pump source.

5.3 Raman fibre laser design

NIR pumping of dysprosium has the previously stated advantage of allowing for the use of standard commercial optical components, perhaps the most important of which is single mode silica telecommunications fibre (SMF-28). Since Raman properties of silica glass are well known, we can start to quantify some parameters relevant to a RFL design. To begin with, we can define a Raman gain coefficient g_r that governs the growth of the Stokes power P_s through [145]

$$\frac{dP_s}{dz} = g_r P_p P_s \tag{5.3}$$

where we see that the Stokes power grows exponentially with pump power P_p. The value of g_r for silica glass is reported in the literature as nominally 1×10^{-13} m/W for a pump wavelength of 1 µm [146]. This value scales inversely with pump wavelength, and though it is small compared to other Raman media, this value can be increased by adding GeO_2 to the glass [147]. Also recall that due to tight confinement and long interaction length, a Raman fibre can generate substantial power with small gain.

To determine the correct pump wavelength we note that the peak Raman gain occurs for a frequency shift of 13.2 THz. Setting the target Stokes wavelength of 1700 nm then allows us to back calculate the pump wavelength as 1582 nm, a value slightly beyond the typical 1550 nm emission of erbium doped fibre lasers, though still achievable. However, the exact specification of pump wavelength can be relaxed somewhat by noting that the Raman gain spectrum of silica is actually quite broad. Though this spectrum can be measured experimentally, Holenbeck and Cantrell take an analytical approach by considering the Raman response in terms of a summation of several vibrational modes of the SiO_2 molecule [148]. The resultant response function is

$$h_R(t) = \sum_{i=1}^{13} \frac{A_i}{\omega_i} \exp(-\gamma_i t) \exp(-\Gamma_i^2 t^2/4) \sin(\omega_i t) \tag{5.4}$$

where A_i is the amplitude of the ith vibrational mode, ω_i the angular frequency, while γ_i and Γ_i are Lorentzian and Gaussian linewidths respectively. The imaginary part of the Fourier transform of this function represents the Raman gain, which we calculate using parameter values given by [148] and present in figure 5.5. We can then use this spectrum to calculate

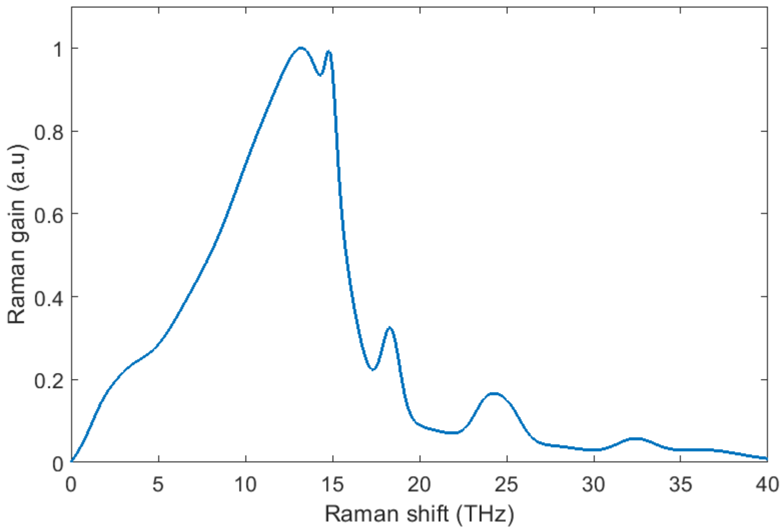

Figure 5.5: Calculated Raman gain spectrum of silica.

the pump wavelength spectrum by setting the target wavelength of 1700 nm as the zero frequency shift, as seen in figure 5.6. We see that there is appreciable gain in the common

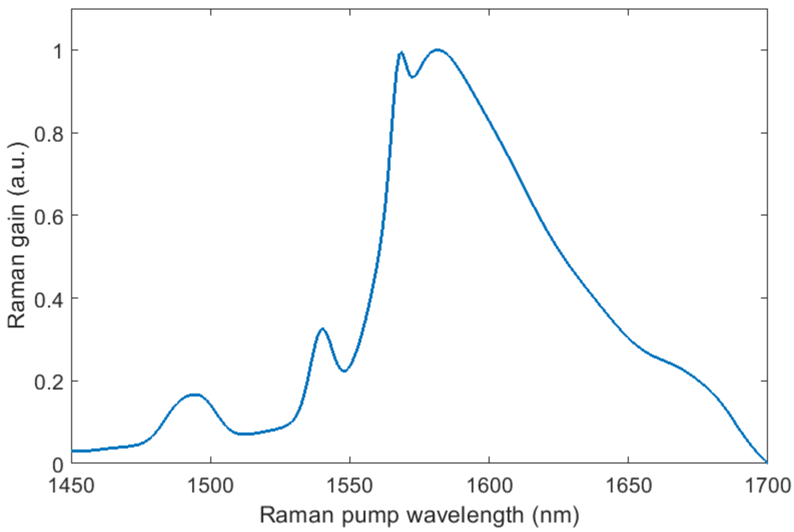

Figure 5.6: Calculated Raman pump spectrum generated by setting 1700 nm as zero frequency shift.

1550 nm emission window of erbium doped fibre lasers, thus this will be a suitable pump source.

As fibre laser cost often scales (even nonlinearly) with output power, we must finally consider the power level required to create a useful 1700 nm pump source. To create an estimate, we can refer to the approximation for Raman threshold P_{th}, which is defined as the pump power at which the Stokes power is equal to the pump power at the fibre exit [149]

$$P_{th} \approx \frac{16A_{eff}}{g_R L_{eff}} \tag{5.5}$$

where $L_{eff} \approx L$ for fibre lengths of a few kilometres or less and $A_{eff} = \pi w^2$ where w is the Gaussian approximated waist of the fundamental fibre mode. Comparing the spectrum to the previously noted peak Raman gain at 1 µm produces threshold power estimates well less than 1 W even for pump wavelengths off the gain peak, provided several km of fibre are used. This threshold power reduces further if a resonator is employed, as we will aim to do.

5.3.1 Er/Yb pump source

Erbium doped fibres are readily commercially available, often employed in erbium doped fibre amplifiers (EDFAs), though one can quite easily employ them as a laser oscillator. Emission around 1550 nm from erbium originates from the ground state terminated $^4I_{13/2} \rightarrow {}^4I_{15/2}$ transition, meaning that, similar to the three micron transition of dysprosium, effective emission requires a relatively high degree of excitation. However, if this is achieved, the emission bandwidth of this transition is actually rather broad, as seen in figure 5.7. In

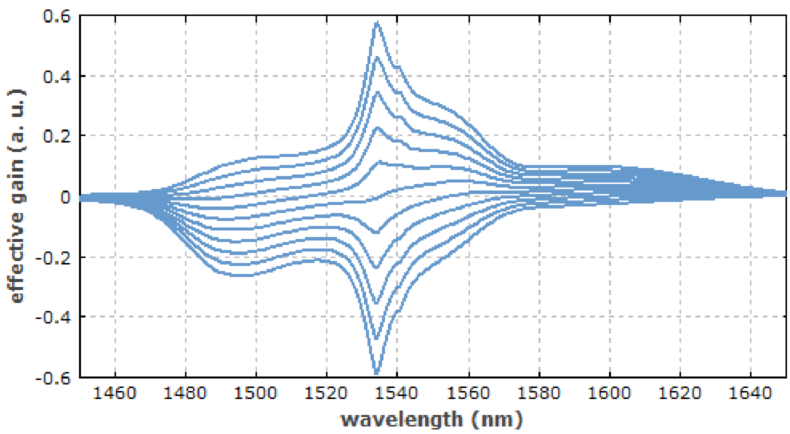

FIGURE 5.7: Effective gain of erbium doped media for increasing levels of excitation. Image adapted from [150].

order achieve a high degree of population inversion, a common technique is to co-dope the gain medium with ytterbium (Yb) [151]. As illustrated in figure 5.8 this has the effect of augmenting pump absorption around 980 nm. While erbium has intrinsic absorption here, it is not particularly strong; ytterbium on the other hand has very strong absorption in this band, and efficiently transfers energy to the erbium ion.

With this in mind, we constructed an in-house Er/Yb laser based on commercial (Nufern SM-EYDF-10P/125-XP) double clad fibre, the schematic of which is shown in figure 5.9.

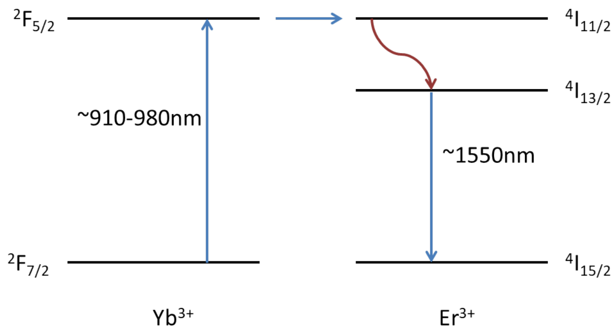

Figure 5.8: Energy level diagram illustrating energy transfer in a Er/Yb co-doped system; the curved arrow indicates fast non-radiative relaxation.

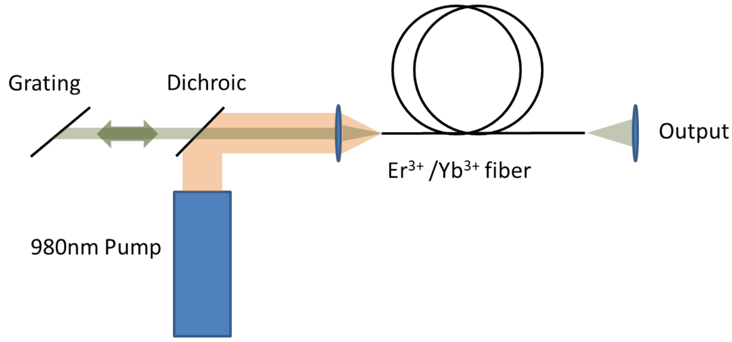

Figure 5.9: Laboratory setup of the Raman pump Er/Yb laser.

Pump light is provided by a high-power 980 nm diode laser (nLight) and is coupled into the cladding 125 µm of the Er/Yb fibre. The Er/Yb fibre has a core diameter of 10 microns, which is larger than standard single mode Er fibre, but still operates in the single mode regime, with a cutoff wavelength of nominally 1510 nm. The fibre operates as a low threshold laser simply with the Fresnel reflection from two perpendicular cleaves serving as the cavity mirrors, although this *free-running* configuration results in emission around 1530 nm, unacceptably low on the Raman gain spectrum shown in figure 5.6. To address this, we implement an extended cavity with a diffraction grating in Littrow configuration providing the required feedback. Doing so allowed for a maximum wavelength emission of 1570 nm, which is near peak Raman gain.

While this laser outputs a maximum power of more than 5 W, a value which should be sufficient for creation of a Raman fibre laser, it was found to suffer from two detrimental effects. One is inherent in the co-doping scheme used, and that is that at sufficient pump power levels, the Yb has parasitic emission effects, in our case in the form of parasitic lasing around 1066 nm. This is detrimental to our efforts in that it inhibits further power scaling of laser output as shown in figure 5.10. We see that the output power is no-longer linearly scalable at higher powers as parasitic lasing becomes more prominent. Additionally, because Yb emission falls well outside of the Raman gain spectrum for generating 1700 nm Stokes light, onset of parasitic Yb emission also sets a limit on Raman output scaling.

The other effect was observed empirically, and that is optical feedback into the Er/Yb laser cavity. While the exact dynamics are not entirely clear, it was conclusively shown

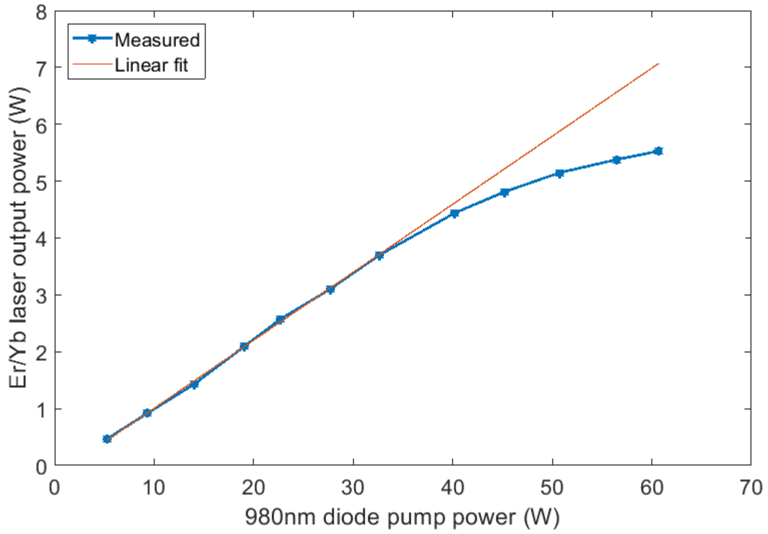

FIGURE 5.10: Output power of the Er/Yb laser as a function of diode laser output. Output power rolls over at high pump powers as compared to a projection of the lower power linear regime due to parasitic Yb oscillation. Output power measured is total power, including any parasitic lasing of Yb.

that even a small amount of feedback (reflections from the input facet of the Raman fibre) into the laser cavity substantially reduced the output power at a given pumping level. To address this a Faraday optical isolator was placed at the output of the Er/Yb laser, ensuring any feedback would be suppressed. While this was effective at eliminating the impact of feedback it introduced a new complication relating to the polarization state of the laser, as the isolator operates on transmission of a defined polarization state. Though the modes derived in chapter 3 are linearly polarized, the fundamental mode then will be degenerate in that any linear polarization state in the fibre can be decomposed into contributions from two orthogonal linearly polarized modes. In theory this is not an issue, as the initial alignment of the optical isolator can be adjusted for any input polarization. In practice however, the Er/Yb laser fibre exhibits some amount of birefringence that can be altered randomly by environmental (thermal in particular) factors during operation. This resulted in the transmission of the isolator drifting with time, and substantially reducing at higher operating powers. In the absence of appropriate wave plates external to the cavity to correct the polarization state during operation, we place a section of the laser fibre in a mechanical polarization controller (based on paddles). By adjusting the orientation of the paddles we are able to both increase and add a higher degree of stability to isolator transmission over the entire operating range.

5.3.2 Raman laser emission at 1700 nm

Despite the limitations in our Raman pump source outlined above, we do achieve watt level output from a Raman fibre laser. Using 1:1 imaging with a pair of aspheric lenses, pump light at 1570 nm can be injected into standard SMF-28 single mode fibre with an efficiency of 80%. Two lengths of fibre were tested for Raman output, 500 meters, and 6 km. Single pass Raman conversion in the shorter section of fibre was not observed at the pump power limit. Single pass Raman conversion was observed in the longer section of fibre, though as seen in figure 5.11 the Stokes signal falls short of our target wavelength of 1700 nm. In

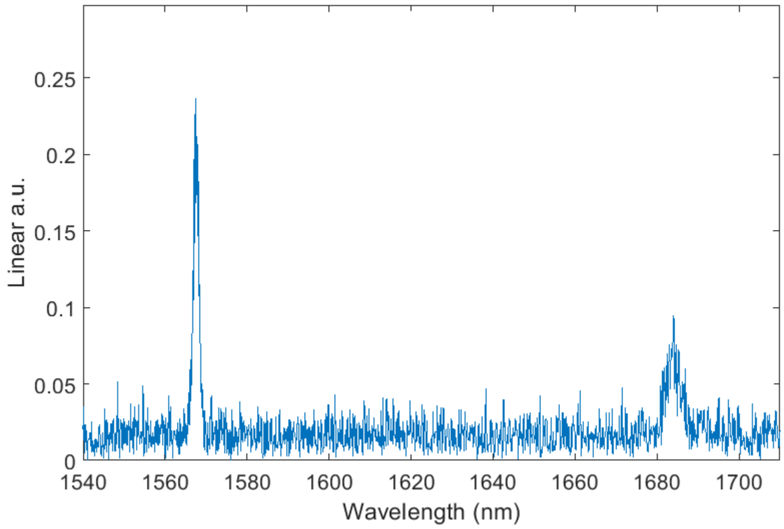

Figure 5.11: Optical spectrum of the single pass Raman output of 6 km of SMF-28 fibre.

order to produce a true Raman *laser*, fibre Bragg gratings (FBGs) serving as cavity mirrors were spliced to each end of the SMF-28 fibre, with the input grating providing a nominal 99% reflectivity at 1700 nm, and a 10% reflector serving as the output coupler at the distal end. This arrangement successfully produced narrowband output at 1700 nm as seen in the optical spectrum in figure 5.12. As the Er/Yb pump laser power is increased, the output of

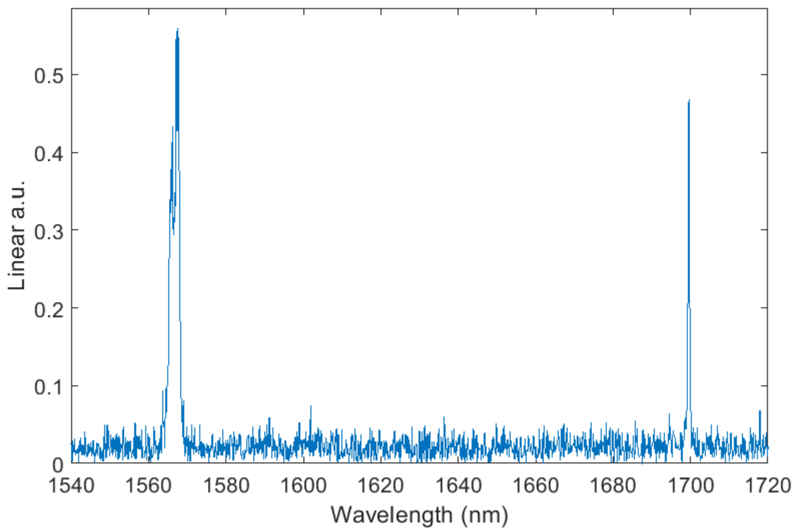

Figure 5.12: Spectral output of the Raman fibre laser (RFL) near conversion threshold.

the RFL is seen to progress towards purely 1700 nm Raman-shifted output as the pump is more efficiently depleted. Output power at 1700 nm as a function of pump laser incident power is presented in figure 5.13. Conversion efficiency of 30% with respect to incident pump

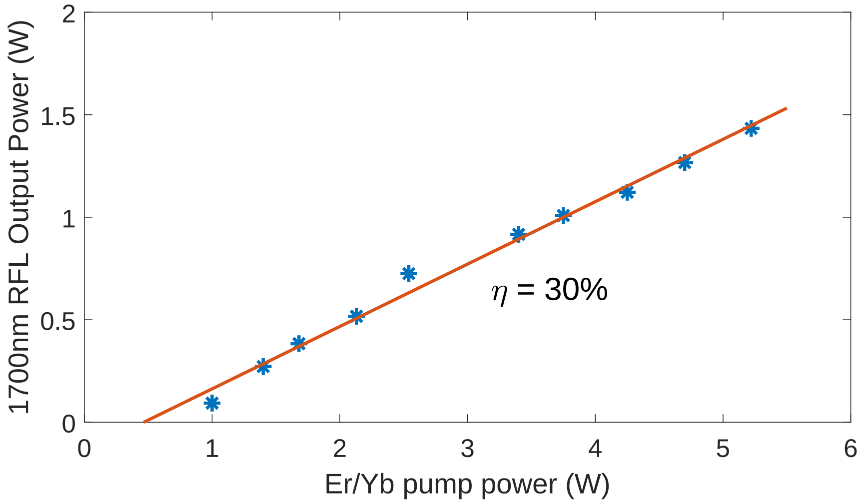

FIGURE 5.13: Raman laser output power as a function of incident pump power. Conversion efficiency of 30% is indicated, with a linear fit conversion threshold calculated as 460mW incident pump power.

power was achieved, with a threshold power of 460 mW, while maximum output power is nominally 1.5 W, as limited largely by the performance limitations of the Er/Yb pump source as discussed above.

5.4 Summary

Several potential sources of 1700 nm laser emission for NIR pumping of dysprosium have been considered. While diode pumping is successfully employed in many other 3 micron class fibre lasers, it is shown by simple analytical argument to not be viable with current available technology. Though this may change in the future, we note that the oscillation thresholds are likely to be multiple watts. However, there may be the possibility of threshold reduction with careful cavity design and specifically engineered fibre (co-doping or small clad-to-core area ratio for example). For present work we focus then on core pumping with fibre laser sources, of which bismuth and thulium doped fibres are considered. Both technologies are promising for this application, and thulium fibre lasers in particular have been shown to well reach the anticipated pump power levels required for dysprosium laser operation. In an effort to mitigate risk however, we decide to pursue rather a Raman fibre laser as it relies on more mature technology of Er/Yb fibre lasers and standard SMF-28 fibre.

Operation of a Raman laser emitting at 1700 nm was successfully achieved, with output power exceeding 1 W. While the performance of the Raman laser is anticipated to suffice for the proof of principle experiments conducted in this work, there are several clear optimizations that could be made in future endeavours. For instance a MOPA (Master Oscillator Power Amplifier) configuration of the Er/Yb pump source should allow for further scaling of useful 1570 nm output power. Further, Raman fibre lasers are routinely demonstrated at much higher conversion efficiency over much shorter lengths of fibre [152]. Higher efficiency could most likely be achieved with this system if SMF-28 fibre was replaced with small core diameter GeO_2 doped fibre, resulting in reduced threshold, increased Raman gain, and reduction in background loss by using substantially shorter lengths of fibre.

6

Near infrared pumping of dysprosium

The previous chapter outlined the motivation to pursue near infrared (NIR) pumping of dysprosium at 1700 nm, and after careful consideration of source candidates a Raman fibre laser (RFL) was deemed the most promising. Following this was the design and successful construction of a RFL emitting watt-level power at 1700 nm. As discussed, there were various technical issues which limited the system performance and may be detrimental to the previously anticipated success of employing the RFL as a pump source for a mid-IR dysprosium laser. In this chapter we will first present an analytical assessment of pump system viability before determining the optimal system design for a Dy^{3+}:ZBLAN fibre laser. Following this we will implement a laboratory demonstration of a NIR pumped dysprosium fibre laser. While successful as a proof of principle effort, this system will ultimately fall short of performance benchmarks set in chapter 4. However, experimental measurements conducted here will allow for a deeper analysis of the dysprosium system itself, and may prove instrumental in shaping future work. Additionally, the wide gain bandwidth offered by removal of the inband gain restriction indicates strong potential for modelocking.

6.1 System design

In chapter 5 we saw how useful analytical calculation of oscillation can be in determining system design, and we will employ similar effort here. From the theoretical discussion of three level laser systems in chapter 3 we know *a priori* that a high cavity 'Q' (low resonator loss) is a desirable condition. Due to this, and the availability of optics, we choose to fix cavity mirrors at $R = 1$ and $R = 0.5$, which is identical to the cavity implemented in the inband pumping work in chapter 4. Using 1 m as an initial estimate of cavity length, we can then use (3.26) to calculate the gain required at threshold, and (3.32) to calculate the absorbed pump power required to generate said gain. This generates an estimate for absorbed pump power threshold of 250 mW. However, this approach ignores ground state depletion, which we not only anticipate, but have previously observed, and also does not include any additional signal loss, therefore for increased accuracy we implement the system of rate equations previously described (chapters 3 and 4) including an additional loss term. Doing so yields an increased threshold of 400 mW, though the available RFL pump power should still suffice.

The value for pump power threshold is in terms of *absorbed* power, thus since we began with an estimate of desired fibre length, we should also be concerned with the absorption per unit length of fibre, as again the three level nature of this system dictates that sections of fibre that remain relatively unpumped will have a direct impact on oscillation in the form of signal re-absorption. As is often done in published work, we could use the small signal absorption coefficient ($\alpha = \sigma_a N_{tot}$) though this would yield greater than 99% absorption in 1 m of fibre. Recall the previously defined quantity pump saturation however (equation (3.31)), and note here that this value is nominally 50 mW, meaning that pump absorption estimates based on small signal values are not valid. Again we can implement the rate equations, and we find that to achieve 400 mW of pump absorption requires an injected power of 460 mW, with 87% pump absorption, thus 1 m length should be well suited.

One additional concern worth mentioning is that the dysprosium doped ZBLAN fibre used for these experiments, though designed for single mode operation in the mid-IR around 3 µm supports multiple modes at the intended pump wavelength of 1700nm, with a designed cutoff wavelength of 2.6 µm. Modal analysis following chapter 3 reveals that the LP_{11} mode is supported in addition to the fundamental LP_{01} mode at 1700 nm. However, integration of the intensity profiles (given by equation (3.17) and (3.18)) over the core region show that overlap for the LP_{11} mode is only slightly reduced. Additionally, by injecting single mode light from the RFL well matched to the fundamental mode size, we do not expect significant excitation of the higher order pump mode. Thus for further calculations the fundamental mode size as defined by the Marcuse equation (3.19) is used with confidence.

6.2 Experimental setup

Very much similar to the inband pumping experiments of chapter 4, we implement two slightly different variants of optical cavity here, one with butt-coupled cavity mirrors, and one an extended cavity version which allows for tuning with a diffraction grating. We outline the setup of each here, while also introducing a new optical element, the off-axis parabola (OAP), to address the impact of lens aberration and focal shift in an extended cavity.

6.2.1 Closed cavity

The setup for the butt-couple mirror cavity (or *closed cavity*) is presented in figure 6.1 The RFL configuration has been previously described in chapter 5 but for completeness will be included in the following system summary. A high power diode laser pumps a length of Er/Yb co-doped fibre. This fibre is in a laser cavity defined by a diffraction grating in Littrow configuration at one end, and a Fresnel reflection from a perpendicular cleave serving as the output coupler. After collimation by a f=11 mm aspheric lens a dichroic mirror reflects the desired 1570 nm laser emission and transmits any unabsorbed 980 nm pump light into a

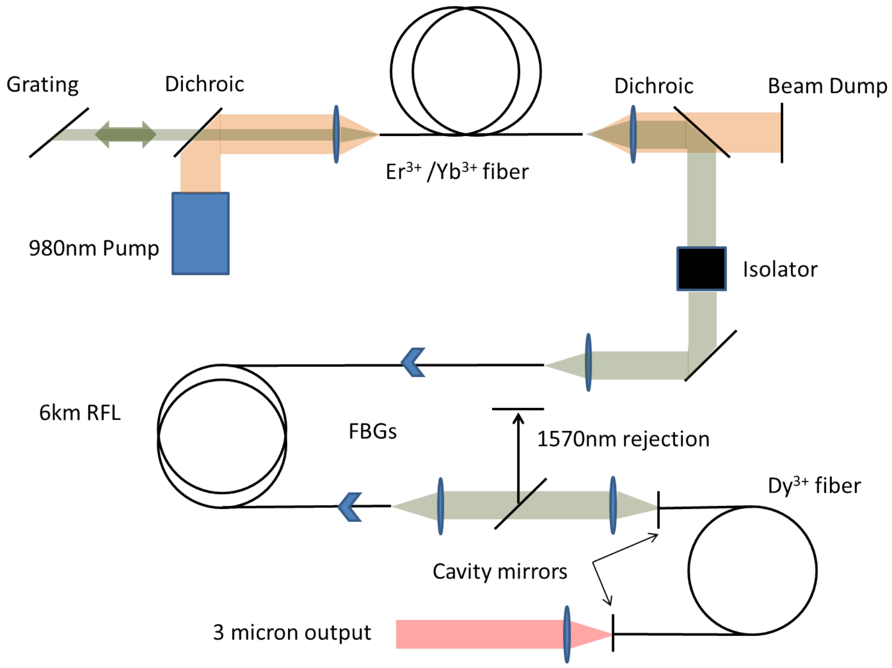

Figure 6.1: Laboratory setup for NIR pumping at 1700nm.

beam dump. Following this is an optical isolator, required to eliminate detrimental feedback into the Er/Yb laser system. Output of the isolator is then focused with a matched f=11 mm aspheric lens into 6 km of SMF-28 silica fibre. The SMF-28 fibre in turn acts as a Raman fibre laser (RFL) with a highly reflective at 1700 nm fibre Bragg grating (FBG) spliced to the input end, and a nominally 10% reflective FBG serving as the output coupler. Output of this fibre is then collimated with a f=25 mm aspheric lens, noting that collimation is tested specifically at the desired 1700nm output wavelength, as at lower operating powers both pump and Stokes power are emitted from the RFL. Due to the un-depleted Raman pump light, a dichroic mirror transmitting only 1700nm is placed between the RFL and target ZBLAN fibre. We note also that though there is no isolation between the RFL and the ZBLAN fibre laser, we observe no impact on RFL performance from any possible back reflections.

RFL pump light is then coupled into Dy^{3+} doped ZBLAN fibre with a matched f=25 mm aspheric lens. The fibre is identical in all specifications to that used in the inband pumping experiments. Note here that the input lens is a standard NIR component and is not sufficiently transparent at 3 microns, dictating that an alternative optical setup would be required if an extended cavity input was desired. The mid-IR laser cavity is comprised of butt-coupled mirrors, the input being highly transmissive at 1700 nm and highly reflective across the 3 µm band, and the output coupler is nominally 50% reflective across the 3 µm band. Laser output is collimated with a f=20 mm CaF_2 plano-convex lens. Output diagnostics include thermal power detection, a pyroelectric camera for visualizing output mode profile, and a high dynamic range optical spectrum analyser (OSA) for measurement of wavelength.

6.2.2 Extended cavity

The extended cavity variant is implemented so that diffraction grating tuning can be implemented. This systems is identical to the setup presented above with the sole exception of the ZBLAN fibre output end where we remove the butt-coupled output coupler. In this arrangement, the plano-convex CaF_2 lens used to collimate output in the closed cavity arrangement is abandoned in favour of an off-axis parabola (OAP). An OAP is a mirror equivalent to a section of a parent parabolic reflector, and though somewhat more difficult to align than a standard lens, offers several advantages in this particular system. To illustrate this we conducted some simple imaging experiments with a Ho^{3+}/Pr^{3+} laser emitting around 2.8 µm. This laser was in-house constructed based on diode pumping of double clad fibre at 1150 nm. This system is well-established in our research group [45, 152] and was selected for these imaging experiments due to its availability, and that it is able to emit stable output power in excess of 100 mW, which allowed for higher accuracy beam width calculation than using a dysprosium source directly. Additionally, the single mode core of this fibre possesses similar specification to the dysprosium fibre in terms of core diameter and single-mode cutoff wavelength. Figure 6.2(a) is the output (visualized with a pyroelectric camera) of the Ho/Pr single mode laser collimated using a plano convex CaF_2 lens. The intensity distribution shows a series of strongly modulated circular rings, which are indicative of spherical aberration. This is a common result of using a simple spherical lens to collimate what is effectively a point source (emission from the fibre core). Whereas figure 6.2(b) is the same output now collimated with an OAP, which results in a clearly Gaussian beam. The difference between the two is more significant than just visual however, as in our case we aim to re-inject the collimated beam into the core of a single mode fibre in an extended cavity arrangement. Any aberration of the beam will directly result in an increase in the achievable spot-size as the beam travels back through the imaging system (lens or OAP) translating to increased cavity loss.

To quantify the impact aberration can have on an extended cavity arrangement we desire to measure the spot size produced by each beam directly. As the pixel size of the camera used for imaging these mid-IR beams is too large to image a spot on the order of dimension of the fibre core, we instead implement a knife-edge measurement. To understand the measurement, note that the intensity profile of a Gaussian beam is represented by

$$I(x,y) = I_0 e^{-2x^2/w_x^2} e^{-2y^2/w_y^2} \tag{6.1}$$

where $w_{x,y}$ are beam waists in the x and y directions. The total power of this beam is the integral of (6.1) with limits $\pm\infty$, but we can more practically define the lower limit as 0 being some point far enough from the beam centre to not effect the actual power measurement. If we introduce a knife edge increasingly blocking the beam from the $+\infty$ direction, the measurement of power will be proportional to the integration up to the location of the knife edge

$$P \propto \int_0^x I(x,y)dx \tag{6.2}$$

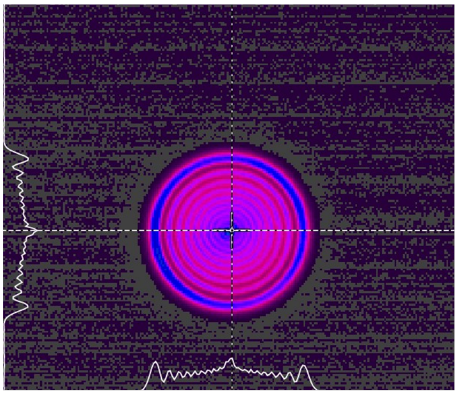

(a)

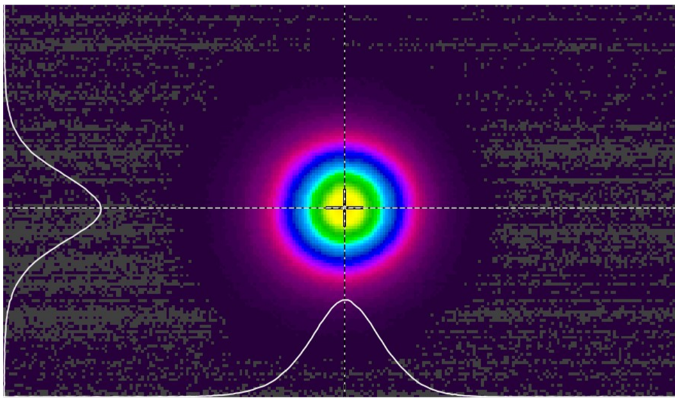

(b)

Figure 6.2: Collimation of the output of a single mode Ho/Pr mid-IR laser achieved with (a) a f=20 mm plano convex lens, (b) an OAP of reflected focal length f=15 mm.

Introducing the error function then

$$\mathrm{erf}(x) = \frac{2}{\sqrt{\pi}} \int_0^x e^{-u^2} du \tag{6.3}$$

indicates that a measurement of power past a translating knife edge obstruction for a Gaussian beam will be proportional to the error function, and indeed with some manipulation, we can generate the following

$$P_{meas} = \frac{c_1}{2} \left[1 \pm \mathrm{erf} \left(\frac{\sqrt{2}(x - c_2)}{c_3} \right) \right] \tag{6.4}$$

where the c's are fitting coefficients, with specifically c_3 representing the $1/e^2$ radius of the Gaussian beam.

For the actual measurement, the Ho/Pr laser output is collimated by either a plano convex lens or an OAP, and then re-focused by a matched element (lens or OAP). A knife edge mounted on a precision x-y-z translation stage allowed us to locate the nominal z-axis location of the focused beam waist. At this position the knife edge is then incrementally translated across the beam in the y-axis and transmitted power is recorded (note that to be complete would require a similar procedure for the x-axis, though we see from figure 6.2 there is a high degree of circular symmetry in both cases). The measured result for the plano-convex lens case, along with a least-squares generated fit to the knife-edge function (6.4) is presented in figure 6.3. While the fit is not ideal, indicating that the focused spot

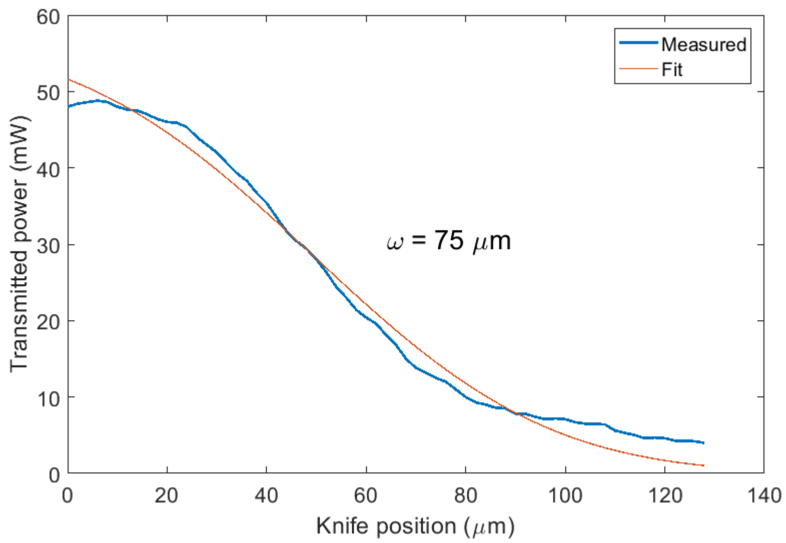

FIGURE 6.3: Measured knife edge data for a beam collimated and focused with a pair of plano-convex lens and a least-squares fit to the transmission function.

deviates from a pure Gaussian, what is more striking is that the waist generated is 75 µm. The fundamental mode of the Ho/Pr fibre is calculated to be nominally 8 microns in waist size, thus this 1:1 imaging should be expected to produce much less than a 75 µm spot at focus. The same measurement for a pair of OAP's with reflected focal length f=15 mm is presented in figure 6.4 The fit to the transmission function here is excellent, and the beam waist calculated is much closer in line with expectations. While the implications of this may be obvious, to put it in even more quantitative terms we make use of the single mode fibre coupling efficiency equation

$$\eta = \frac{4\omega_1^2\omega_2^2}{(\omega_1^2 + \omega_2^2)^2} \tag{6.5}$$

Strikingly, if use ω_1=8 µm from the Ho/Pr fibre, this equation would yield coupling efficiency of 85% for the OAP case, and 10% for the plano-convex case. Clearly spherical aberration is an issue when coupling light into single mode fibre; a fact that though should be practically obvious has been often overlooked in some published research. Before moving on there is an additional benefit to OAPs not yet mentioned, and that is because they rely on reflection not refraction, they are inherently achromatic, exhibiting no focal shift with wavelength, a very useful property when attempting to design broadband or widely tunable laser sources.

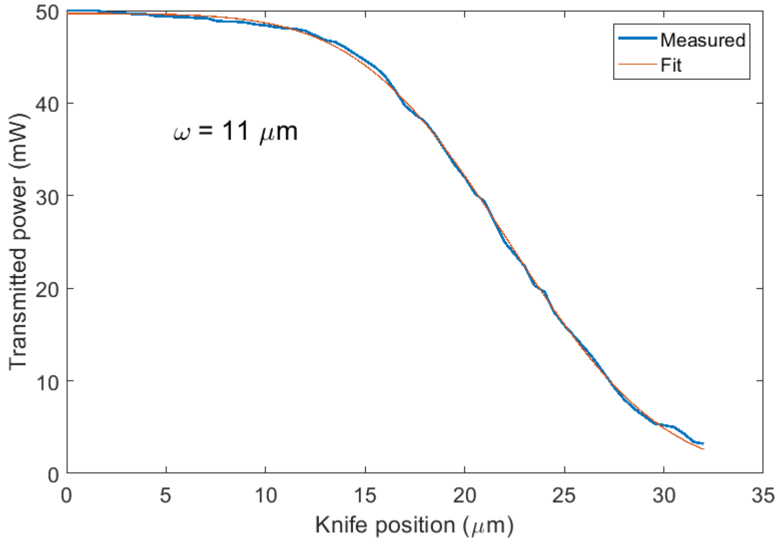

Figure 6.4: Measured knife edge data for a beam collimated and focused with a pair of OAP mirrors lens and a least-squares fit to the transmission function.

6.3 Results

6.3.1 Closed cavity

For the initial case of butt-coupled mirrors we used as outlined a 1 m length of dysprosium doped ZBLAN. Oscillation was however not achieved up to the limit of available RFL power. Though we will discuss in greater detail the characterization measurements and analysis that point to the possible explanation for this, we note here that the absorption of pump power in this length of fibre was measured as abnormally high. Recall from the calculations in section 6.1 that this length of fibre should approach oscillation near 500 mW of injected pump power, with more than 10% of said pump power exiting the distal end of the fibre un-absorbed. In actuality, we measure less than 1% residual pump transmission even at maximum RFL injected power.

While the imaging system to inject RFL power (two aspheric lenses) is calculated to produce a focused spot that is well matched to the fundamental mode of the ZBLAN fibre, given the recent discussion of aberration in section 6.2.2, it may be tempting to point to poor coupling efficiency as an explanation for the lack of residual pump transmission, and the associated failure to reach oscillation. However as we have noted previously, at low Er/Yb power pumping, the RFL output is both 1700nm and 1570 nm. We can take advantage of this by further reducing the pump power to the RFL such that only 1570 nm is emitted, and as this is by definition co-linear with the 1700nm beam, and well removed from the intrinsic absorption by Dy^{3+} at 1700nm we can use this as a probe to make a fairly accurate estimate of coupling efficiency. Doing so yields a value of 80%, an acceptable value for free space coupling of two single mode fibre sources.

Ignoring for the moment the possible physical reasoning, we take a practical experimentalist point of view and simply reduce the fibre length until we achieve the targeted nominal

90% pump absorption our initial calculations called for. After several incremental length reductions this resulted in a fibre length of 42 cm, and a pump absorption of 87%. At this point we bring the cavity mirrors into contact with the fibre tips, closing the cavity, and successfully produce mid-IR laser emission from the system centred at 2916 nm as seen in the measured spectrum in figure 6.5. The output power as a function of launched RFL

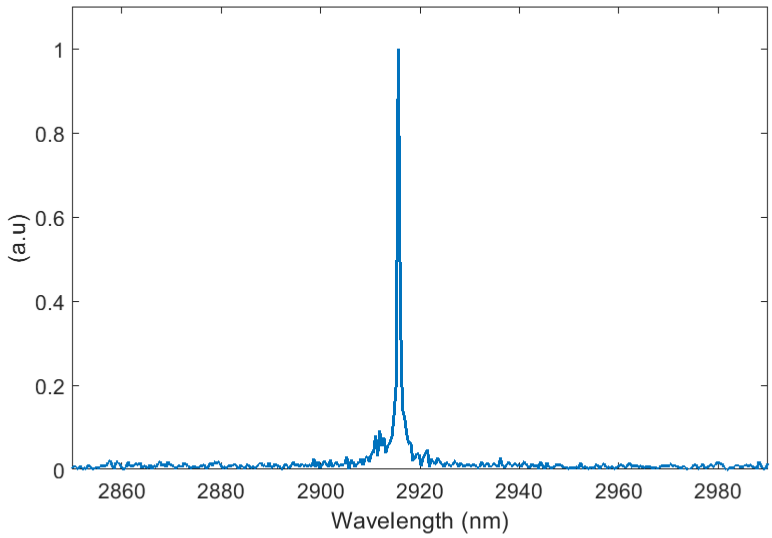

FIGURE 6.5: Measured optical spectrum of emission from a L=42 cm Dy:ZBLAN fibre laser pumped at 1700nm.

power is presented in figure 6.6, where we see that the efficiency with respect to launched power was 13% and the maximum output power generated was 30 mW for an injected power of 1.2 W.

6.3.2 Continuous tuning

It is of importance to note that the laser demonstrated with butt-coupled mirrors is fairly close to oscillation threshold even at the maximum of available RFL pump power. This is a direct negative indicator for the potential success of an extended cavity arrangement, as the extended cavity even with careful implementation is almost guaranteed to introduce some additional loss. This highlights the importance of correct selection of optical elements, as given the calculations regarding aberration, an extended cavity employing spherical lenses would almost certainly not oscillate given the limitation in pump power. However, at maximum available pump power, with careful system alignment, oscillation across a wide range was achieved.

Due to the proximity to oscillation threshold, and the limitation in pump power, we decide to take a binary approach to measurement of tunable output i.e. *lasing* or *not lasing*. For this we place a CaF_2 optic in the extended cavity section at a 45 degree angle to the collimated beam. This optic is anti-reflection (AR) coated across the 3 micron band on one side, and uncoated on the other, allowing for outcoupling a small fraction of the cavity light. This reflected signal, while too weak for reliable thermal detection, is directed at a fixed

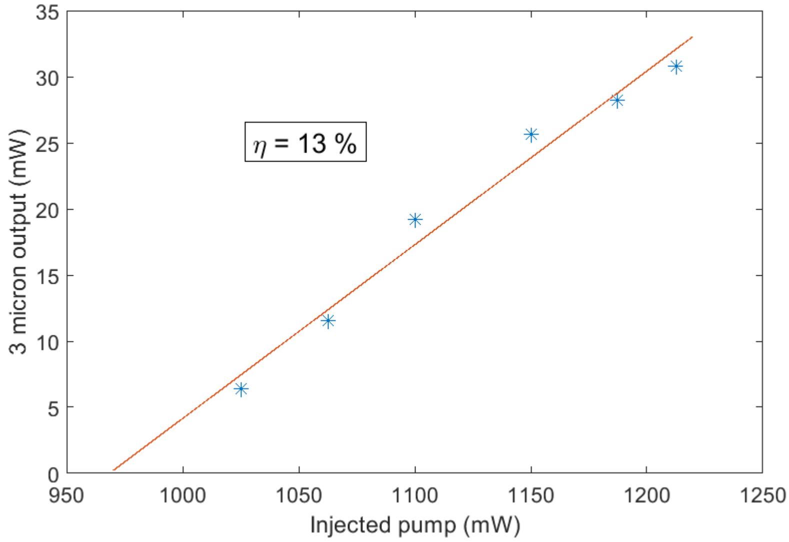

Figure 6.6: 3 micron output power as a function of launched NIR pump power. Slope efficiency is 13% and oscillation threshold is 970 mW.

probe fibre of the mid-IR OSA. The sensitivity of the spectrum analyser is such that even low levels of output power are detectable as a narrow emission peak, thus indicating *lasing*. Though not a calibrated power measurement, we can nonetheless use the OSA signal peak height as a substitute for output power, and we plot this value over the achieved tuning range in figure 6.7. Output is achieved from 2820 to 3240 nm, representing 420 nm total

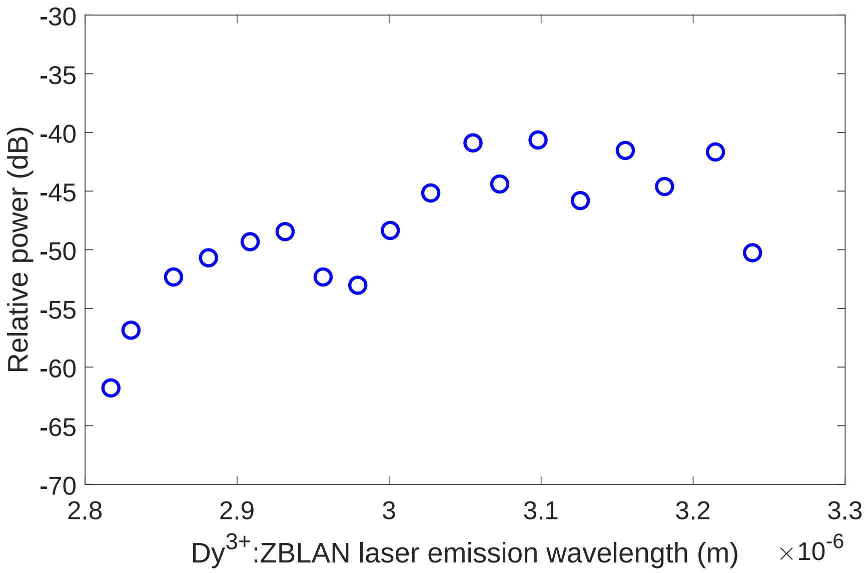

Figure 6.7: Output of a diffraction grating continuously tuned dysprosium ZBLAN fibre laser. Y-axis values are taken from peaks heights as measured by an optical spectrum analyser.

tuning range. While this is comparable to the tuning range achieved for inband pumping, note here that the short-wavelength side of the range is extended by nearly 200 nm.

6.4 Further analysis

As the performance of this system falls short of the expectations set out by the initial numerical approach, we are left to pose the familiar question: why? In an attempt to answer this question, we split our approach into two areas. First, the tuning range as inferred both from theoretical standpoint and the performance of the inband pumped system appears to fail to meet expectations. Second, and likely more important to the understanding of the dysprosium ion itself, we attempt to understand what manifested in experiment as anomalous absorption of pump radiation. For this we need to consider the possibility of excited state absorption (ESA), a phenomenon that while common in rare earth doped lasers as a whole, was expected to be non-existent in the inband pumped system, and negligible here.

6.4.1 Tuning limits

One of the key motivations of pursuing NIR pumping at 1700nm as opposed to inband pumping is that it does not place a fundamental restriction on the wavelength of emission. While in practice we do indeed observe that emission is achievable at substantially shorter wavelengths, it seems to have, in this instance, come at the expense of a large portion of the longer wavelength range. We've already addressed the concept of a minimum fibre length to achieve oscillation with equations (4.10) and (4.11) in chapter 4 and those hold here as well. This was introduced there in the context that inband pumping fundamentally limits the fractional population inversion to 60%, while in theory the limit here is 100%, or total inversion. However, if this inversion was actually achieved, we would have also seen pump transparency as the ground state would be completely depleted. Given what we actually observed is essentially the opposite (anomalously large pump absorption), it would be a fair assumption that the inversion here is less than complete. To illustrate graphically the effect this has, we calculate a minimum length of fibre required for oscillation based on 75% inversion (averaged over the length of fibre), with the result shown in figure 6.8. We see that this inversion estimate actually yields fair agreement to experiment, indicating that the fibre is not a sufficient length to reach longer wavelengths. Of course in this instance longer fibre lengths will be counterproductive as we have already discussed, thus to achieve longer wavelengths in this system would require higher fractional inversion, possibly with bi-directional pumping for example.

While the effect limiting long wavelength emission is identical to the inband pumping case, the limit on the short wavelength side requires a new explanation. To facilitate this we are able to measure here the amplified spontaneous emission (ASE) spectrum of this length of fibre in the absence of cavity mirrors. As expected from the measurements of transition cross sections, the measured ASE spectrum in figure 6.9 is peaked around 2.9 µm, though with the measured data overlaid there are a few interesting observations to be made. First, *lasing* is achieved at the highest signal levels for emission wavelengths well into the long wavelength tail of the ASE spectrum, with lasing achievable in regions barely above the noise floor in the ASE spectrum. This can be explained by recalling that signal re-absorption is reduced at longer wavelengths, which will shift the wavelength of maximum output from the emission cross section peak if the system is not fully inverted; a conclusion we have already loosely made in section 4.4.2. Further, the sharp drop off in observed signal

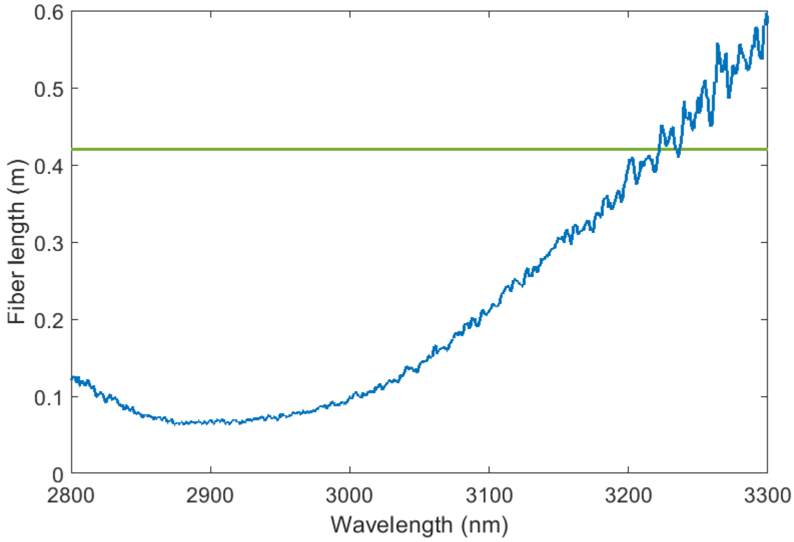

Figure 6.8: Minimum length of Dy:ZBLAN fibre required to reach oscillation threshold for a 75% fractional inversion. The horizontal line indicates the fibre length used in tuning experiments.

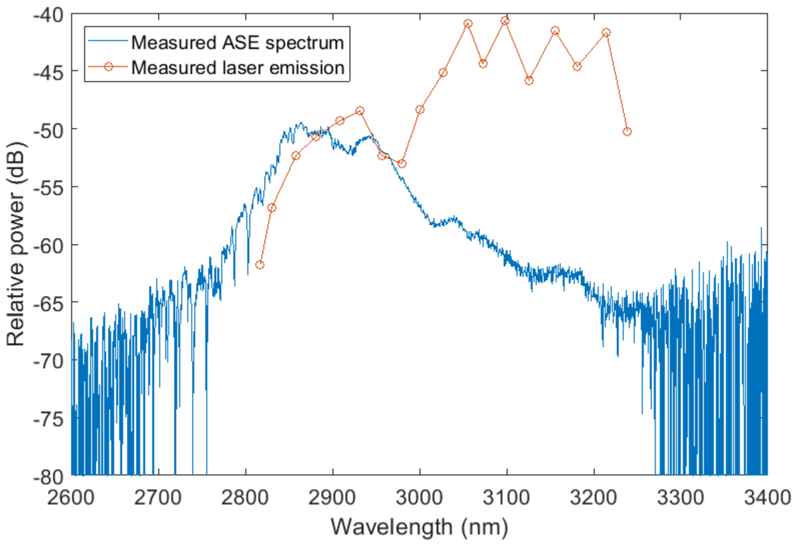

Figure 6.9: ASE spectrum of L=42 cm of Dy:ZBLAN fibre pumped at maximum RFL power. OSA peak heights as measured in the continuous tuning experiment are indicated.

power at long wavelengths is consistent with the minimum fibre length argument.

The short wavelength side of continuously tunable output falls off in a region where the magnitude of the ASE spectrum well exceeds that of the longer wavelengths. This is curious until we consider the effect of atmospheric absorption, as the extended cavity setup required for tunable operation contains a free space section of nominally 60 cm. A simulation of the atmospheric transmittance function over this wavelength range (HITRAN database) plotted with the ASE spectrum and the measured data is shown in figure 6.10. Atmospheric transmittance over this range (as one may have already noted from chapter 1) exhibits

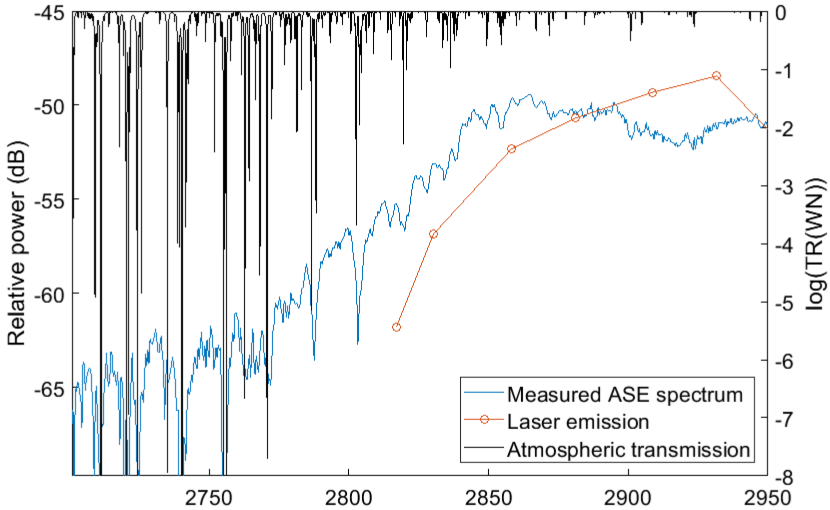

FIGURE 6.10: HITRAN database simulation of transmittance function for atmospheric propagation of 60 cm along with measured ASE from Dy:ZBLAN and laser emission data.

several closely spaced features, associated largely with absorption by water vapour molecules. Several strong absorption features map clearly to the ASE spectrum, and the increasing frequency of absorption lines follows a similar shape to the laser emission measurements. It is then a likely conclusion that atmospheric absorption is the limiting factor in achieving shorter wavelength emission here. However it is worth re-iterating that laser performance indicates that we are not well above oscillation threshold, thus small contribution from atmospheric absorption can have a significant impact. It is therefore likely that increased inversion, coupled with a reduction in free-space cavity length would result in an increase in emission range to shorter wavelengths. Incidentally, though in this instance a net negative for laser performance, the high sensitivity to molecular absorption here is a good example of the utility of mid-IR optical sources for sensing applications.

6.4.2 Excited state absorption

Excited state absorption was introduced in section 2.1.3 and discussed briefly in section 2.2.2 in regards to previous demonstrations of dysprosium 3 µm fibre lasers. The ESA process under strong 1.1 µm pumping was also illustrated explicitly in figure 2.5 as this process was observed experimentally [51], and while possible ESA is mentioned for pumping at 1.3 µm, up to this point we have not considered it in detail for the work presented here. However, the experimental evidence from pumping at 1700nm, both in terms of pump absorption and oscillator performance, suggest that ESA may be a factor.

To begin the analysis we again present the energy level diagram of Dy^{3+} in ZBLAN, with the four pump wavelengths which have been investigated and the possible ESA channels for each in figure 6.11. As we have already pointed out, all of the levels up to $^6F_{3/2}$ are non-radiatively quenched in ZBLAN, with the exception of the upper 3 micron laser level $^6H_{13/2}$, though as noted this level also exhibits significant non-radiative decay. Of the pump

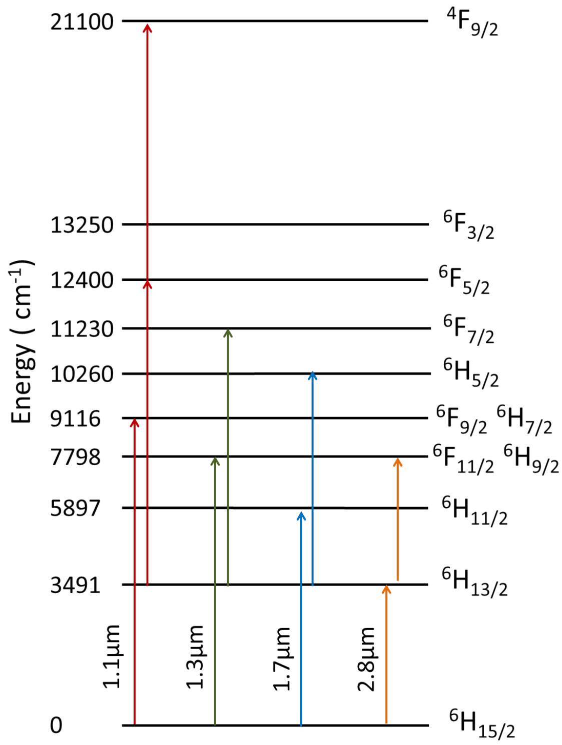

Figure 6.11: Possible excited state absorption channels in Dy:ZBLAN for each infrared pump wavelength.

wavelengths, only photons at 1.1 µm are energetic enough to bridge the energy gap between the highest non-radiatively coupled level $^6F_{3/2}$ and $^4F_{9/2}$. As $^4F_{9/2}$ has an inherently long lifetime, and is characterized by efficient radiative emission, this is a substantial source of energy loss, and was clearly observed experimentally, contributing to overall poor system performance. As the remainder of possible ESA channels result in excitation to non-radiatively coupled levels, it is difficult in practice to observe the presence or impact of ESA on laser operation.

As a first order method of estimating ESA probability, we can simply calculate in terms of energy the proximity of the discrete levels to ESA position. For example, pump photons exciting $^6F_{9/2}+{}^6H_{7/2}$ directly have an energy of 9116 cm^{-1}, thus absorption of these photons from the $^6H_{13/2}$ upper laser level at 3491 cm^{-1} results in an excitation energy of 12607 cm^{-1} which is nearly equivalent to the energy of level $^6F_{5/2}$ at 12400 cm^{-1}. The ratio of the difference in energy ΔE of these two values to the excited state level position (12400 cm^{-1} in this case) is in a sense an inverse Q-factor indicating degree of resonance. This value calculated for the most probable ESA process for each pump wavelength is presented in table 6.1. Using this simple metric would indicate that ESA is less resonant for both of the pumping schemes investigated here. However for these calculations to carry any real physical meaning we must include some information about the natural bandwidth of each level. To generate an estimate for this we look back to the ground state absorption spectrum in figure 2.4. The width of each absorption peak will be proportional to contributions from the splitting of both the ground and excited state. Since each absorption shares the

Pump λ (µm)	ESA level	$\frac{\Delta E}{E}$ (%)
1.1	$^6F_{5/2}$	1.7%
1.3	$^6F_{7/2}$	0.5%
1.7	$^6F_{9/2} + {}^6H_{7/2}$	3%
2.8	$^6F_{11/2} + {}^6H_{9/2}$	10.5%

TABLE 6.1: Estimation of ESA resonance based on energy level positions for various pump wavelengths. All transitions originate from the upper laser level at $^6H_{13/2}$.

same ground state in common, one could infer to first order that the observed bandwidth of the absorption carries some information then about the splitting of the excited state. Following this logic allows for generation of an upper bound for ESA resonance as follows: the normalized bandwidth $\Delta E/E$ (where ΔE here = FWHM) of the $^6H_{13/2}$ ground state absorption is 6%, while the same normalized bandwidth for $^6F_{11/2} + {}^6H_{9/2}$ is nominally 5%; thus an ESA transition between these two levels could be estimated to have a bandwidth roughly proportional to the convolution of the two, which assuming Gaussian shapes would yield a normalized bandwidth of $\sqrt{0.06^2 + 0.05^2} = 8\%$. Referring back then to table 6.1 we see that the calculated resonance condition exceeds this bandwidth. If however we carry out the same procedure now using the terminal ESA level for 1700 nm pumping $^6F_{9/2} + {}^6H_{7/2}$, we find that normalized bandwidth of the convolution is equivalently 8% and see that the ESA condition as defined is substantially less than this value, indicating, at least by this method, that pump ESA at 1700 nm is allowed. While this method is admittedly crude, and a more sound approach would require further spectroscopic measurement grounded in Judd-Ofelt theory, it does provide some direction, and as we will see, a simple ESA model shows reasonable agreement to laboratory measurement.

In the previous inband pumping experiment, we found that measurements of pump absorption were helpful in determining an estimate for background fibre loss. The same procedure is applied here, but while ESA largely manifests as an additional loss, to handle it correctly in the system of rate equations requires a key difference. Previously, the equation governing propagation of the pump intensity took the form

$$\frac{dI_p}{dz} = I_p(\sigma_{e,p}N_2 - \sigma_{a,p}N_1 - \delta) \tag{6.6}$$

As ESA is proportional to the population in the excited state, here the equation for pump intensity is

$$\frac{dI_p}{dz} = I_p(\sigma_{e,p}N_2 - \sigma_{a,p}N_1 - \delta - \sigma_{ESA}N_2) \tag{6.7}$$

where we have now defined an ESA cross-section σ_{ESA} which translates to a loss which now has a length dependence and requires knowledge of the inversion at each point along the fibre.

Measurement of residual pump power transmission as a function of fibre length for injection of the maximum available RFL power is shown in figure 6.12 along with multiple variant of numerical model. The best fit using only a linear loss still deviates substantially from measurement. Further, the value used for linear loss here is 7400 dB km^{-1}, which considering

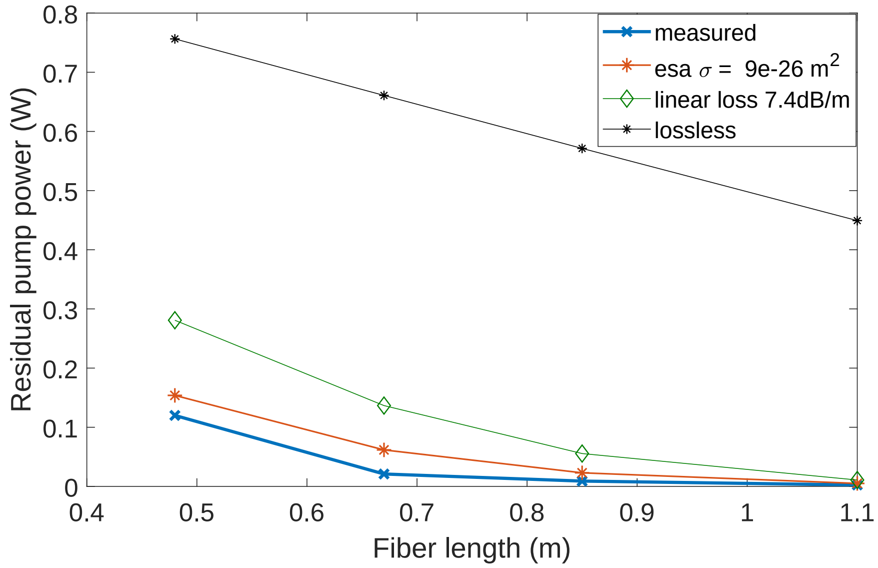

Figure 6.12: Residual pump transmission for injection of maximum RFL pump power. Numerical model is applied for loss-less, linear loss, and ESA loss.

there are no obvious ZBLAN impurities which exhibit absorption in this range is likely not physically believable. Using rather an ESA mechanism for loss provides a much better fit.

As ESA is proportional to the population in the excited state, it is perhaps a more revealing measurement to investigate pump transmission as a function of injected power for a fixed length of fibre, as the behaviour of linear loss and ESA should show clear deviation. Figure 6.13 shows measurement of residual pump transmission for a L=48 cm length of Dy:ZBLAN fibre over a range of injected RFL power, along with numerical model output using both loss mechanisms. Again we see that a best fit based solely on linear loss deviates from measurement, while ESA-based loss provides a reasonable fit. If we then use this ESA cross section value and the previously estimated value for signal loss around 3 microns, a full rate equation simulation of laser action yields an injected threshold of 500 mW and a slope efficiency of 9%. While not an exact match to experiment, the overall trend in these measurements clearly suggest that both fibre loss at 3 microns, and ESA resulting from 1700nm pump absorption are negatively impacting laser performance. Cross section for ESA by absorption of 1.3 µm pump photons from $^6H_{13/2}$ has been estimated in the spectroscopic work [80] and the value there of 4.68×10^{-24} m^2 is more than an order of magnitude larger than the cross section value 1×10^{-25} m^2 produced here. This is at least qualitatively consistent with the ESA resonance conditions derived earlier.

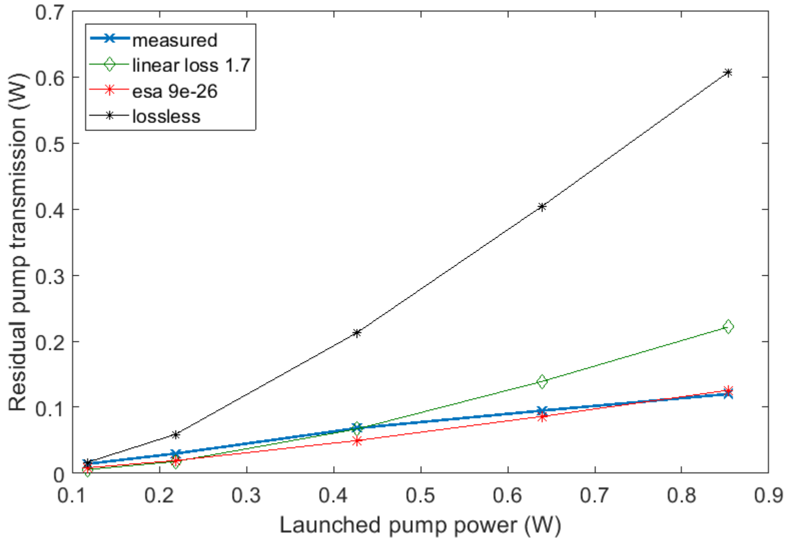

FIGURE 6.13: Measurement of residual pump transmission for a 48 cm length of Dy:ZBLAN fibre at various injected RFL power. Numerical model output is shown for the loss-less case, and best fits based on linear or ESA loss.

6.5 Mode-locking implications

At the outset of this work, progressing dysprosium mid-IR fibre lasers to pulsed or even more ideally *mode-locked* operation was a stated goal. Due to the bandwidth limitations imposed by the in-band pumped system, as well as the increased complexity of a system composed entirely of mid-IR optical components, NIR pumping was thought to be the best case scenario for achieving pulsed operation. As the data presented above clearly shows, the system performance fell short of expectation, and though mode-locked operation was not achieved, some of the measurements made here are relevant to a discussion of the future potential of mode-locked dysprosium mid-IR fibre lasers. Rigorous treatment of mode locking and ultrafast optics, as well as thorough review of the current state of pulsed mid-IR fibre lasers can be found elsewhere [48, 153]. Here we will approach mode-locking from a basic point of view, as that will prove to be sufficient for discussion of the potential of a Dy:ZBLAN pulsed fibre laser.

Longitudinal modes were introduced in chapter 3 and it was noted that even in a narrow linewidth CW laser, there can often be many longitudinal modes oscillating concurrently. As these modes have no fundamental phase correlation, they will generally exhibit a random distribution of optical phase. The output then is a superposition of all the modes, with the temporal behaviour of the optical intensity being characterized by random noise about an average value equal to the CW output power. If however the modes share some common phase relationship the behaviour is quite different as seen in figure 6.14. If the cavity modes have some phase correlation, the output exhibits intensity spikes at intervals equal to the cavity round trip time. If we take this further to the modes all having the *exact same* phase, the output will consist only of the spikes, now well defined pulses. The modes are then said to be *locked*, hence *mode-locking*.

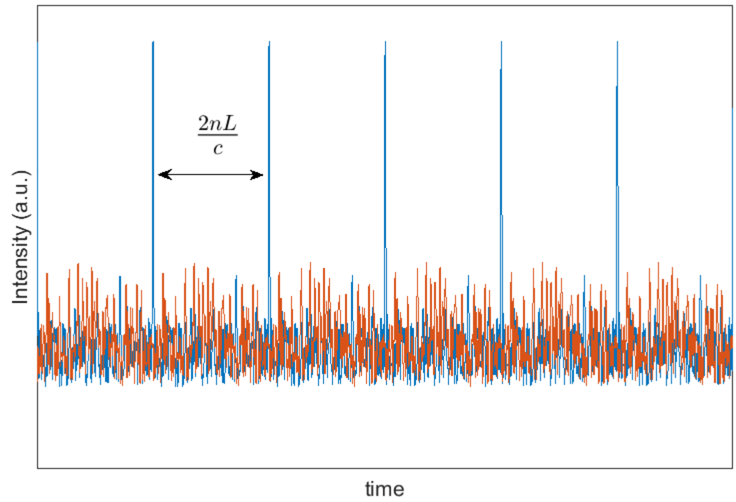

Figure 6.14: Representative laser output demonstrating mode-locking principle. Modes with random phase (red) result in noise about a CW output power. Modes with phase correlation (blue) lead to sharp spikes in output intensity at a fixed frequency of $c/2nL$.

To achieve this phase relationship between the cavity modes one must periodically modulate the cavity loss at the cavity round trip frequency (or multiple thereof). There are a variety of methods to achieve this, all of which can be grouped as either *active*, or *passive*. In terms of mid-IR fibre lasers, active modulation by an acousto-optic modulator (AOM) has been used to successfully generate nanosecond-scale pulses [154, 155], while passive modulation based on a physical saturable absorber element achieved emission on the picosecond scale [156]. However the most successful pulsed mid-IR fibre laser systems, both in shortest pulse duration and peak output power have been based on passive modulation by an artificial saturable absorber employing the Kerr nonlinearity [49, 50] which have produced femtosecond scale pulses.

All of the mentioned methods of achieving the required cavity modulation require the introduction of increased cavity loss, indeed the fundamental principle of mode-locking requires that loss be high for for all output except high intensity pulses. As a result, the current performance limitations of a NIR pumped dysprosium fibre will not allow for mode-locked operation, but should these issues be overcome, there is clear potential.

The lower limit in optical pulse duration is defined by the time-bandwidth product

$$C = \Delta\tau\Delta\nu \tag{6.8}$$

where $\Delta\tau$ and $\Delta\nu$ are full width half maximum values for time and spectral bandwidth and C is a constant roughly equal to 0.315 for the sech^2 pulse shapes encountered in mid-IR fibre lasers. ASE spectra are generally well indicative of the maximum $\Delta\nu$ achievable, as it is a direct measurement of the gain bandwidth. Hu et. al [49] demonstrated a passively mode-locked mid-IR fibre laser based on erbium doping, and despite the broad measured ASE spectrum of erbium, the spectral width of the pulse was substantially less, as seen in figure 6.15. This was attributed to the effect of atmospheric absorption, as this laser cavity included

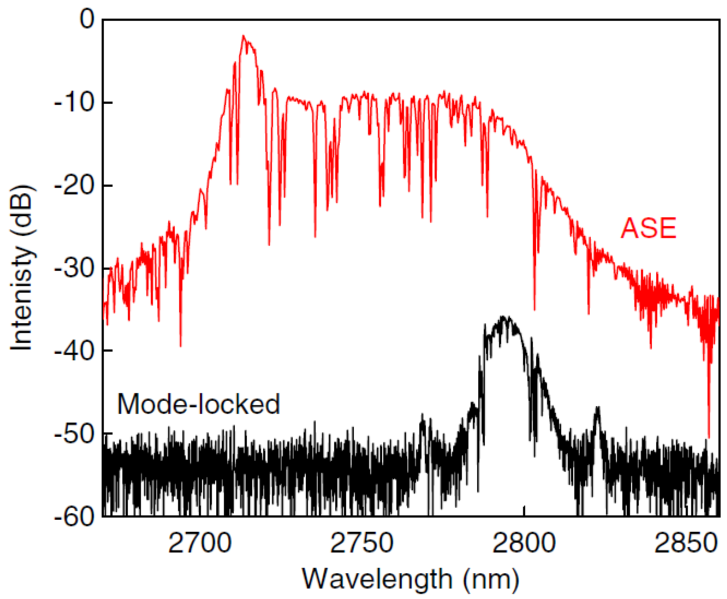

FIGURE 6.15: Erbium ASE spectrum and mode-locked pulse spectrum as achieved by Hu et al. [49].

free space propagation, and as we have seen already in figure 6.10, atmospheric absorption can be significant in this range. Antipov et. al further solidified this argument by successfully demonstrating a similar laser cavity with a holmium doped fibre emitting at slightly longer wavelengths [50] which further avoided atmospheric absorption. The result was a 180 fs pulse which exhibited a 60 nm spectral width, covering almost all of the ASE spectrum. We can propose in theory to carry this further with dysprosium by comparing the measured ASE spectra of both holmium and dysprosium, as seen in figure 6.16. The dysprosium ASE

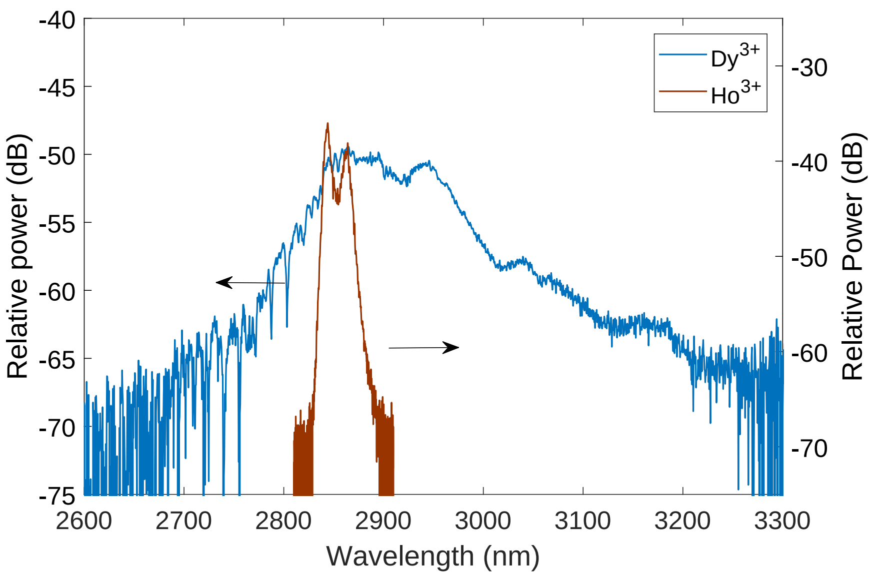

FIGURE 6.16: Measured ASE spectra of both holmium and dysprosium in ZBLAN.

spectrum is not only further removed from the strong influence of atmospheric absorption but is substantially broader. Further, it is significant that even in the performance limited system presented here, oscillation was achieved well out to the long wavelength tail of the ASE spectrum, indicating that accessing a substantial portion of the gain bandwidth should be possible in an ultrafast pulse given sufficient pump power and proper system design.

6.6 Summary

We have demonstrated in this chapter a dysprosium fibre laser pumped by a NIR Raman fibre laser source at 1700 nm. As a proof of principle exercise, this demonstration was clearly successful in that oscillation was achieved, and at a conversion efficiency more than double the only other instance of a NIR fibre laser pumped dysprosium mid-IR laser [51]. Additionally, continuous tuning was achieved, demonstrating laser emission well shorter than the in-band pumped system was capable of. However, the performance limitations of the RFL pump laser as outlined in chapter 5 proved to be a distinct limitation. Engineered solutions to the pump power limitation would allow for further development and power scaling of these NIR pumped systems even in the presence of possible fibre loss and excited state absorption processes.

The identification of ESA as a likely limiting factor in these systems, while unanticipated, allowed for investigation which should further our understanding of the underlying dynamics of dysprosium in ZBLAN. The measurements presented here regarding ESA, while convincing on a preliminary basis, could certainly be augmented by an investigation specifically targeted at ESA and energy transfer processes in Dy:ZBLAN, which would likely require for example a pump/probe experimental setup.

While the current system limitations prevented operation of this system in the pulsed regime, ASE measurements are encouraging for future development. By simple comparative argument, dysprosium is shown to have clear potential as a mode-locked system, specifically when pumped at NIR wavelength.

7
Conclusion

This thesis began with the aim to show that dysprosium as a mid-infrared rare earth ion has been mistakenly overlooked by the majority of the mid-IR fibre laser community. To that end we laid out a plan that hoped to not only address the shortcomings of previous dysprosium systems, but potentially offer solutions for mid-IR fibre laser development that were superior to alternative systems. In-band pumping would enable ultra-high efficiency, allowing for output power scaling to outpace the incremental improvement seen in recent years. while NIR pumping would enable low cost and robust systems with tunable output covering upwards of 700 nm across regions of the mid-IR spectrum inaccessible directly by other fibre laser sources, as well as opening the door for pulsed dysprosium fibre lasers. Though we have devoted two chapters exclusively to theory, chapter 2 focusing on rare-earth ions and chapter 3 covering key aspects of optical fibre and laser theory, at its heart this work has been highly experimental in nature. As with most experimental research projects, not all of the goals set out at the start can claim complete success.

Before summarizing the faults, it is important to note the relative successes, as despite not achieving every lofty expectation, what we have demonstrated experimentally here certainly still supports the view that dysprosium fibre lasers offer unique potential worthy of further investigation and investment by the greater community. Chiefly, at the time of writing the in-band pumped dysprosium system represents the highest conversion efficiency in three micron class lasers, despite falling short of the Stokes limit. While it may be fair to note that the wall-plug efficiency is not extraordinarily high, as this system relies on an erbium laser which itself is nominally 30% efficient, the potential for increased output power remains as it has been the thermal load on ZBLAN fibres that is a major factor in power scaling. One could easily envision a system of beam combined erbium mid-IR lasers pumping a single highly efficient dysprosium laser. The reliance on a ZBLAN laser pump source as well can be viewed as a positive, as ZBLAN-ZBLAN splicing is considerably more reliable than ZBLAN-silica for example given the difference in glass transition temperature. Thus one could realize a nearly *all-fibre* system emitting near the C-H resonance around 3.4 microns, given that we have shown emission close to that point even with a demonstrably lossy cavity.

The NIR pumping demonstration offers some potential progress towards an all fibre construction as well, with a pump source that could easily be converted to a true all-fibre construction given that FBG's are readily available for all relevant wavelengths. Even the possible MOPA solution offered to extend the total pump source power output can be fibre-ized as fibre coupled pump diodes are common in this range. And despite falling short of the Stokes limit, NIR pumping here exhibited a three-fold increase in efficiency over the previous effort which relied on fibre pumping. Further, though pumping near 1.3 µm was reported as more efficient with respect to absorbed power, reliance on a solid state laser with poor beam quality means that NIR pumping here was actually comparably if not more efficient with respect to incident pump power. Additionally, to the best of our knowledge, the ASE spectrum presented here is the first directly measured ASE spectrum from a Dy:ZBLAN fibre. This is significant in that beyond the spectral character already known from fluorescence measurements, it indicates directly, particularly in conjunction with laser output measurements, the available gain bandwidth of this NIR-pumped system. Drawing from comparison to demonstrated pulsed ZBLAN fibre lasers, this has strong implication for the potential of mode-locked dysprosium fibre lasers.

Though inevitably we have encountered some setbacks and system limitations, it is important that rather than discourage continued effort to develop mid-IR dysprosium lasers, these can help shape the direction of future work. Of perhaps the most importance among these is the issue of fibre background loss. The loss estimates produced here, in combination with the estimates afforded by the Galzerano group, while representing a fair amount of variance, strongly suggest that background loss in this dysprosium ZBLAN fibre is a key design issue. With this particular draw of fibre, obviously there is no rectifying background loss fundamentally, but certainly further spectroscopic investigation of it would prove useful in terms of informing how to minimize the impact through more optimized system design for example. It is also important to remember that fibre quality has been a persistent issue across the field of fibre optics since the first drawn glass fibre. It has taken years and countless dollars and man-hours to bring the quality of common silica fibre to where it is today. Clearly if we had just given up on this technology our world would look drastically different. ZBLAN in this sense is still in its formative years as an optical fibre technology, particularly so for rare earth doped variants as we are concerned with here. Even in passive variants, fibre loss in the mid-IR has been shown to vary greatly over the (relatively few) commercial suppliers, and even amongst the offering of a single manufacturer. Further, currently only one supplier offers standard doped fibre, and this is an erbium variant, which itself required much development effort. As with almost all technology, custom products, even when available, come with a higher degree of uncertainty in terms of quality and consistency.

The issue of ESA on the other hand is different, as this is more fundamental and the exact nature is dysprosium specific. We have generated an estimate for ESA cross section based on straight-forward laboratory measurement, and a model well grounded in physical meaning. While the value we produce is smaller than for example the ESA cross section estimated for pumping at 1.3 µm, the performance of the system would seem to indicate, at least currently, that ESA is a significant factor. Direct measurement of ESA cross sections can often prove difficult though previous iteration of dysprosium fibre laser have sought to minimize ESA by altering the output coupling, the thought process being that increased intra-cavity flux depletes the upper laser level, reducing the impact of ESA. This could alternatively be viewed as a decrease in inversion required for threshold, which considering the RFL output power limitation is not feasible currently, but surely has promise. Going beyond just the system development point of view, the measurement of a cross section (albeit indirect) of an ESA process not previously observed should be considered in itself a valuable contribution to knowledge of dysprosium as a rare earth. As we point out early on, comparatively to other ions, there have been very few spectroscopic studies of dysprosium in any host, making each new piece of information crucial to the overall picture.

No successful technology has ever been invented and developed in a vacuum. It takes a village to raise a child is a common proverb, and in science it is no different. It can sometimes be the case that a technology does not attract significant attention from the greater community, whether that be scientific or industrial. History shows us that occasionally this has been a serious error in judgment. For example, a Western Union memo in 1876 supposedly read “This ‘telephone’ has too many shortcomings to be seriously considered as a means of communication. The device is inherently of no value to us”. While published work on mid-IR ZBLAN fibre lasers is demonstrably increasing, and commercial suppliers have begun to appear, it would be difficult to argue against the view that if there is to be wide-scale success, we are still in the early days. Let the work presented here contribute to a further step in the right direction.

References

[1] T. H. Maiman. *Stimulated optical radiation in ruby.* Nature **187**(4736), 493 (1960).

[2] K. Kao and G. A. Hockham. *Dielectric-fibre surface waveguides for optical frequencies.* In *Proceedings of the Institution of Electrical Engineers*, vol. 113, pp. 1151–1158 (IET, 1966).

[3] C. J. Koester and E. Snitzer. *Amplification in a fiber laser.* Applied Optics **3**(10), 1182 (1964).

[4] L. Dong and B. Samson. *Fiber Lasers: Basics, Technology, and Applications* (Crc Press, 2016).

[5] V. Dominic, S. MacCormack, R. Waarts, S. Sanders, S. Bicknese, R. Dohle, E. Wolak, P. Yeh, and E. Zucker. *110 W fiber laser.* In *Conference on Lasers and Electro-Optics*, p. CPD11 (Optical Society of America, 1999).

[6] V. Fomin, M. Abramov, A. Ferin, A. Abramov, D. Mochalov, N. Platonov, and V. Gapontsev. *10 kW Single mode fiber laser.* In *SyTu-1.3, Symposium on High-Power Fiber Lasers, 14th International Conference, Laser Optics* (2010).

[7] IPG. URL `http://www.ipgphotonics.com/en/products/lasers/high-power-cw-fiber-lasers`.

[8] D. Ma, Y. Cai, C. Zhou, W. Zong, L. Chen, and Z. Zhang. *37.4-fs Pulse generation in an Er:fiber laser at a 225 Mhz repetition rate.* Optics Letters **35**(17), 2858 (2010).

[9] G. P. Agrawal. *Nonlinear Fiber Optics* (Academic press, 2007).

[10] D. R. Paschotta. *Mid-infrared laser sources* (2017). URL `https://www.rp-photonics.com/mid\_infrared\_laser\_sources.html`.

[11] A. B. Seddon, B. Napier, I. Lindsay, S. Lamrini, P. M. Moselund, N. Stone, and O. Bang. *Mid-infrared spectroscopy/bioimaging: moving toward mir optical biopsy.* Laser Focus World **52**(2), 50 (2016).

[12] C. W. Rudy. *Mid-ir lasers: power and pulse capability ramp up for mid-ir lasers.* Laser Focus World **50**(05), 63 (2014).

[13] J. Sanghera, L. Shaw, L. Busse, V. Nguyen, P. Pureza, B. Cole, B. Harrison, I. Aggarwal, R. Mossadegh, F. Kung, *et al.* *Development and infrared applications of chalcogenide glass optical fibers.* Fiber & Integrated Optics **19**(3), 251 (2000).

[14] Vision-Systems. URL `http://www.vision-systems.com/articles/print/volume-21/issue-8/features/choosing-a-camera-for-infrared-imaging.html`.

[15] F. Adler, P. Masłowski, A. Foltynowicz, K. C. Cossel, T. C. Briles, I. Hartl, and J. Ye. *Mid-infrared fourier transform spectroscopy with a broadband frequency comb.* Optics Express **18**(21), 21861 (2010).

[16] S. Amini-Nik, D. Kraemer, M. L. Cowan, K. Gunaratne, P. Nadesan, B. A. Alman, and R. D. Miller. *Ultrafast mid-ir laser scalpel: protein signals of the fundamental limits to minimally invasive surgery.* PLoS One **5**(9), e13053 (2010).

[17] X. Shi, B. Thapa, W. Li, and H. B. Schlegel. *Controlling chemical reactions by short, intense mid-infrared laser pulses: comparison of linear and circularly polarized light in simulations of $ClCHO^+$ fragmentation.* The Journal of Physical Chemistry A **120**(7), 1120 (2016).

[18] J. Faist, F. Capasso, D. L. Sivco, C. Sirtori, A. L. Hutchinson, A. Y. Cho, *et al.* *Quantum cascade laser.* Science-AAAS-Weekly Paper Edition-including Guide to Scientific Information **264**(5158), 553 (1994).

[19] B. S. Williams, S. Kumar, Q. Hu, and J. L. Reno. *Operation of terahertz quantum-cascade lasers at 164 K in pulsed mode and at 117 K in continuous-wave mode.* Optics Express **13**(9), 3331 (2005).

[20] P. Q. Liu, A. J. Hoffman, M. D. Escarra, K. J. Franz, J. B. Khurgin, Y. Dikmelik, X. Wang, J.-Y. Fan, and C. F. Gmachl. *Highly power-efficient quantum cascade lasers.* Nature Photonics **4**(2), 95 (2010).

[21] S. O. Antipov, V. A. Kamynin, O. I. Medvedkov, A. V. Marakulin, L. Minashina, A. S. Kurkov, and A. Baranikov. *Holmium fibre laser emitting at 2.21 μm.* Quantum Electronics **43**(7), 603 (2013).

[22] L. Sojka, Z. Tang, D. Furniss, H. Sakr, A. Oladeji, E. Bereś-Pawlik, H. Dantanarayana, E. Faber, A. Seddon, T. Benson, *et al.* *Broadband, mid-infrared emission from Pr^{3+} doped GeAsGaSe chalcogenide fiber, optically clad.* Optical Materials **36**(6), 1076 (2014).

[23] T. Schweizer, D. Hewak, B. Samson, and D. Payne. *Spectroscopic data of the 1.8-, 2.9-, and 4.3-μm transitions in dysprosium-doped gallium lanthanum sulfide glass.* Optics Letters **21**(19), 1594 (1996).

[24] T. Schweizer, D. Hewak, D. Payne, T. Jensen, and G. Huber. *Rare-earth doped chalcogenide glass laser.* Electronics Letters **32**(7), 666 (1996).

[25] A. B. Seddon, Z. Tang, D. Furniss, S. Sujecki, and T. M. Benson. *Progress in rare-earth-doped mid-infrared fiber lasers.* Optics Express **18**(25), 26704 (2010).

[26] A. Seddon, Z. Tang, D. Furniss, H. Sakr, L. Sojka, E. Barney, T. Benson, and S. Sujecki. *Review of recent progress towards mid-infrared fiber lasers for 4-9 μm window.* In *Novel Optical Materials and Applications*, pp. NoW2C–1 (Optical Society of America, 2017).

[27] M. Bernier, V. Fortin, N. Caron, M. El-Amraoui, Y. Messaddeq, and R. Vallée. *Mid-infrared chalcogenide glass raman fiber laser.* Optics Letters **38**(2), 127 (2013).

[28] D. D. Hudson, S. Antipov, L. Li, I. Alamgir, T. Hu, M. El Amraoui, Y. Messaddeq, M. Rochette, S. D. Jackson, and A. Fuerbach. *Toward all-fiber supercontinuum spanning the mid-infrared.* Optica **4**(10), 1163 (2017).

[29] IR-Fibers. URL `http://leverrefluore.com/products/ir-fibers/`.

[30] R. S. Quimby and M. Saad. *Dy:Fluoroindate fiber laser at 4.5 μm with cascade lasing.* In *Advanced Solid State Lasers*, pp. AM2A–7 (Optical Society of America, 2013).

[31] R. S. Quimby and M. Saad. *Comparison of fluoroindate and fluorozirconate rare earth doped glasses for mid-ir lasers.* In *Frontiers in Optics*, pp. FW2D–2 (Optical Society of America, 2014).

[32] J. A. Harrington. *Infrared Fibers and their Applications* (SPIE press Bellingham, WA, 2004).

[33] M. Poulain, M. Poulain, and J. Lucas. *Verres fluores au tetrafluorure de zirconium proprietes optiques d'un verre dope au Nd^{3+}.* Materials Research Bulletin **10**(4), 243 (1975).

[34] M. Poulain, M. Chanthanasinh, and J. Lucas. *New fluoride glasses.* Mater. Res. Bull.;(United States) **12**(2) (1977).

[35] A. Lecoq and M. Poulain. *Lanthanum fluorozirconate glasses.* Journal of Non-Crystalline Solids **34**(1), 101 (1979).

[36] A. Lecoq and M. Poulain. *Fluoride glasses in the ZrF_4 BaF_2 YF_3 AlF_3 quaternary system.* Journal of Non-Crystalline Solids **41**(2), 209 (1980).

[37] K. Ohsawa and T. Shibata. *Preparation and characterization of ZrF_4-BaF_2-LaF_3-NaF-AlF_3 glass optical fibers.* Journal of Lightwave Technology **2**(5), 602 (1984).

[38] F. Gan. *Optical properties of fluoride glasses: a review.* Journal of Non-Crystalline Solids **184**, 9 (1995).

[39] D. S. Starodubov, S. Mechery, D. Miller, C. Ulmer, P. Willems, J. Ganley, and D. Tucker. *Zblan fibers: From zero gravity tests to orbital manufacturing.* In *Applied Industrial Optics: Spectroscopy, Imaging and Metrology*, pp. AM4A–2 (Optical Society of America, 2014).

[40] J. Schneide, C. Carbonnier, and U. B. Unrau. *Characterization of a Ho^{3+}-doped fluoride fiber laser with a 3.9-μm emission wavelength.* Applied Optics **36**(33), 8595 (1997).

[41] H. Tobben. *Room temperature cw fibre laser at 3.5 μm in Er^{3+}-doped ZBLAN glass.* Electronics Letters **28**(14), 1361 (1992).

[42] O. Henderson-Sapir, S. D. Jackson, and D. J. Ottaway. *Versatile and widely tunable mid-infrared erbium doped zblan fiber laser.* Optics Letters **41**(7), 1676 (2016).

[43] L. Wetenkamp. *Efficient cw operation of a 2.9 μm Ho^{3+}-doped fluorozirconate fibre laser pumped at 640 nm.* Electronics Letters **26**(13), 883 (1990).

[44] M.-C. Brierley and P. France. *Continuous wave lasing at 2.7 μm in an erbium-doped fluorozirconate fibre.* Electronics Letters **24**(15), 935 (1988).

[45] S. D. Jackson. *Single-transverse-mode 2.5-W holmium-doped fluoride fiber laser operating at 2.86 μm.* Optics Letters **29**(4), 334 (2004).

[46] V. Fortin, M. Bernier, S. T. Bah, and R. Vallée. *30 W fluoride glass all-fiber laser at 2.94 μm.* Optics Letters **40**(12), 2882 (2015).

[47] Y. O. Aydın, V. Fortin, F. Maes, F. Jobin, S. D. Jackson, R. Vallée, and M. Bernier. *Diode-pumped mid-infrared fiber laser with 50% slope efficiency.* Optica **4**(2), 235 (2017).

[48] X. Zhu, G. Zhu, C. Wei, L. V. Kotov, J. Wang, M. Tong, R. A. Norwood, and N. Peyghambarian. *Pulsed fluoride fiber lasers at 3 μm.* JOSA B **34**(3), A15 (2017).

[49] T. Hu, S. D. Jackson, and D. D. Hudson. *Ultrafast pulses from a mid-infrared fiber laser.* Optics Letters **40**(18), 4226 (2015).

[50] S. Antipov, D. D. Hudson, A. Fuerbach, and S. D. Jackson. *High-power mid-infrared femtosecond fiber laser in the water vapor transmission window.* Optica **3**(12), 1373 (2016).

[51] S. D. Jackson. *Continuous wave 2.9 μm dysprosium-doped fluoride fiber laser.* Applied Physics Letters **83**(7), 1316 (2003).

[52] Y. H. Tsang, A. E. El-Taher, T. A. King, and S. D. Jackson. *Efficient 2.96 μm dysprosium-doped fluoride fibre laser pumped with a Nd:YAG laser operating at 1.3 μm.* Optics Express **14**(2), 678 (2006).

[53] USGS. URL `https://pubs.usgs.gov/fs/2002/fs087-02/`.

[54] Mineralprices. URL `http://mineralprices.com/`.

[55] M. J. Digonnet. *Rare-Earth-Doped Fiber Lasers and Amplifiers, Revised and Expanded* (CRC press, 2001).

[56] W. Koechner. *Solid-State Laser Engineering*, vol. 1 (Springer, 2013).

[57] W. J. Miniscalco. *Optical and electronic properties of rare earth ions in glasses.* Rare Earth Doped Fiber Lasers and Amplifiers (1993).

[58] G. H. Dieke and H. Crosswhite. *The spectra of the doubly and triply ionized rare earths.* Applied Optics **2**(7), 675 (1963).

[59] M. G. Mayer. *Rare-earth and transuranic elements.* Physical Review **60**(3), 184 (1941).

[60] A. Einstein. *Strahlungs-emission und absorption nach der quantentheorie.* Deutsche Physikalische Gesellschaft **18** (1916).

[61] B. Judd. *Optical absorption intensities of rare-earth ions.* Physical Review **127**(3), 750 (1962).

[62] G. Ofelt. *Intensities of crystal spectra of rare-earth ions.* The Journal of Chemical Physics **37**(3), 511 (1962).

[63] M. P. Hehlen, M. G. Brik, and K. W. Krämer. *50th anniversary of the judd–ofelt theory: An experimentalist's view of the formalism and its application.* Journal of Luminescence **136**, 221 (2013).

[64] B. M. Walsh. *Judd-ofelt theory: principles and practices.* In *Advances in Spectroscopy for Lasers and Sensing*, pp. 403–433 (Springer, 2006).

[65] RP-photonics. *Füchtbauer-Ladenburg equation.* URL `https://www.rp-photonics.com/fuchtbauer_ladenburg_equation.html`.

[66] D. McCumber. *Einstein relations connecting broadband emission and absorption spectra.* Physical Review **136**(4A), A954 (1964).

[67] W. J. Miniscalco and R. S. Quimby. *General procedure for the analysis of Er^{3+} cross sections.* Optics Letters **16**(4), 258 (1991).

[68] M. J. Digonnet, E. Murphy-Chutorian, and D. G. Falquier. *Fundamental limitations of the mccumber relation applied to er-doped silica and other amorphous-host lasers.* IEEE Journal of Quantum Electronics **38**(12), 1629 (2002).

[69] R. Martin and R. Quimby. *Experimental evidence of the validity of the mccumber theory relating emission and absorption for rare-earth glasses.* JOSA B **23**(9), 1770 (2006).

[70] L. A. Riseberg and H.-W. Moos. *Multiphonon orbit-lattice relaxation of excited states of rare-earth ions in crystals.* Physical Review **174**(2), 429 (1968).

[71] R. Reisfeld and C. K. Jørgensen. *Excited state phenomena in vitreous materials.* Handbook on the Physics and Chemistry of Rare Earths **9**, 1 (1987).

[72] S. D. Jackson and T. A. King. *Theoretical modeling of tm-doped silica fiber lasers.* Journal of Lightwave Technology **17**(5), 948 (1999).

[73] H. Pask, A. Tropper, and D. Hanna. *A Pr^{3+}-doped zblan fibre upconversion laser pumped by an Yb^{3+}-doped silica fibre laser.* Optics Communications **134**(1), 139 (1997).

[74] A. F. H. Librantz, S. D. Jackson, F. H. Jagosich, L. Gomes, G. Poirier, S. J. L. Ribeiro, and Y. Messaddeq. *Excited state dynamics of the Ho^{3+} ions in holmium singly doped and holmium, praseodymium-codoped fluoride glasses.* Journal of Applied Physics **101**(12), 123111 (2007).

[75] X. Zhu and N. Peyghambarian. *High-power zblan glass fiber lasers: review and prospect.* Advances in OptoElectronics **2010** (2010).

[76] R. Reisfeld. *Radiative and non-radiative transitions of rare-earth ions in glasses.* Rare Earths pp. 123–175 (1975).

[77] L. Wetenkamp, G. West, and H. Többen. *Optical properties of rare earth-doped zblan glasses.* Journal of Non-Crystalline Solids **140**, 35 (1992).

[78] R. Wyatt. *Spectroscopy of rare earth doped fibres.* In *OE/FIBERS'89*, pp. 54–64 (International Society for Optics and Photonics, 1990).

[79] J. Adam, A. Docq, and J. Lucas. *Optical transitions of Dy^{3+} ions in fluorozirconate glass.* Journal of Solid State Chemistry **75**(2), 403 (1988).

[80] L. Gomes, A. F. H. Librantz, and S. D. Jackson. *Energy level decay and excited state absorption processes in dysprosium-doped fluoride glass.* Journal of Applied Physics **107**(5), 053103 (2010).

[81] R. Piramidowicz, M. Klimczak, and M. Malinowski. *Short-wavelength emission analysis in Dy:ZBLAN glasses.* Optical Materials **30**(5), 707 (2008).

[82] S. Bowman, S. OConnor, and N. Condon. *Diode pumped yellow dysprosium lasers.* Optics Express **20**(12), 12906 (2012).

[83] N. P. Barnes and R. E. Allen. *Room temperature Dy:YLF laser operation at 4.34 μm.* IEEE Journal of Quantum Electronics **27**(2), 277 (1991).

[84] H. Jelínková, M. Doroshenko, M. Jelínek, J. Šulc, T. Basiev, V. Osiko, V. Badikov, and D. Badikov. *Resonant pumping of dysprosium doped lead thiogallate by 1.7 μm Er:YLF laser radiation.* Laser Physics Letters **8**(5), 349 (2011).

[85] H. Jelínková, M. E. Doroshenko, M. Jelínek, J. Šulc, V. V. Osiko, V. V. Badikov, and D. V. Badikov. *Dysprosium-doped $PbGa_2S_4$ laser generating at 4.3 μm directly pumped by 1.7 μm laser diode.* Optics Letters **38**(16), 3040 (2013).

[86] R. Quimby, L. Shaw, J. Sanghera, and I. Aggarwal. *Modeling of cascade lasing in Dy:chalcogenide glass fiber laser with efficient output at 4.5 μm.* IEEE Photonics Technology Letters **20**(2), 123 (2008).

[87] S. Sujecki, L. Sójka, E. Bereś-Pawlik, Z. Tang, D. Furniss, A. Seddon, and T. Benson. *Modelling of a simple Dy^{3+} doped chalcogenide glass fibre laser for mid-infrared light generation.* Optical and Quantum Electronics **42**(2), 69 (2010).

[88] L. Johnson and H. Guggenheim. *Laser emission at 3 μ from Dy^{3+} in BaY_2F_8.* Applied Physics Letters **23**(2), 96 (1973).

[89] B. M. Antipenko, A. Ashkalunin, A. A. Mak, B. Sinitsyn, Y. V. Tomashevich, and G. Shakhkalamyan. *Three-micron laser action in Dy^{3+}.* Soviet Journal of Quantum Electronics **10**(5), 560 (1980).

[90] N. Djeu, V. Hartwell, A. Kaminskii, and A. Butashin. *Room-temperature 3.4-μm Dy:$BaYb_2F_8$ laser.* Optics Letters **22**(13), 997 (1997).

[91] Y. Tsang and A. El-Taher. *Efficient lasing at near 3 μm by a Dy-doped zblan fiber laser pumped at 1.1 μm by an Yb fiber laser.* Laser Physics Letters **8**(11), 818 (2011).

[92] R. Quimby and M. Saad. *Anomalous nonradiative decay in Dy-doped glasses and crystals.* Optics Letters **42**(1), 117 (2017).

[93] Y. Ohishi, E. Snitzer, G. H. Sigel, T. Kanamori, T. Kitagawa, and S. Takahashi. *Pr^{3+}-doped fluoride fiber amplifier operating at 1.31 μm.* Optics Letters **16**(22), 1747 (1991).

[94] M. Shinn, W. Sibley, M. Drexhage, and R. Brown. *Optical transitions of Er^{3+} ions in fluorozirconate glass.* Physical Review B **27**(11), 6635 (1983).

[95] J. A. Buck. *Fundamentals of Optical Fibers* (John Wiley & Sons, 2004).

[96] O. G. Okhotnikov. *Fiber Lasers* (John Wiley & Sons, 2012).

[97] T. Okoshi. *Optical Fibers* (Elsevier, 2012).

[98] P. France. *Fluoride Glass Optical Fibres* (Springer Science & Business Media, 2012).

[99] W. Sellmeier. *Zur erkarung der abnormen farbenfolge im spectrum einiger. substanzen.* Annalen der Physik und Chemie **219**, 272 (1871).

[100] E. Snitzer. *Cylindrical dielectric waveguide modes.* JOSA **51**(5), 491 (1961).

[101] D. Gloge. *Weakly guiding fibers.* Applied Optics **10**(10), 2252 (1971).

[102] D. Marcuse. *Loss analysis of single-mode fiber splices.* Bell Labs Technical Journal **56**(5), 703 (1977).

[103] E. Snitzer, H. Po, F. Hakimi, R. Tumminelli, and B. McCollum. *Double clad, offset core Nd fiber laser.* In *Optical Fiber Sensors*, p. PD5 (Optical Society of America, 1988).

[104] D. Faucher, M. Bernier, G. Androz, N. Caron, and R. Vallée. *20 W passively cooled single-mode all-fiber laser at 2.8 μm.* Optics Letters **36**(7), 1104 (2011).

[105] A. E. Siegman. *Lasers* (University Science Books, 1986).

[106] O. Svelto and D. C. Hanna. *Principles of Lasers* (Springer, 1998).

[107] A. Yariv. *Quantum Electronics, 3rd Edn.* (John Wiley & Sons, 1989).

[108] M. Digonnet. *Theory of superfluorescent fiber lasers.* Journal of Lightwave Technology **4**(11), 1631 (1986).

[109] C. Barnard, P. Myslinski, J. Chrostowski, and M. Kavehrad. *Analytical model for rare-earth-doped fiber amplifiers and lasers.* IEEE Journal of Quantum Electronics **30**(8), 1817 (1994).

[110] M. J. Digonnet and C. Gaeta. *Theoretical analysis of optical fiber laser amplifiers and oscillators.* Applied Optics **24**(3), 333 (1985).

[111] H. Pask, R. J. Carman, D. C. Hanna, A. C. Tropper, C. J. Mackechnie, P. R. Barber, and J. M. Dawes. *Ytterbium-doped silica fiber lasers: versatile sources for the 1-1.2 μm region.* IEEE Journal of Selected Topics in Quantum Electronics **1**(1), 2 (1995).

[112] M. Digonnet. *Theory of operation of three-and four-level fiber amplifiers and sources.* In *OE/FIBERS'89*, pp. 8–26 (International Society for Optics and Photonics, 1990).

[113] M. J. Digonnet. *Closed-form expressions for the gain in three-and four-level laser fibers.* IEEE Journal of Quantum Electronics **26**(10), 1788 (1990).

[114] M. Morin, R. Larose, and F. Brunet. *Q-switched fiber lasers.* In M. J. Digonnet, ed., *Rare-Earth-Doped Fiber Lasers and Amplifiers*, pp. 341–394 (CRC press, 2001).

[115] A. E. Siegman. *How to (maybe) measure laser beam quality.* In *Diode Pumped Solid State Lasers: Applications and Issues*, p. MQ1 (Optical Society of America, 1998).

[116] M. R. Majewski and S. D. Jackson. *Highly efficient mid-infrared dysprosium fiber laser.* Optics Letters **41**(10), 2173 (2016).

[117] M. R. Majewski and S. D. Jackson. *Tunable dysprosium laser.* Optics Letters **41**(19), 4496 (2016).

[118] D. Hanna, R. Percival, I. Perry, R. Smart, P. Suni, J. Townsend, and A. Tropper. *Continuous-wave oscillation of a monomode ytterbium-doped fibre laser.* Electronics Letters **24**(17), 1111 (1988).

[119] E. Desurvire, C. Giles, J. R. Simpson, and J. Zyskind. *Efficient erbium-doped fiber amplifier at a 1.53-μm wavelength with a high output saturation power.* Optics Letters **14**(22), 1266 (1989).

[120] E. Desurvire. *Analysis of erbium-doped fiber amplifiers pumped in the* $^4I_{15/2} - ^4I_{13/2}$ *band.* IEEE Photonics Technology Letters **1**(10), 293 (1989).

[121] Coractive. *OEM Lasers.* URL `http://coractive.com/products/mid-ir-fibers-lasers/oem-lasers/index.html`.

[122] P. Sprangle, A. Ting, J. Peñano, R. Fischer, and B. Hafizi. *Beam combining: high-power fiber-laser beams are combined incoherently.* Laser Focus World **45** (2009).

[123] S. Augst, S. Redmond, C. Yu, D. Ripin, T. Fan, G. Goodno, P. Thielen, J. Rothenberg, and A. Sanchez. *Coherent and spectral beam combining of fiber lasers.* In *Proc. SPIE*, vol. 8237, p. 823704 (2012).

[124] T. Hosoda, D. Wang, G. Kipshidze, W. Sarney, L. Shterengas, and G. Belenky. *3 μm Diode lasers grown on (Al)GaInSb compositionally graded metamorphic buffer layers.* Semiconductor Science and Technology **27**(5), 055011 (2012).

[125] M. Pollnau and S. D. Jackson. *Erbium* 3μm *fiber lasers.* IEEE Journal of Selected Topics in Quantum Electronics **7**(1), 30 (2001).

[126] L. Jian-Feng and S. D. Jackson. *Theoretical study and optimization of a high power mid-infrared erbium-doped zblan fibre laser.* Chinese Physics B **20**(3), 034205 (2011).

[127] M. C. Gonçalves and R. M. Almeida. *Incorporation of OH species in fluorozirconate glasses: nature and influence on physical properties.* Journal of Non-Crystalline Solids **194**(1-2), 180 (1996).

[128] T. Fernandez, Y. Wang, A. Gambetta, N. Coluccelli, P. Laporta, and G. Galzerano. *Dy^{3+} doped zblan fiber amplifier pumped by a single frequency 1064 nm laser for mid infrared applications.* In *Transparent Optical Networks (ICTON), 2016 18th International Conference on*, pp. 1–3 (IEEE, 2016).

[129] S. Duval, J.-C. Gauthier, L.-R. Robichaud, P. Paradis, M. Olivier, V. Fortin, M. Bernier, M. Piché, and R. Vallée. *Watt-level fiber-based femtosecond laser source tunable from 2.8 to 3.6 μm.* Optics Letters **41**(22), 5294 (2016).

[130] J. Swiderski. *High-power mid-infrared supercontinuum sources: Current status and future perspectives.* Progress in Quantum Electronics **38**(5), 189 (2014).

[131] A. Miotello and P. M. Ossi. *Laser-Surface Interactions for New Materials Production*, vol. 130 (Springer, 2010).

[132] I. Mingareev, F. Weirauch, A. Olowinsky, L. Shah, P. Kadwani, and M. Richardson. *Welding of polymers using a 2μm thulium fiber laser.* Optics & Laser Technology **44**(7), 2095 (2012).

[133] V. V. Alexander, K. Ke, Z. Xu, M. N. Islam, M. J. Freeman, B. Pitt, M. J. Welsh, and J. S. Orringer. *Photothermolysis of sebaceous glands in human skin ex vivo with a 1,708 nm raman fiber laser and contact cooling.* Lasers in Surgery and Medicine **43**(6), 470 (2011).

[134] Y. Fujimoto and M. Nakatsuka. *Infrared luminescence from bismuth-doped silica glass.* Japanese Journal of Applied Physics **40**(3B), L279 (2001).

[135] E. M. Dianov, V. Dvoyrin, V. M. Mashinsky, A. A. Umnikov, M. V. Yashkov, and A. N. Gur'yanov. *Cw bismuth fibre laser.* Quantum Electronics **35**(12), 1083 (2005).

[136] S. Firstov, S. Alyshev, M. Melkumov, K. Riumkin, A. Shubin, and E. Dianov. *Bismuth-doped optical fibers and fiber lasers for a spectral region of 1600–1800 nm.* Optics Letters **39**(24), 6927 (2014).

[137] S. Firstov, S. Alyshev, K. Riumkin, M. Melkumov, O. Medvedkov, and E. Dianov. *Watt-level, continuous-wave bismuth-doped all-fiber laser operating at 1.7 μm.* Optics Letters **40**(18), 4360 (2015).

[138] J. Geng and S. Jiang. *Fiber lasers: The 2 μm market heats up.* Opt. Photon. News **25**(7), 34 (2014). URL `http://www.osa-opn.org/abstract.cfm?URI=opn-25-7-34`.

[139] Z. Li, S. Alam, Y. Jung, A. Heidt, and D. Richardson. *All-fiber, ultra-wideband tunable laser at 2 μm.* Optics Letters **38**(22), 4739 (2013).

[140] C. Guo, D. Shen, J. Long, and F. Wang. *High-power and widely tunable tm-doped fiber laser at 2 μm.* Chinese Optics Letters **10**(9), 091406 (2012).

[141] J. Daniel, N. Simakov, M. Tokurakawa, M. Ibsen, and W. Clarkson. *Ultra-short wavelength operation of a thulium fibre laser in the 1660–1750 nm wavelength band.* Optics Express **23**(14), 18269 (2015).

[142] C. V. Raman. *A new radiation* (1928).

[143] G. Woodbury and W. Ng. *Stimulated raman emission in a normal ruby laser.* Proceedings of the IRE **50**, 1236 (1962).

[144] K. Hill, B. Kawasaki, and D. Johnson. *Low-threshold cw raman laser.* Applied Physics Letters **29**(3), 181 (1976).

[145] R. W. Boyd. *Nonlinear optics* (Academic press, 2003).

[146] R. Stolen and E. Ippen. *Raman gain in glass optical waveguides.* Applied Physics Letters **22**(6), 276 (1973).

[147] N. Shibata, M. Horigudhi, and T. Edahiro. *Raman spectra of binary high-silica glasses and fibers containing GeO_2, P_2O_5 and B_2O_3.* Journal of Non-Crystalline Solids **45**(1), 115 (1981).

[148] D. Hollenbeck and C. D. Cantrell. *Multiple-vibrational-mode model for fiber-optic raman gain spectrum and response function.* JOSA B **19**(12), 2886 (2002).

[149] R. G. Smith. *Optical power handling capacity of low loss optical fibers as determined by stimulated raman and brillouin scattering.* Applied Optics **11**(11), 2489 (1972).

[150] RP-Photonics. *Er-doped gain media.* URL https://www.rp-photonics.com/erbium_doped_gain_media.html.

[151] J. Townsend, W. Barnes, and S. Crubb. *Yb^{3+} Sensitised Er^{3+} doped silica optical fibre with ultra high transfer efficiency and gain.* MRS Online Proceedings Library Archive **244** (1991).

[152] S. Crawford, D. D. Hudson, and S. D. Jackson. *High-power broadly tunable 3-μm fiber laser for the measurement of optical fiber loss.* IEEE Photonics Journal **7**(3), 1 (2015).

[153] A. Weiner. *Ultrafast optics*, vol. 72 (John Wiley & Sons, 2011).

[154] T. Hu, D. D. Hudson, and S. D. Jackson. *Actively q-switched 2.9 μm Ho^{3+} Pr^{3+}-doped fluoride fiber laser.* Optics Letters **37**(11), 2145 (2012).

[155] T. Hu, D. Hudson, and S. Jackson. *High peak power actively q-switched Ho^{3+} Pr^{3+}-co-doped fluoride fibre laser.* Electronics Letters **49**(12), 766 (2013).

[156] T. Hu, D. D. Hudson, and S. D. Jackson. *Stable, self-starting, passively mode-locked fiber ring laser of the 3 μm class.* Optics Letters **39**(7), 2133 (2014).